UNIVERSIDADE DE LISBOA
FACULDADE DE CIÊNCIAS
DEPARTAMENTO DE BIOLOGIA ANIMAL

Using satellite imagery to identify foraging habitats for shorebirds and model their distribution in the mudflats of the Bijagós archipelago, Guinea-Bissau

João Ricardo Moreira de Freitas Belo

Mestrado em Biologia da Conservação

Dissertação orientada por:
Doutor José Pedro Granadeiro
Doutora Teresa Catry

2019

DEDICATÓRIA E AGRADECIMENTOS

Dedicatória

Dedico esta tese de mestrado ao meu padrinho e tio, Vasco, que infelizmente faleceu no passado Verão, mas que vai sempre continuar na minha memória.

Agradecimentos

Gostaria de começar por agradecer à fundação MAVA que financiou uma parte importante do meu trabalho de campo, através do projeto "Waders of the Bijagós: Securing the ecological integrity of the Bijagós archipelago as a key site along the East Atlantic Flyway" e à Fundação para a Ciência e Tecnologia que também financiou o meu trabalho, através do projeto "MigraWebs: Migrants as a seasonal ecological force shaping communities and ecossystem functions in temperate and tropical coastal wetlands" (ref. PTDC/BIA-ECO/28205/2017).

Gostaria também de agradecer ao Instituto da Biodiversidade e das Áreas Protegidas da Guiné-Bissau (IBAP), em especial ao Justino Biai, Aissa Regalla, Emanuel Dias, e também ao restante pessoal, pela boa vontade e disponibilidade que sempre mostraram. Facilitaram tudo durante a minha estadia na Guiné-Bissau.

Também quero agradecer à Faculdade de Ciências da Universidade de Lisboa por ser a minha segunda casa desde que saí do ensino secundário e por me ter concedido a oportunidade de aprender com especialistas de topo.

Claro que não pode faltar um agradecimento muito especial. Aos meus dois orientadores, Doutor José Pedro Granadeiro e Doutora Teresa Catry, um obrigado gigante. Só graças a vocês é que tudo foi possível e podem ter a certeza de que este ano foi o que aprendi mais. Obrigado pela vossa disponibilidade (mesmo carregados de coisas para fazer) e paciência. Aprendi mesmo muito convosco e este ano foi espetacular. Obrigado a sério!

Obrigado Filipe "El comandante", Jorge, Edna e Patrícia, pela vossa boa disposição e ajuda preciosa. Para mim, foram sempre 5 estrelas.

Paulino e Mohamed, de vocês nem vale a pena falar. Só digo uma coisa: espero que saibam que só consegui fazer esta tese por causa da vossa ajuda. Obrigado mesmo a sério, gostei muito de trabalhar convosco!

Claro que tenho de agradecer à minha família e amigos pelo apoio que me deram. Mas vocês sabem, não vale a pena estar a escrever porque já vos disse pessoalmente. Mãe sabes que não há ninguém como tu e desde que tu estejas orgulhosa, está tudo perfeito para mim.

Telma claro que te tenho de agradecer! Tu és muito importante para mim e sem ti talvez fosse (ainda) mais difícil. Obrigado pelo teu apoio incondicional e por me teres ajudado sempre. Também agradeço pela tua paciência, sei que às vezes não sou fácil de aturar.

Quero só deixar também um agradecimento também ao pessoal do grupo Atlantic Migrants/ Tidal wings por me terem aceite este ano e pelas sugestões que me foram dando! Também quero agradecer a todos os meus colegas e professores de mestrado pelo ano letivo de 2018/2019, que foi um ano fantástico que pude partilhar convosco.

RESUMO

As áreas intertidais situam-se na interface entre os ambientes marinhos e terrestres. Estas são áreas que estão expostas ao ar durante o período de baixa-mar e submersas pela água do mar durante o período de preia-mar. Como tal, estas áreas estão sujeitas a flutuações ambientais extremas e os organismos que aí habitam têm de ser capazes de tolerar estas variações (a salinidade elevada, o tempo de exposição ao ar e o de imersão no mar, por exemplo). Como as tolerâncias dos diferentes organismos são distintas, forma-se um gradiente vertical (desde a linha de água até às áreas superiores da costa), dividido em secções, nas quais os organismos se distribuem – processo chamado de zonação. Existem também outros gradientes, como o do tamanho médio do grão de sedimento, que leva a uma enorme diversidade de habitats: desde as amplas planícies estuarinas de grão fino até às costas rochosas de grão mais grosso.

Os estuários e outras áreas intertidais encontram-se entre os ecossistemas mais produtivos do globo. Devido a esta enorme produtividade, estas áreas podem albergar grandes populações de vertebrados, como peixes e aves costeiras.

As aves costeiras pertencem a um grupo vasto, composto principalmente por aves de pequeno e médio porte, e ocorrem sobretudo em zonas costeiras e zonas húmidas. Estas aves têm um caracter altamente migratório e todos os anos migram de zonas de elevada latitude, onde se encontram as suas principais áreas de reprodução, e dispersam para zonas mais a sul, para as suas áreas de invernada. Para tal, usam rotas migratórias que interligam diversas áreas chave do Planeta onde vão parando, até atingirem o seu destino final, as áreas de invernada. Aí alimentam-se essencialmente de invertebrados bentónicos, como poliquetas, crustáceos e bivalves, a fim de atingirem os seus requerimentos energéticos para migrarem de volta para as áreas de reprodução. No entanto, as populações de aves costeiras estão em declínio acentuado, e esta observação já foi feita em diversas partes do Planeta. As principais causas deste decréscimo estão relacionadas com o aumento da pressão das atividades humanas em áreas intertidais (estuários e zonas costeiras, por exemplo). Um dos exemplos é maior taxa de ocupação destas áreas devido ao crescimento da população humana. Também a subida média do nível da água do mar já tem sido relatada como uma ameaça crescente, pois leva à perda de áreas intertidais e, consequentemente, afeta as populações de aves.

A rota migratória do Atlântico Este é percorrida por milhões de aves costeiras, anualmente. Esta rota liga as zonas de reprodução do Ártico (desde o Canadá até à Sibéria) à Costa Oeste de África. O arquipélago dos Bijagós localiza-se nesta região africana e faz parte da Guiné-Bissau (11º52’ N, 15º 36’ W), sendo um dos locais de invernada mais importantes para estas aves. Todos os anos alberga cerca de 700000 a 900000 aves costeiras e foi classificado como Reserva da Biosfera pela UNESCO (2011) e como sítio Ramsar pela Convenção Ramsar (2014).

Neste arquipélago existe uma espécie de caranguejo-violinista *Afruca tangeri* que se encontra distribuído por todo o arquipélago. Estes caranguejos são considerados engenheiros de ecossistemas, uma vez que alteram as características do sedimento, afetando também os padrões de biodiversidade que aí ocorrem. No entanto, este arquipélago dos Bijagós é dos menos estudados em África. Torna-se, portanto, imperativo aumentar o conhecimento existente sobre este local extremamente importante para a biodiversidade e sobretudo para as aves costeiras que, apesar de muito ameaçadas, encontram aqui uma área de extrema importância. Torna-se importante também perceber quais os fatores que afetam a sua distribuição nas zonas de invernada.

Este estudo tem como objetivos principais (1) mapear a variabilidade de sedimentos existentes nas planícies intertidais do arquipélago dos Bijagós, usando técnicas de sensoriamento remoto aplicado a imagens de satélite de alta resolução, e (2) perceber quais os fatores ambientais que influenciam a distribuição de aves costeiras em alimentação no ecossistema intertidal dos Bijagós, através de um exercício de modelação espacial. Pretende-se construir mapas preditivos da ocorrência de várias espécies de aves costeiras nesta área de importância global. Este estudo encontra-se dividido em dois capítulos, que se encontram sumariamente abaixo descritos.

No primeiro capítulo é apresentado um exercício de classificação e mapeamento da variabilidade dos sedimentos da área intertidal, no arquipélago dos Bijagós. Este estudo foi realizado numa ampla planície intertidal (com uma área de cerca de 1000 ha), localizada na parte sul do Parque Nacional de Orango. Para tal, obteve-se uma imagem detetada pelo sensor do satélite do Sentinel-2 MSI (*Multi-spectral Instrument*), lançado pela Agência Espacial Europeia. No campo, foram amostradas 228 unidades de área homogénea em termos de composição do sedimento, a fim de serem usadas como áreas de treino e de validação para implementar uma classificação supervisionada. Em cada área foi estimada visualmente a sua dimensão, a percentagem de cobertura de água, de macroalgas, de conchas e de áreas ocupadas pelos caranguejos-violinistas (*Afruca tangeri*). Também foi tirada uma amostra de sedimento em cada área, para mais tarde determinar o conteúdo de partículas finas (partículas< 0.63µm) e o conteúdo de matéria orgânica do sedimento. Após recolhidas todas as amostras, foram estabelecidas quatro classes de habitat, com base em duas das variáveis recolhidas – a percentagem do sedimento coberta por áreas de caranguejo-violinista e a percentagem de partículas finas do sedimento. As classes de habitat definidas foram: *Sand-FBA* (áreas com: percentagem de partículas finas < 10% e cobertura de área ocupada por caranguejo > 30%); *Sand* (áreas com: percentagem de partículas finas < 10% e cobertura de área ocupada por caranguejo < 30%); *Muddy* (áreas com: percentagem de partículas finas >10% e cobertura de área ocupada por caranguejo < 30%) e *Muddy-FBA* (áreas com: percentagem de partículas finas > 10% e cobertura de área ocupada por caranguejo < 30%). Após definidas as classes realizou-se uma classificação supervisionada, utilizando o algoritmo *Random Forest*. A imagem a ser classificada foi composta por várias camadas: dez bandas espectrais, um modelo de inundação (gerado também com base numa série de imagens de satélite), uma camada contendo os valores de NDWI (Normalized Difference Water Index) para cada pixel e as cinco componentes principais resultantes de uma análise de componentes principais. As eficácias de classificação foram elevadas, variando desde 0.89 (*Muddy*) até 0.99 (*Muddy-FBA*). Além da classificação, foi também efetuada uma comparação entre dois métodos classificativos: um em que cada tipo de habitat foi classificado em etapas diferentes, dependente das diferenças da assinatura espetral de cada habitat (método 1), ou seja, habitats com espetros distintos vão sendo sucessivamente separados da restante área, até toda a área intertidal se encontrar classificada; e outro em que a classificação foi feita numa só etapa, ou seja, com todas as classes de habitat (método 2). As eficácias de classificação aplicando ambos os métodos foram semelhantes, contudo foram ligeiramente mais elevadas aquando da aplicação do método 1. Também foram comparadas as eficácias de classificação entre duas imagens detetadas remotamente com um mês de diferença. As principais conclusões foram que (1) aplicando o método descrito, áreas intertidais semelhantes a esta podem ser classificadas com elevada eficácia; (2) áreas de caranguejos-violinistas podem ser distinguidas claramente de outras áreas e (3) este método pode ser replicado através da extração da assinatura espetral de cada tipo de habitat.

No segundo capítulo, o objetivo foi perceber quais as variáveis ambientais que mais influenciam a distribuição de aves costeiras em alimentação para conseguir identificar áreas importantes para a sua conservação. A área de estudo foi a mesma que a descrita anteriormente. Definiram-se 67 áreas de contagem (na maior parte dos casos tinham uma dimensão de 250*250 metros), onde foram contadas aves em alimentação. Cada área foi contada duas vezes. Estas áreas foram caracterizadas em termos de diferentes habitats utilizando o mesmo conjunto de variáveis descritos acima e também foi recolhida a penetrabilidade de cada tipo de habitat. Determinaram-se, através de programas de sistemas de

informação geográfica, as distâncias desde o centroide de cada área até ao limite da área de mangal, ao limite de bancos de areia e até ao canal mais próximo. Em seguida aplicaram-se modelos de distribuição de espécies GAMs (*Generalized additive models*) para testar quais destas variáveis tinham mais influência e mais poder explicativo na ocorrência e na abundância de 11 e 7 espécies de aves costeiras, respectivamente. Os preditores mais selecionados pelos modelos foram o tempo de exposição dos sedimentos (i. e. o tempo em que estão fora de água), a percentagem de partículas finas, a percentagemde área ocupada por caranguejos-violinistas, a distância à mancha de mangal mais próxima e a distância ao canal de água mais próximo. No geral, o poder explicativo dos modelos (medido em percentagens) foi elevado, sendo que as abundâncias do Maçaricos-galego, *Numenius phaeopus*, por exemplo, foram explicadas em 60%. De seguida, estes preditores foram usados para classificar a área intertidal, através de técnicas de deteção remota, e obtiveram-se mapas preditivos relativos a toda a área de estudo. As principais conclusões foram que (1) a aplicação de GAMs permitiu predições eficazes e relações interpretáveis entre as aves e o habitat, (2) espécies diferentes têm diferentes preferências de habitat, sendo que a manutenção da diversidade encontrada nestas áreas é de extrema importância no âmbito da conservação destas espécies e (3) os mapas preditivos foram eficazes uma vez que existe elevada concordância entre as frequências de ocorrência observadas e as probabilidades de ocorrência previstas.

Este estudo tem potenciais de aplicação relevantes em termos de conservação, uma vez que quer os sistemas intertidais, quer as aves costeiras encontram-se atualmente fortemente ameaçados. A ligação entre os dois capítulos é feita a partir dos mapas preditivos, pois conseguiu-se prever as probabilidades de ocorrência das espécies numa área relativamente abrangente, através da utilização de técnicas de deteção remota. No futuro, este estudo pode ser expandido para uma escala maior, para todo o arquipélago. Isto é de extrema importância uma vez que este local é um dos mais relevantes ao longo da rota migratória do Atlântico. Este e a identificação de áreas importantes para a aves costeiras pode ser crítico para a definição de ações de conservação.

Palavras-chave: Áreas intertidais, Aves costeiras, modelos preditivos, Deteção Remota, Sentinel-2A

SUMMARY

The intertidal zone is the area of marine sediments that is exposed to air at low tide and submersed by seawater at high tide. Intertidal areas have extreme environmental fluctuations as they are cyclically covered by the sea and exposed at the air. The interface sea-air generates a vertical gradient that shapes the distribution of intertidal organisms, from the lower to the upper shore. The biological response to that gradient is zonation, i.e., organisms are distributed through different sections, according to their ability to cope with physical factors (e.g. desiccation) and biological processes. Wave action, tide dynamics and the geological history of the shore are responsible for creating the particle-size gradient, that leads to a wide variety of intertidal areas ranging from large-particle rocky shores to fine-particle estuarine mudflats.

Estuaries and other intertidal areas are among the most productive ecosystems on Earth. Due to this high productivity, they can support large populations of vertebrates, including fishes and shorebirds.

Shorebirds are a large group of small to medium-sized birds that occur namely in coastal or wetland habitats during the winter, all over the globe. These species are highly migratory, as they breed in high-latitude areas and then disperse to the non-breeding areas. Every year, shorebirds migrate along flyways that encompass a network of key-sites, usually estuaries, where they rest and refuel while in migration or where they spend the winter. Here, they feed on the invertebrate prey, such as polychaetes, bivalves and crustaceans and at some stage feed intensively to put up reserves in order to migrate back to the breeding areas. However, shorebird populations are threatened at a global scale, representing a matter of international conservation concern. The main reasons are related to the loss of the intertidal areas mainly due to high pressure of human activities over estuarine areas, such as land reclamation and sediment dredging), and due to sea-level rise. These threats ultimately result in habitat degradation/loss of suitable habitat for foraging shorebirds.

The East Atlantic Flyway (EAF) is one of the major flyways for shorebirds, and it used by millions of shorebirds annually. It connects the Artic breeding grounds (from Canada to Central Siberia) to the entire western coast of Africa.The Bijagós archipelago is located off the coast of Guinea-Bissau (11º52’ N, 15º 36’ W) and it comprises 88 islands and islets. It is the second most important African site along the EAF for shorebirds, just after the Banc d’Arguin, in Mauritania . Several shorebird species reach the south edge of their winter distributions here, highlighting the importance of such area. Due to its biodiversity and ecological relevance, the Bijagós archipelago was classified as a Biosphere Reserve by UNESCO (2011) and as Ramsar site under the Ramsar Convention (2014).

In this archipelago there is a widespread fiddler crab species *Afruca tanferi* that is considered to be a ecosystem engineer as it alters the sediment characteristics, affecting the biodiversity patterns that occur there. However, this archipelago is one of the most poorly known in the African continent. Therefore, it is imperative to increase our knowledge about this really important site for the biodiversity and particularly about shorebirds that find here one of the most important non-breeding areas.

In chapter 1, we used Sentinel-2 Multispectral Instrument imagery to map foraging habitats for shorebirds in an important mudflat of the Bijagós archipelago. We established and characterized 228 homogeneous training plots (total area of 132.35 ha) in ca. 1,000 ha of intertidal area, in which we

characterized the percentage coverage by surface water, African Fiddler Crab *Afruca tangeri* burrows, macroalgae, shells, and drainage channels and measured the mud (silt + clay) fraction of the sediment. We defined four types of habitat: sand; sand-FBA (fiddler crab burrow area); muddy and muddy-FBA. We performed a step wise supervised classification (method 1), using Random Forest based on: (1) 10 spectral bands of a Sentinel-2A scene, (2) an inundation model for the area, (3) the NDWI and (4) the first five Principal Components applied to the satellite scene. The balanced accuracy of the habitat classification ranged from 0.89 (Muddy) to 0.99 (Muddy-FBA) and the model had an overall accuracy of 0.92 (kappa=0.88). We also performed a supervised classification in one only step (method 2) to compare the accuracy with the first method. Overall accuracies were slightly higher and uncertainties were lower in method 1. To assess replicability, we applied the same method to an image from a different date, and accuracies were similar. This work can be used to model shorebird occurrences in relation to high-density fiddler crab areas, as these crustaceans are known ecosystem engineers, and to monitor changes in intertidal habitats over the years.

In chapter 2, we investigate the biotic and abiotic variables driving foraging shorebird distributions in the Bijagós archipelago, an important East Atlantic Flyway non-breeding area. This allowed to map important foraging areas for shorebird species on an important mudflat. To achieve this, we (1) counted shorebirds in 67 plots during low tide, (2) collected biotic and abiotic data within the counted plots, and (3) used species distribution models (GAMs) to test which variables can better explain the variations in shorebird occurrences (n=11 species) and abundances (n=7 species) throughout the sampling plots. The most significant predictors were the exposure period, mud fraction, fiddler crab burrow area, distance to mangrove patches (m) and distance to channels/creeks. GAMs offered accurate occurrence predictions and interpretable shorebird-habitat relationships. Overall explained deviances reached high values (e.g. abundances of whimbrels had 60% of its deviance explained). The best predictors for shorebird distributions were used to classify the intertidal area using remote sensing techniques (Sentinel-2A), and suggested predictions for shorebird distributions within the study area. This work can be expanded to the whole Bijagós archipelago, providing an important tool to identify priority areas and to inform conservation actions.

This study is relevant as intertidal areas and shorebirds are highly threatened. The link between the two chapters are the predictive maps. We could predict areas with higher probability of occurrence for 11 shorebird species, using information that could hardly be obtained without the use of remote sensing tools. The exercise used in this thesis can be expanded to larger scales if the sampling effort is higher. We consider our work to be relevant in terms of conservation, as intertidal areas and shorebirds face several threats. Although being poorly studied, the Bijagós archipelago is one of the key non-breeding areas for shorebirds along the East Atlantic Flyway. Therefore, identifying priority areas for shorebirds in this critical site can be of major importance for the definition of conservation actions.

Key-words: Intertidal areas, Predictive models, Remote sensing, Sentinel-2A, Shorebirds

I presented this work in the International Wader Study Group (IWSG) conference held in Morecambe, United Kingdom, in September 2019.

CONTENTS

LIST OF ABREVIATIONS

BX	Bands (X corresponds to the number of the spectral band of Sentinel2 MSI)
EDF	Effective Degrees of Freedom
ESA	European Space Agency
FBA	Fiddler crab Burrow Area
GAM	Generalized Additive Model
IH	Instituto Hidrográfico
MF	Mud Fraction
NDVI	Normalized Difference Vegetation Index
NDWI	Normalized Difference Water Index
NIR	Near Infra-Red
PC	Principal Component
PCA	Principal Component Analysis
SWIR	Short-wave Infra-Red

LIST OF FIGURES AND TABLES

FIGURES

TABLES

GENERAL INTRODUCTION

The intertidal zone is the area of marine sediments that is exposed to air at low tide and submersed by seawater at high tide. Intertidal areas have extreme environmental fluctuations as they are cyclically covered by the sea and exposed to air. This ultimately generates a vertical gradient that shapes the distribution of intertidal organisms, from the lower to the upper shore. The biological response to that gradient is zonation, i.e., organisms are distributed through different sections, according to their ability to cope with physical factors (e.g. desiccation) and biological processes (e.g. competition; Rafaelli & Hawkins, 1999; Gibson et al., 2001). Wave action, tide dynamics and the geological history of the shore are responsible for creating the particle-size gradient, that leads to a wide variety of intertidal areas ranging from large-particle rocky shores to fine-particle estuarine mudflats (Rafaelli & Hawkins, 1999).

Estuaries and other intertidal areas are among the most productive ecosystems on Earth (Schelske & Odum, 1962). Due to this high productivity, they can support large populations of vertebrates, including fishes and shorebirds (Wallace et al., 1984; Russi et al., 2013; Liu et al., 2016; Sagar et al., 2017).

Shorebirds are a large group of small to medium-sized birds that occur namely in coastal or wetland habitats during the winter, all over the globe (Brown, 2018). These species are highly migratory, as they breed in high-latitude areas and then disperse to the non-breeding areas. Every year, shorebirds migrate along flyways that encompass a network of key-sites, usually estuaries, where they rest and refuel while in migration or where they spend the winter (Delany et al., 2009). Here, they feed on the invertebrate prey, such as polychaetes, bivalves and crustaceans (Beninger & Paterson, 2018) and at some stage feed intensively to put up reserves in order to migrate back to the breeding areas. However, shorebird populations are threatened at a global scale, representing a matter of international conservation concern (IUCN, 2019). The main reasons are related to the loss of the intertidal areas mainly due to high pressure of human activities over estuarine areas, such as land reclamation and sediment dredging (Cayford, 1993; Day Jr et al., 2013), and due to sea-level rise (Galbairth et al., 2005; Murray et al., 2019). These threats ultimately result in habitat degradation/loss of suitable habitat for foraging shorebirds.

The East Atlantic Flyway (EAF) is one of the major flyways for shorebirds, and it used by millions of shorebirds annually. It connects the Artic breeding grounds (from Canada to Central Siberia) to the entire western coast of Africa (van Roomen et al., 2018). The Bijagós archipelago is located off the coast of Guinea-Bissau (11º52' N, 15º 36' W) and it comprises 88 islands and islets. It is the second most important African site along the EAF for shorebirds, just after the Banc d'Arguin, in Mauritania (Dodman & Sá, 2005). Several shorebird species reach the south edge of their winter distributions here, highlighting the importance of such area. Due to its biodiversity and ecological relevance, the Bijagós archipelago was classified as a Biosphere Reserve by UNESCO (2011) and as Ramsar site under the Ramsar Convention (2014). Yet, this archipelago is one of the most poorly known in Africa (Rebelo & Catry, 2011).

The aim of this study is to map important areas for foraging shorebirds in the Bijagós archipelago. This was achieved by classifying the relevant intertidal habitats for foraging shorebirds, using remote sensing techniques based on recent sensors imagery (Sentinel-2), and by modelling

shorebird occurrences and abundances in relation to environmental variables. Such an approach enabled the production of predictive maps for the patterns of occurrence and abundance of shorebirds.

CHAPTER1: USING SENTINEL-2A MULTI-SPECTRAL INSTRUMENT TO CLASSIFY INTERTIDAL HABITATS BASED ON SEDIMENT FEATURES, IN THE MUDFLATS OF THE BIJAGÓS ARCHIPELAGO

Abstract: Estuaries and other intertidal areas are among the most productive ecosystems on Earth, but are threatened at a global scale, affecting shorebird populations that depend on these systems. Therefore, mapping these areas and the micro habitats within, is crucial for monitoring changes. The Bijagós archipelago is one of the most important non-breeding areas for shorebirds along the East Atlantic Flyway. In this study, we used Sentinel-2 Multispectral Instrument imagery to map foraging habitats for shorebirds in an important mudflat of the Bijagós archipelago. During the low tide period, we established and characterized 228 homogeneous training plots (total area of 132.35 ha) in ca. 1 000 ha of intertidal area, in which we characterized the percentage coverage by surface water, African Fiddler Crab *Afruca tangeri* burrows, macroalgae, shells, and drainage channels and measured the mud (silt + clay) fraction of the sediment. We defined four types of habitat: sand; sand-FBA (fiddler crab burrow area); muddy and muddy-FBA. We performed a stepwise supervised classification (method 1), using Random Forest based on: (1) 10 spectral bands of a Sentinel-2A scene, (2) an inundation model for the area, (3) the NDWI and (4) the first five Principal Components applied to the satellite scene. The balanced accuracy of the habitat classification ranged from 0.89 (Muddy) to 0.99 (Muddy-FBA) and the model had an overall accuracy of 0.92 (kappa=0.88). We also performed a supervised classification in one only step (method 2), using the same algorithm, to compare the accuracy with the first method. Overall accuracies were slightly higher and uncertainties were lower with method 1. To assess replicability, we applied the same method to an image from a different date, and accuracies were similar. This work can be used to model shorebird occurrences in relation to high-density fiddler crab areas, as these crustaceans are known ecosystem engineers, and to monitor changes in intertidal habitats over the years.

Key-words: Bijagós archipelago, classification of intertidal habitats, Random Forest, Sentinel-2A, shorebirds

INTRODUCTION

Despite providing a wide range of important ecosystem services, such as shore protection or carbon storage, intertidal areas are threatened at a global scale (Galbairth et al., 2002; Lotze et al., 2006; Russi et al., 2013; Murray et al., 2019). The main threats are related to high pressure of human activities (e.g. disturbance and land-reclamation; Goss-Custard & Yates, 1992; Cayford, 1993; Day Jr et al., 2013) and sea-level rise (Watkinson et al., 2004; Galbraith et al., 2002; Murray et al., 2019). As a result, the total area covered by these systems declined over the last three decades at an accelerated rate (Murray et al., 2019), highlighting the need to identify and monitor these changes in order to delineate effective conservation actions.

Remote sensing has been successfully used to map coastal wetlands over the last three decades (Tiner, 1996; Dahl, 2006). Several authors used this tool to map intertidal sediments (e.g. Yates et al., 1993; Rainey et al., 2003; Ryu et al., 2004), delineate the coastline and coastline dynamics (e.g. Liu & Jezek, 2004b; Yu & Acton, 2004; Li & Gong, 2016), assess the seasonality in microphytobenthos (e.g. Brito et al., 2013), assess changes in the distribution of tidal flats (e.g. Murray et al., 2019) and the variation in extent of mangrove cover (Cardoso, 2017). Intertidal sediment distribution and dynamics are key factors for the understanding of coastal erosion and estuarine ecology (Ryu et al., 2004). Mapping such distribution can be achieved by recognizing which sediment features (biotic and abiotic) are the most important in determining the spectral signature of the sediment. The general profile of the radiometric spectrum (defined as the set of mean values of reflectance of all bands of a particular area) is strongly influenced by the mud-sand contents (Broeckman & Stelzer, 2008). Muddy areas retain more organic matter and therefore the absorption of wavelengths in the blue and red region areas are higher and in the region between 700 and 750 nm (wavelengths between the red and the infra-red region) are lower than sandy areas (Broeckman & Stelzer, 2008). In fact, the organic matter contents is relevant in discriminating between sediment classes (Deronde et al., 2006). However, sediment grain size is also described as one of the major key features promoting spectral differences between substrates (Doerffer & Murphy, 1989; Rainey et al., 2000). Shell banks and macroalgae and microalgae coverage are also described as critical variables in shaping the spectral signature of intertidal sediments (Doerffer & Murphy, 1989; Thomson et al., 1998). Topography (related to other sediment features) can also explain a high proportion of the variance in the spectral signature of the sediment (Doerffer & Murphy, 1989). The spectral signature also depends on the water contents and the superficial water coverage, as with the increase of the water contents, there is a sharp decrease of the reflectance for higher wavelengths in the infra-red region (Rainey et al., 2000; Stelzer et al., 2004; Broeckman & Stelzer, 2008).

During low tide, the surface water coverage and the interstitial water contents, can be a major obstacle while mapping intertidal sediments (Broeckman & Stelzer, 2008). The spectrum of "wet" muddy and sandy areas is often similar and could therefore prevent an accurate classification (Rainey et al., 2000; Stelzer et al., 2004). One possible way to overcome such complexity is to use linear mixture modelling as it can be successful in unmixing data from similar environments (Mertes et al., 1993; Yates et al., 1993). However, the success of this approach seems to be limited, mainly due to temporal differences between image acquisition and the validation in the field. Hence, the date of image acquisition should be temporally coincident with field surveys (Dyer et al., 2000). In addition, Bryant et al. (1996) demonstrated that the short-wave infra-red region (SWIR – 1.4-3.0 μm) of the spectrum is of major importance in distinguishing sediments with different moisture contents, and this approach has been successfully used for estimating soil moisture in terrestrial environments by several authors (e.g. Lobell & Asner, 2002; Kwon et al., 2016). Rainley et al. (2000) showed *in-situ* that image acquisition after drying out the sediment would maximize the differences between the spectra of mud and sand

areas. However, this can be difficult to apply under natural conditions. Hence, it is recommended to use an image corresponding to the lowest available tide (Rainley et al., 2000). Kwon et al. (2016) classified intertidal sediments, using a two-step principal component analysis (PCA). This method was performed in order to extract the principal component related to the superficial water and then classify the intertidal sediments. PCAs have been successfully used in several other remote sensing exercises (e.g. Lhermitte et al., 2011; Ammanollahi et al., 2011; Muñoz-Robles et al., 2012).

Mapping intertidal sediments offers other challenges. Yates et al. (1993) could hardly distinguish between sandy and muddy areas in the Wash estuary due to a thin layer of mud covering sandy areas.

More recently, the development of high spatial and spectral resolution sensors significantly enhanced the success of mapping and classifying habitats (Klemas, 2011). As part of Copernicus, the European Earth Observation Programme, the Sentinel satellite constellation of the European Space Agency (ESA) comprising several satellite families (Sentinel-1, 2 and 3), provides free information for the scientific community (Drusch et al., 2012). Sentinel-2 has a Multi-Spectral Instrument (MSI), which is a high-resolution optical sensor. Several studies compared the characteristics between this sensor and others such as Landsat or SPOT. Table 1.1. displays the main characteristics of the spectral bands of both sensors. The finer spatial resolution of Sentinel-2 MSI allows to more accurately classify land cover habitats than Landstat-8 (Pesaresi et al., 2016; Kwang et al., 2017). In particular, the red-edge region provided by Sentinel-2 (Fig. 1.1) offers advantages when classifying different types of vegetation due to its narrow wavelength width and to the fact that it occupies a region in the spectrum that is included in the panchromatic band in Landsat. This allows a better discrimination of soil proprieties (Fourkour et al., 2018). Fourkour et al. (2018) verified that when using Sentinel-2 red-edge bands in mapping different land covers in Burkina Faso, the classification accuracy improved by 4 % compared to the accuracy obtained with Landsat OLI (Operational Land Imager) sensor. The red-edge bands have also been selected as the most influential when estimating the canopy coverage of boreal forest (Korhonen et al., 2017). The classification of different land uses in the city of Istanbul had an increment of 3-6 % in the accuracy when using Sentinel-2 (Topaloglu et al., 2016). Manzo et al. (2015) verified that the bands on the red-edge have great potential for the detection of Chlorophyll-a in turbid water. Hedley et al. (2012) showed that Sentinel-2 MSI sensor had a better performance in the classification of macroalgae and sand areas. Another feature that differentiates Sentinel-2 from Landsat-8 is the higher visit frequency of the first one (10 versus 16 days; Li & Roy, 2017). According to Li & Roy (2017), tiles in Sentinel-2 are wider than Landsat-8. These two characteristics allow Sentinel-2 to have higher availability of images of the same tile per year (Sentinel-2: 61 images and Landsat-8: 39 images).

Table1.1- Comparison between Landsat-8 bands (NASA, 2017), L8, on the left, and Sentinel-2 bands (ESA, 2017b), S2, on the right (Central wavelength, in µm; wavelength range, in µm; bandwidth, in µm; and resolution in m).

L8 Band		CW (µm)	Wavelength (lower-upper)	Bandwidth	Res. (m)		S2 Band		CW (µm)	Wavelength (min-max)	Bandwidth	Res. (m)
1	C/A	0.443	0.435 - 0.451	0.016	30	C/A	1	C/A	0.443	0.421 - 0.457	0.036	60
2	Blue	0.482	0.452 - 0.512	0.060	30	Blue	2	Blue	0.494	0.439 - 0.535	0.096	10
3	Green	0.561	0.533 - 0.590	0.057	30	Green	3	Green	0.560	0.537 - 0.582	0.045	10
4	Red	0.655	0.636 - 0.673	0.037	30	Red	4	Red	0.665	0.646 - 0.685	0.039	10
							5	VRE	0.704	0.694 - 0.714	0.020	20
							6	VRE	0.740	0.731 - 0.749	0.018	20
							7	VRE	0.781	0.768 - 0.796	0.028	20
							8	NIR	0.834	0.767 - 0.908	0.141	10
5	NIR	0.865	0.851 - 0.879	0.028	30	NIR	8a	NIR	0.864	0.848 - 0.881	0.033	20
							9	WV	0.944	0.931 - 0.958	0.027	60
9	Cirrus	1.373	1.363 - 1.384	0.020	30	Cirrus	10	Cirrus	1.375	1.338 - 1.414	0.076	60
6	SWIR	1.609	1.567 - 1.651	0.085	30	SWIR	11	SWIR	1.612	1.539 - 1.681	0.142	20
7	SWIR	2.201	2.107 - 2.294	0.187	30	SWIR	12	SWIR	2.194	2.072 - 2.312	0.240	20
8	Pan	0.590	0.503 - 0.676	0.172	15							
10	TIRS	10.895	10.60 - 11.19	0.590	100 *							
11	TIRS	12.005	11.50 - 12.51	1.010	100 *							

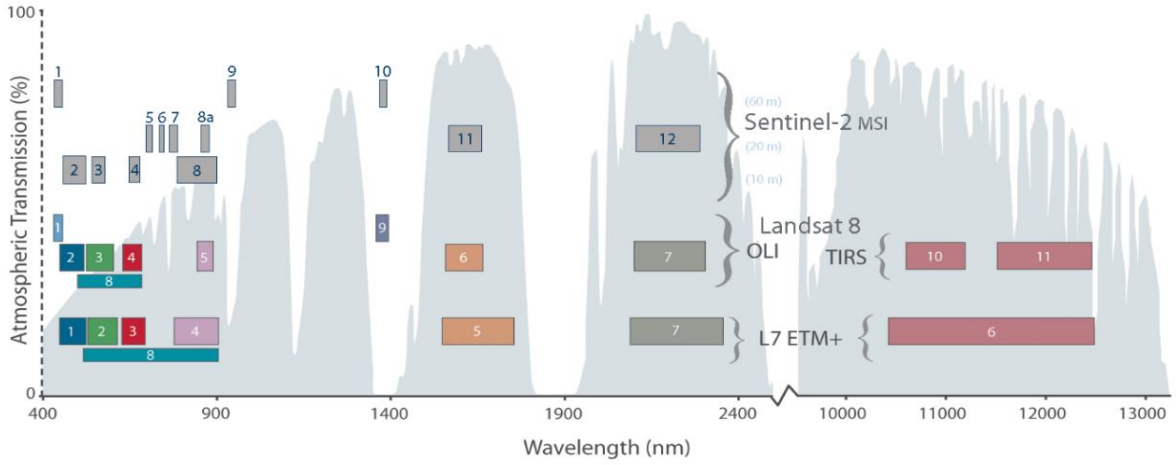

Figure 1.1- Graphical representation of the spectral ranges of the different bands by different bands in Sentinel-2 MSI, Landsat-8 and Landsat-7 (source: NASA, 2015).

The Bijagos archipelago is located off the coast of Guinea-Bissau (11º52' N, 15º 36' W) and comprises a set of 88 islands and islets. This archipelago was classified as Biosphere Reserve by UNESCO (UNESCO, 2011) and as Ramsar site under the Ramsar Convention (2014). Yet, this archipelago is one of the most poorly known in Africa (Rebelo & Catry, 2011). The intertidal area of the Bijagós archipelago extends over than 140 000 ha of mud and sand flats, 35 000 ha of which are covered by mangroves (Campedron & Catry, 2016). Most of the tidal area is composed by a mixture of fine and coarse sediments (Zwarts, 1988). Intertidal areas of the Bijagós support a high biodiversity, with relevance for the large populations of fish and wintering shorebirds (Zwarts, 1988; Dodman & Sá, 2005; Campredon & Catry, 2016).

Another key organism in this ecosystem is the fiddler crab *Afruca tangerii* (Eidux, 1835), which is widespread in the mudflats of the archipelago (Zwarts, 1988). Fiddler crabs are distributed in patchy areas of both muddy and sandy flats, inhabiting holes that they excavate (Zwarts, 1985). These crabs are considered as ecosystem engineers as they force the ascension of organic matter and deep sediments to the surface (Gutiérrez et al., 2006, Kristensesn, 2008), increase carbon fluxes (Genoni, 1991) and alter the topography and geochemistry of the sediment (e.g. particle-size and drainage; Mouton and Felder,

1996; Botto and Iribarne, 2000, Kristensen, 2008). Thus, it is expected that areas with high densities of fiddler crabs have a different spectral signature from areas with low densities.

In this study, the objective was to develop methods to classify intertidal sediments in the Bijagós archipelago. To achieve this, we selected a large intertidal area in southern part of Orango National Park and tested the effectiveness of Sentinel-2 images to identify different types of sediment. We also carried out extensive validation work on the ground, estimated several sediment features, such as the mud fraction, the cover of fiddler crab burrowing area, superficial water, coverage by shells and by macroalgae. We also used a novel method based on a sequence of Sentinel-2 images to obtain an inundation model and therefore calculate the heights of every pixel.

METHODS

STUDY AREA

Fieldwork took place in an extensive intertidal flat in south part of Orango National Park, which comprises an area of roughly 1000 ha (Fig. 1.2.). Flats are surrounded by mangroves with a thin sandbank that acts as a barrier. The study area is characterized by a semi-diurnal tidal regime, where the tidal range varies from approximately 3m during neap tides to approximately 4.5m during spring tides (estimated from Instituto Hidrográfico da marinha portuguesa – IH, 2019).

GROUND TRUTHING

In the field, we selected 228 sampling polygons that were characterised (Fig. 1.2.) and used to supervise the classification of the satellite scene. We took into account three factors when selecting these polygons: (1) uniformity: each selected area should be relatively homogeneous in terms of sediment type, water, algae, shell and fiddler crab burrow area coverage, as judged by visual inspection, (2) conservativeness: the limits were set by making all efforts to avoid including heterogeneous areas; and (3) representativeness: the number of samples of each class was roughly proportional to the area occupied by each habitats (Campbell & Wynne, 2011). The area of sampling polygons was estimated by attributing a radius value (in m) to each plot in relation to the position of the observer. When the whole sampling polygons proved to have the same type of surface cover, we used it directly, as a polygon. In each sampling polygon, we estimated at 5% intervals, the surface cover percentage of superficial water, shells, macroalgae, drainage channels, and fiddler crab burrow area. We also collected a sediment sample per habitat, with a volume of 40-60 ml and a depth of approximately 5 cm, to determine the fine particle and organic matter contents and classify the habitat types accordingly.

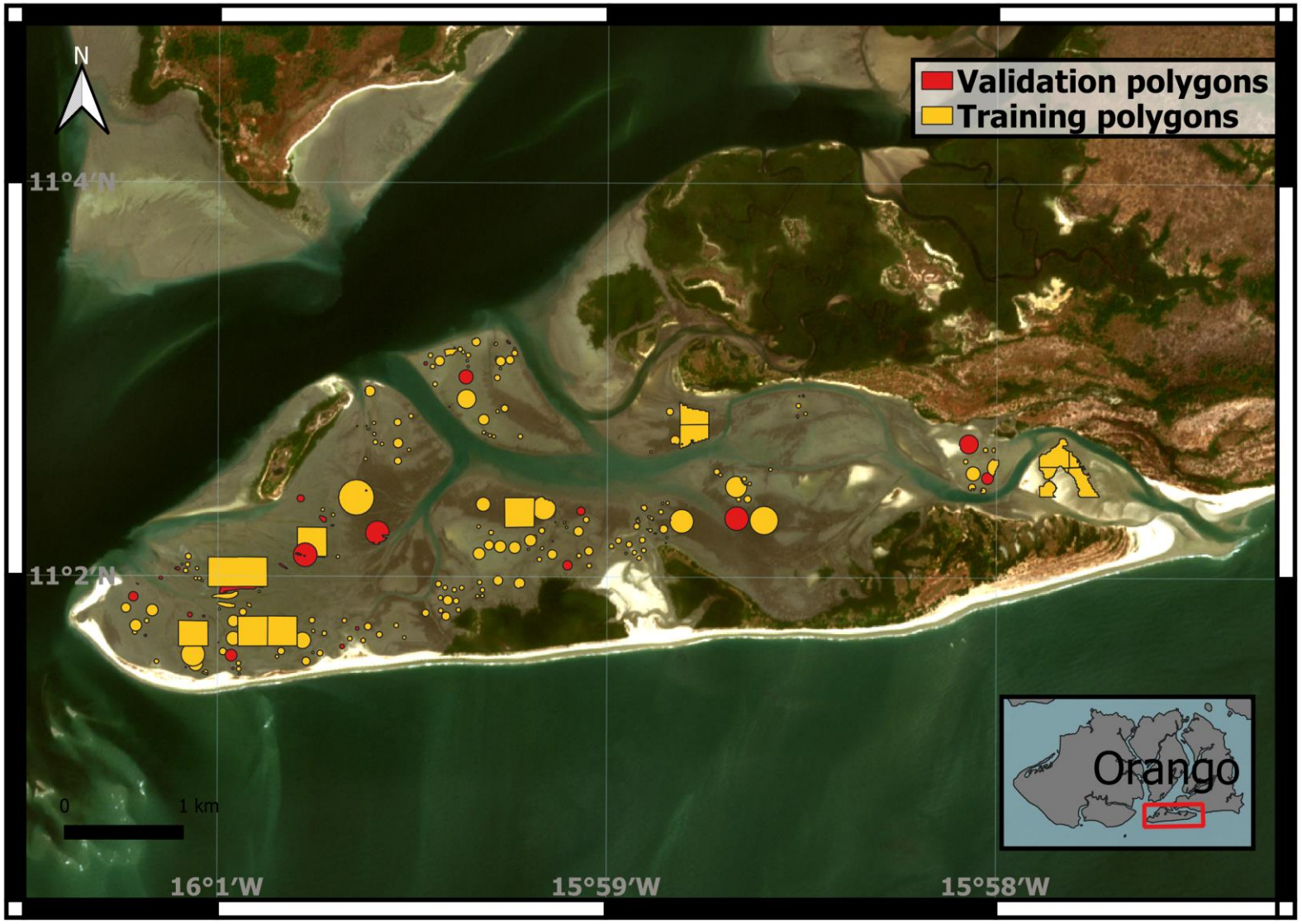

Figure 1.2. - Map of the sampling polygons for ground truthing (n=228) in the intertidal area of Adonga. Training polygons in orange (n= 202) and validation polygons in red (n= 26)

SEDIMENT SAMPLE PROCESSING

Each sediment sample collected in the field was divided in two sub-samples, one used to determine mud fraction or fine particles contents (silt + clay) and the other to quantify organic matter contents. Sediment samples were dried for 48h at 60ºC and the initial dry mass was quantified (to the nearest 0.01mg). To determine the mud fraction (particles<63 µm dry weight/ total sample dry weight) of each sample (n = 228) we first used a sodium pyrophosphate solution (c= 30g/l) to disperse the sediment particles before wet sieving through a 63µm mesh. The remaining sample was dried for 120h at 60ºC. After this period, we measured the final dry mass and divided this by the initial dry mass (Quintino et al., 1989).

The organic contents of the sediment was measured in 80 samples. We calculated the difference between the initial dry mass of the sediment and the dry mass after ignition at 580ºC for 3 hours in a muffle furnace, dividing the result by the initial dry mass.

The fine-particle contents and the organic matter contents were highly correlated, as expected (r^2=0.90; n=80). Therefore, we chose to use only the fine particle fraction of the sediment on further analyses.

CLASSIFICATION OF THE INTERTIDAL AREA OF ADONGA

Inundation model and intertidal area delimitation

In order to delimitate the intertidal area, we built an inundation model following Catalão (2018). Firstly, 24 images of the study area, sensed by Sentinel-2 MSI, were downloaded from Copernicus Hub of the European Space Agency (site: https://scihub.copernicus.eu/). Areas were selected as to provide different phases of the tide process, i.e., tiles portraying different position of the water line in the tidal area. The tiles comprised the period between December 2017 and May 2018 and were constrained to have up to 3% of cloud cover. Afterwards, we estimated tide heights at time of capture of each image based on IH (2019). The reconstruction of the bathymetry was based on a methodology developed by Catalão (2018). The process started by stacking the images. The next step was to classify the area based on the Normalized Difference Water Index (NDWI) values of three pixel classes: water, land and intertidal. NDWI, defined by McFeeters (1996) is the most appropriated index for water bodies mapping (ESA, 2017c). It is calculated as:

$$NDWI = \frac{B03 - B08}{B03 + B08} \quad (1.1)$$

Where B03 corresponds to the green band, with wavelengths ranging between 0.537 and 0.582 µm and B08 corresponds to the near infra-red band, with wavelengths ranging between 0.767 and 0.908 µm (ESA, 2017c) Permanent water and dry soil pixels have a much lower temporal variability, since they represent still conditions, whereas the NDWI of intertidal areas change due to cyclic exposure and coverage of the area. Thus, pixels with high temporal variability were selected as the intertidal area. We selected all pixels with NDWI values between -0.05 and 0.15, which represent intertidal pixels. Then, a logistic regression was applied to each pixel using the NDWI values as independent variable and the corresponding tidal height at scene capture as dependent variable, in order to estimate the inflection

point (tidal height for NDWI=(max(NDWI)-min(NDWI))/2), which corresponds to the altitude value per pixel. We extracted those pixels and obtained a layer of the intertidal area of the Bijagós archipelago. Pixels with heights lower than 2.5 m were excluded as they are related to the presence of draining channels and the presence of superficial water can change the spectral signature of a class (Kwon et al., 2016).

Tile acquisition for the classification of the intertidal area

In this study, we resorted to Sentinel-2A MSI imagery. This sensor collects high-resolution information, containing a total of 13 spectral bands covering visible (2,3 and 4), red edge (5,6 and 7), near infrared (8 and 8A) and short-wave infrared (11 and 12) regions. The products used were classified as Level-2A, meaning that they provide orthorectified Bottom-Of-Atmosphere (BOA) reflectance, with sub-pixel multispectral registration (ESA, 2017a) and with a radiometric resolution of 12-bits, i.e., digital numbers have values between 0 and 4096. The tile was acquired from Copernicus Hub of the European Space Agency (site: https://scihub.copernicus.eu/). Tiles have a dimension of 100×100 km^2 and are projected in WGS84 (EPSG: 4326), being downloaded in GeoTiff format (Georeferenced Tagged Image File Format). The selection criteria were the sensing date – date similar to the fieldwork period (16/03/2019); the cloud cover percentage (0%) and the available image with the lowest tide height (approx. 1.3 m – estimated by IH (2019)). Figure 1.3 shows the coverage of the selected tile (tile code: T28PCT).

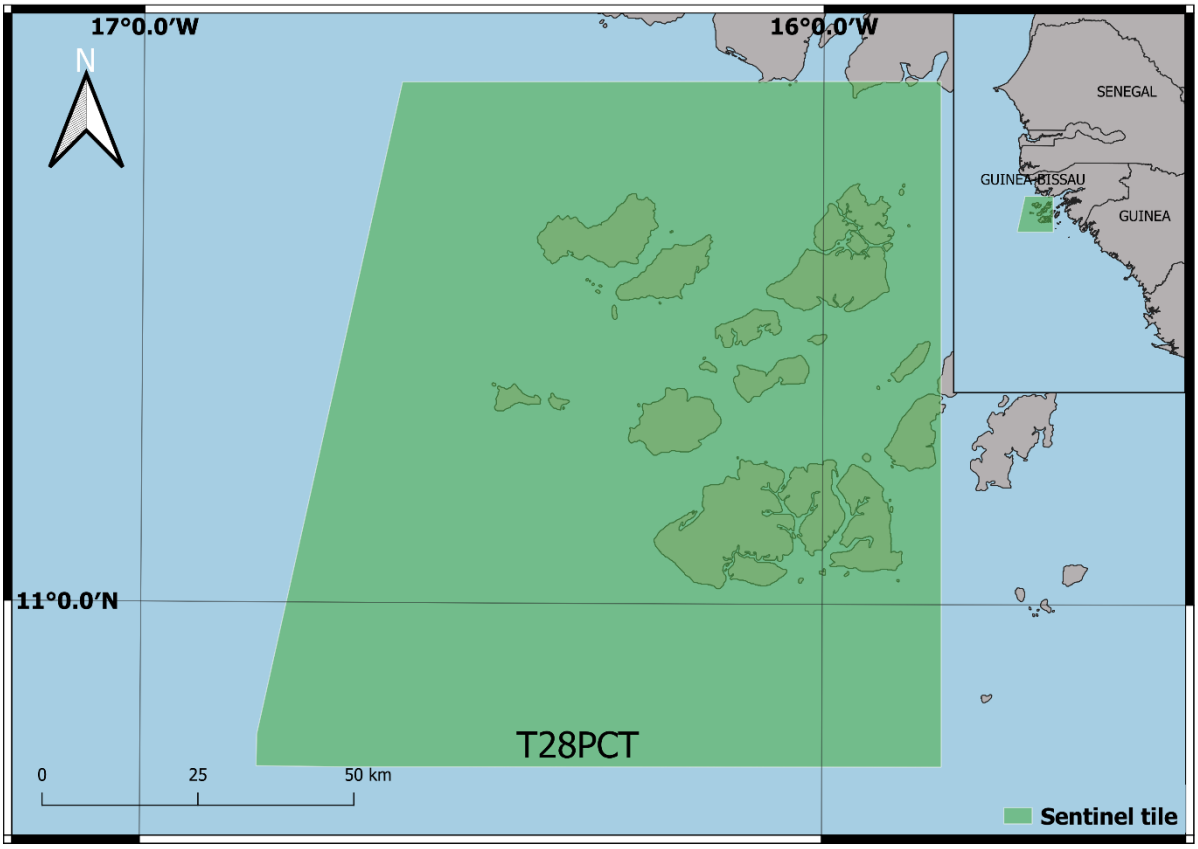

Figure 1.3. - Coverage of the used tile of Sentinel-2 MSI (Sentinel code: T28PCT)

Image pre-processing

After decompressing, the bands abovementioned were imported to Sentinel Application Platform (SNAP, v.6.0). All spectral bands with a resolution of 20 m were resampled to obtain a resolution of 10 m. We used the nearest neighbour resampling method. The reflectance values were divided by the quantification number (10 000) to obtain reflectance values per pixel (European Space Agency, 2019). Afterwards, we re-projected the all spectral bands into WGS84/ UTM zone 28N (EPSG: 32628). We stacked all spectral bands, obtaining a multi-spectral image, and then cropped the area containing the study region with ca 1000 ha (defined as Xmin= 387040.9 m, Xmax= 399262.9 m, Ymin= 1218359 m and Ymax= 1223248 m). Also, we stacked the inundation model to the multi-spectral image. Afterwards we calculated NDWI values for each pixel of the intertidal area of Adonga, obtaining a layer, and then we stacked it to the image abovementioned.

Definition of land cover/habitat classes

Several preliminary thresholds and methods were tested to find the best possible set of variables and classes that could be the subject of classification. We could not detect small variations in individual variables such as sediment grain-size, water coverage and fiddler-crab burrow area. We had to define thresholds for grain-size and fiddler crab burrow area, and then define habitat classes with these two classes as other collected environmental variables, such as superficial water, macroalgae and shell coverage, did not have enough representativeness in order to form new classes of habitat type. However, we calculated the mean values of these variables and associated them to each habitat class. For the definition of habitat classes using fine particles sediment contents, we followed the classification of sediment using mud contents when defining habitat types (after Folk et al., 1970, modified and re-drawn, Beninger & Paterson, 2018). Areas with a fine particle contents below 10% were considered to be sand and areas above this threshold were classified as muddy, therefore including muddy-sands (10 to 50%), sandy-muds (50 to 90%) and muds (90 to 100%). We established four classes based on mud fraction of the sediment (MF) and fiddler crab burrow area (FBA): *sand* (MF<10% and FBA<30%); *muddy* (MF>10% and FBA<30%); *sand-FBA* (MF<10% and FBA>30%) and *muddy-FBA* (MF>10% and FBA>30%), showed in figure 1.4. Thereafter, we built the spectral signature of each class using the mean reflectance value to each band. This allows us to identify which spectral bands or layers (e.g. the NDWI values layer, the inundation model layer) are more prone to be candidates for discriminating between classes.

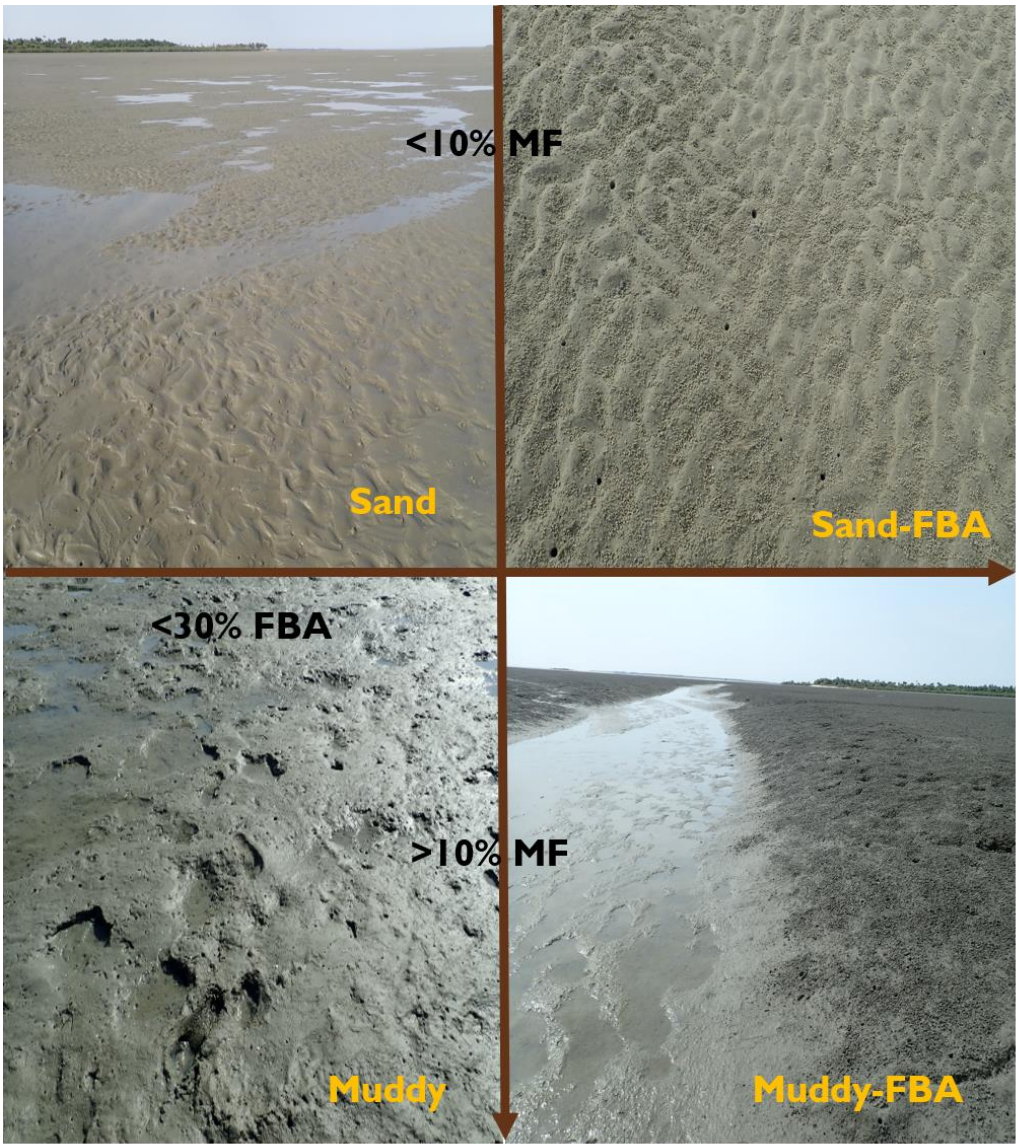

Figure 1.4 – The four types of habitat. The habitat type Sand had a value of mud fraction (MF) lower than 10% while the habitat type Muddy had a value of mud fraction higher than 10%. If one of the habitat types abovementioned had a cover percentage of fiddler-crab burrow area (FBA) higher than 30%, the habitat types were Sand-FBA and Muddy-FBA, respectively.

Training and validation samples

In order to perform a supervised classification of land cover/use, it is recommended to have different datasets for training the model and for assessing its accuracy (Wegmann et al., 2016). The number of validation pixels was selected based on the total number of pixels that were described in the field per class of habitat type. It is also recommended that each class has a similar proportion of validation pixels (Wegmann et al., 2016). Table 1.2. shows the number of total, training and validation pixels and the percentage of validation pixels, for each class of habitat type. Also, our validation and training sets were selected from different polygons defining the sampling polygons to minimise spatial autocorrelation.

Table 1.2 - Number of total, training and validation pixels for the different habitat types. Validation pixel percentage correspond to the ratio between validation and total number of pixels.

Habitat type	Total pixels	Training pixels	Validation pixels	Validation pixels percentage (%)
Sand-FBA	1898	1673	225	12
Sand	5146	4567	579	11
Muddy	2270	2006	264	12
Muddy-FBA	4358	3717	641	15
Total	13672	11963	1709	13

Supervised classification

Classification procedures were all performed using 'RStoolbox v 0.2.4' package (developed by Leutner et al., 2018) in R (v. 3.5.3). The intertidal sediment classification was performed using the ten spectral bands abovementioned stacked with the inundation model and the NDWI layer. In most cases, band-to-band correlation is very high, resulting from a lot of redundancy in the spectral signal (Wegmann et al., 2016). This can be a limitation as many statistic tests or models have difficulty to cope with high correlation between variables. Therefore, reducing the dimension and number of variables and transform them into uncorrelated variables can be useful. To accomplish this, we performed a Principal Component Analysis, using 'rasterPCA' of the package 'RStoolsbox', running in R (v. 3.5.3). We used as layers the first five principal components (PC), which explained 99% of the variability.

We used the 'RandomForest' algorithm (Breiman, 2001). This algorithm is considered to be highly efficient (Rodriguez-Galiano et al., 2012), showing low sensitivity to outliers, training sample size and imbalance (Chen et al., 2004; Na et al., 2010). The results achieved by the application of this algorithm are more accurate than the ones obtained by other algorithms, such as the Maximum likelihood (Attarchi & Gloaguen, 2014), and can be comparable to those obtained by neuronal networks (Khatami et al., 2016). We used the default options for the number of trees (*ntree*=500) and for the subset of variables used at each tree node (*mtry*).

We compared a classification using all defined habitat classes in one single step (method 2) with a stepwise classification (method 1). Before implementing the later procedure, we built the spectral signatures of each habitat class. Thereafter, we visually analysed which class had the most distinct spectral signature, as the higher proportion of the variability between classes is explained by this class. The class with the most distinct spectral signature was then separated from the remaining ones through a classification procedure, and later used to mask the intertidal area. We repeated this procedure to the other habitat classes, resulting in a three-step classification.

We converted all obtained classified rasters into shape files in order to build a landcover map, using QGIS (v. 3.6.1). We also classified the image using one step only – method 2 - to later compare the accuracy of both methods.

IMPORTANCE OF THE DIFFERENT LAYERS IN SEPARATING HABITAT CLASSES

When applying method 1, the most important layers in distinguishing classes were identified using the function 'importance' of the package 'RStoolbox'. This function measures the total decrease in node impurities (Mean Decrease in Gini) from splitting one variable, averaged over all trees (Han et al., 2016). The Mean Decrease in Gini is a measure of variable importance. The node impurity is measured by Gini index – Gini impurity. The Gini impurity is a metric used in decision trees that determines how to split the data into smaller groups, selecting which variable and which threshold will be used. The Mean Decrease in Gini is the average of a variable's total decrease in node impurity, weighted by the proportions of samples reaching that node in each individual decision tree in the random forest. A higher value of Mean Decrease in Gini indicates higher variable importance (Han et al., 2016).

ESTIMATION OF THE FINAL AREA OF THE DIFFERENT HABITAT CLASSES

We estimated the area occupied by each class within the intertidal area of Adonga by multiplying the number of classified pixels by the area of each pixel. We applied this methodology for both classification methods.

CLASSIFICATION ACCURACY ASSESSMENT FOR BOTH METHODS

There are several approaches to estimate the classification accuracy, although those based on the analysis of the confusion matrix are among the most recommended (Congalton, 1991). The overall accuracy can be misleading, and the assessment should be complemented with class-wise accuracies (Wegman et al., 2016). Hence, an analysis of accuracies between classes is crucial to understand which model has a better performance.

In our study we built confusion matrix in order to estimate the commission and omission errors, producer's and user´s accuracy, balanced accuracy of the classes and the overall accuracy and kappa coefficient (Congalton, 1991). Commission errors refer to those related with the incorrect inclusion of pixels of a certain class from classification errors of other classes. Omission errors refer to the error related to the exclusion of pixels that should belong to one class but were incorrectly assigned to other classes. The producer's accuracy is the probability of a pixel from a known class being classified as such. User's accuracy is the probability of the class attributed to a certain pixel correspond to the same class recorded in the field. Kappa coefficient is generated from a statistical test and it evaluates whether the classification results are better compared to just randomly assigned values. Kappa ranges between -1 to 1 and a value of 0 indicates that the classification is not better than a random classification. The balanced accuracy of a class is the result of the quotient of the sum of true positives and true negatives by the total number of pixels, while the overall accuracy is similar but using all classes. Every accuracy measure ranges between zero and one, with one indicating high accuracy. We used the same approach to assess the accuracy of method 2.

UNCERTAINTY ASSESSMENT FOR BOTH METHODS

Assessing the percentage of uncertain classified pixels and the spatial distribution of uncertainties can help to assess the reliability of a map (Wegmann et al., 2016). At each step of the classification, we classified the image using the 'superclass' function, changing the prediction type to 'prob'. This function gives the pixels uncertainty probability of correct classification, within the same class. Values near or equal to 1 show that the model is certain that one pixel belongs to the class assigned by the model. Values near or equal 0 show that the model is certain that one pixel does not belong to the

concerned class. Values near or equal to 0.5 show that the model is uncertain whether the pixel belongs to one or another class. To have a clearer view of which pixels were classified with more uncertainty, we extracted pixels with uncertainty probability ranging from 0.4 to 0.6, at each step. We then calculated the ratio between pixels with high uncertainty and the total number of pixels of each class for both methods.

COMPARISON OF CLASSIFICATION ACCURACIES BETWEEN METHODS

When assessing whether one model has a better performance than the other, one can focus on the overall accuracy or kappa coefficient. Models with higher values for these two parameters will be more accurate (Cingolani et al., 2004). However, a comparison between classes accuracies can show where are the major weaknesses of the different models (Wegmann et al., 2016). Despite differences being found between classes in corresponding accuracies, not every difference is statistically significant. An alternative approach is the McNemar test (Foody, 2004). This is a non-parametric test and it is grounded on correct and incorrect classes allocations. The McNemar test is based on the standarized normal test statistic (z-test). According to Foody (2004), the square of z-test follows a chi-square distribution, so the chi-square is equivalent to:

$$\chi^2 = \frac{(|b-c|)^2}{b+c} \tag{1.2}$$

Here, b is the sum of misclassified pixels from one model and c is the sum of misclassified pixels from another model. The chi-square distribution is continuous and therefore a correction for continuity is recommended (Dietterich, 1998; Rozenstein & Karnieli, 2011):

$$\chi^2 = \frac{(|b-c|-1)^2}{b+c} \tag{1.3}$$

We used equation 1.3 to evaluate if there were significant differences between the two methods in terms of the whole classification and class-wise accuracy.

REPEATABILITY OF BOTH METHODS

We applied the same methods to a different Sentinel 2 tile obtained 29 days later (in 15/04/2019) to assess the replicability of this approach using the same methodological approach.

RESULTS

The mean characteristics obtained in training polygons within each habitat type are presented in Table 1.3. *Muddy-FBA* areas had the highest mean mud fraction, followed by *Muddy* areas. In opposite, both *Sand-FBA* and *Sand* had the lowest mud fraction, as expected. As fine particle contents is known to be correlated with the organic matter contents of the sediment, the results of these two parameters were similar, with *Muddy-FBA* having the highest mean values. In terms of water coverage, *Muddy* areas had higher values, followed by *Sand* areas. *Muddy-FBA* and *Sand-FBA* areas had the lowest values. The areas with highest percentage of shell cover were *Muddy* ones, followed by *Sand*, *Sand-FBA* and *Muddy-FBA*, respectively. The drainage channels cover percentage was higher in *Muddy-FBA* and *Muddy* areas. The other two habitat classes had lower values. As expected, *Muddy-FBA* and *Sandy-FBA* had the highest percentages of fiddler crab burrow areas. Concerning the topography of the different areas, *Sand-FBA* areas had the highest mean height. *Sand* and *Muddy* areas had similar mean heights, while *Muddy-FBA* areas had the lowest mean height.

Table 1.3 - Mean characteristics of the sampled areas based on the 228 samples (Sand-FBA: n= 48; Sand: n=57; Muddy: n=69; Muddy-FBA: n= 54). The organic matter contents was estimated based on 80 samples (Sand-FBA: n=16 ; Sand: n=19 ; Muddy: 26; Muddy-FBA: n= 19

Habitat type	Mud fraction (%)	Water coverage (%)	Organic matter contents (%)	Shells coverage (%)	Channels coverage (%)	FBA coverage (%)	Height (m)
Sand-FBA	4.6±2.7	2.9±6.0	0.9±0.5	1.2±3.3	0.06±0.3	91.9±18.2	3.6±0.4
Sand	4.9±2.5	18.9±16.3	0.9±0.3	1.4±4.5	0.2±1.3	0.5±2.7	3.2±0.2
Muddy	26.4±19.7	29.1±21.5	2.7±1.2	2.4±4.6	1.3±2.5	1.1±4.1	3.1±0.2
Muddy-FBA	34.4±22.45	9.6±13.0	4.7±2.7	0.3±0.9	3.6±5.4	100±0	2.8±0.1

CLASSIFICATION OF THE INTERTIDAL AREA OF ADONGA

Figure 1.5. (on the left side) shows the difference between the mean spectral signature of different habitat cover. Figure 1.7. shows the supervised classification scheme, using method 1.

The steps of the classification were (see Fig 1.7.):

Step 1- distinguish *sand-FBA* from the other habitat types (*not sand-FBA)*, based on the spectral signature of these two habitat classes (Fig. 1.5., on the right side) and by using 1673 and 10290 pixels (Table 1.2), respectively. We obtained 2 layers of habitat classes: *sand-FBA* and *not sand-FBA* (Fig. 1.7).

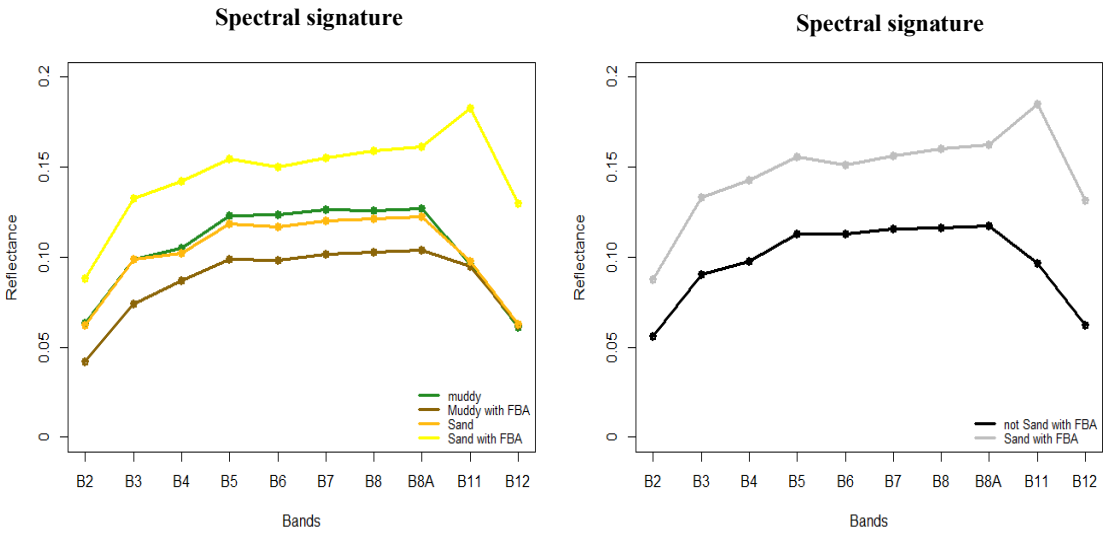

Figure 1.5 – The spectral signature of all habitat types: Sand-FBA, Sand, Muddy and Muddy-FBA (on the left side). Comparison between the spectral signature of the class Sand-FBA and the remaining habitat classes (on the right side).

Step 2 – discriminate *muddy-FBA* from the other types of habitats (*not muddy-FBA*), based on the spectral signature of these two habitat classes (Fig. 1.6, on the left side) and by using 3717 and 6573 pixels (Table 1.2), respectively. We obtained 2 layers of habitat classes: *muddy-FBA* and *not-muddy-FBA* (Fig. 1.7).

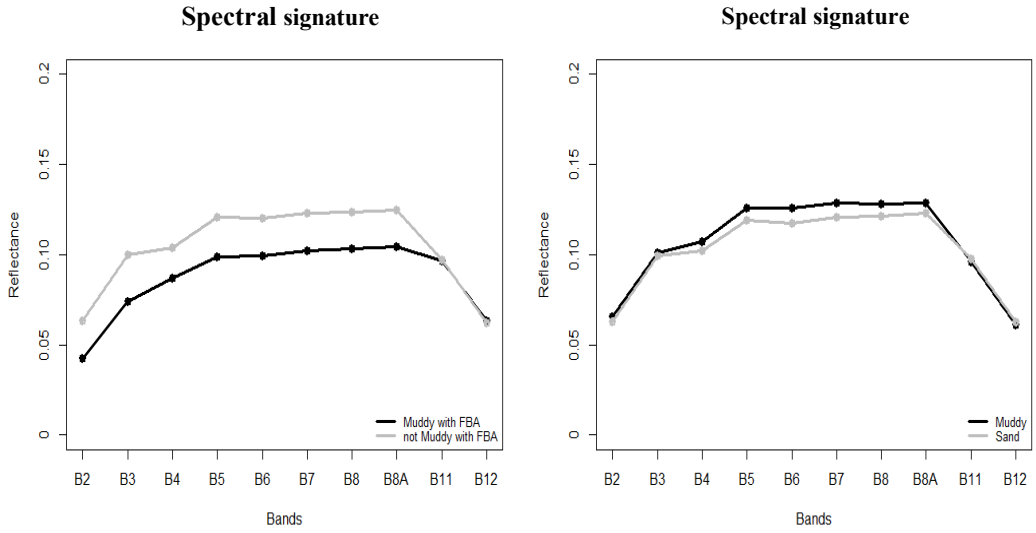

Figure 1.6- Comparison between the spectral signature of the class Muddy-FBA and the mean spectrum of the remaining habitat classes (on the left side). Comparison between the spectral signature of the class Muddy and of the class Sand (on the right side).

Step 3 – discriminate *muddy* from *sand,* based on the spectral signature of these two habitat classes (Fig. 1.6, on the right side) and by using 2006 and 4567 pixels (Table 1.2), respectively. We obtained two layers of habitat classes: *muddy* and *sand* (Fig. 1.7).

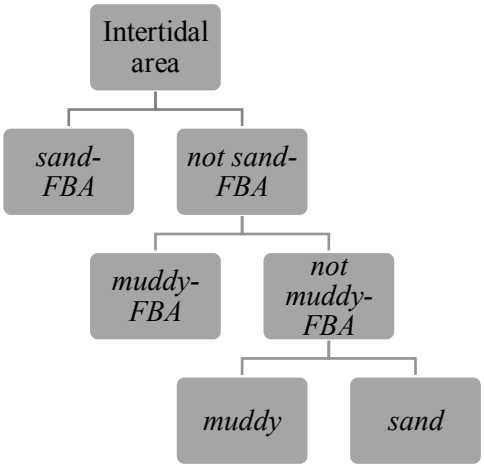

Figure 1.7- Classification steps. In each step, two classes are obtained: one corresponding to a defined habitat type and the other to the other defined habitats types.

The map obtained after the classification procedure of method 1 is displayed on figure 1.8. Areas with fiddler crabs are associated to the main and to secondary channels, while muddy and sand areas are located in the centre of the intertidal area.

Figure 1.8 - Classification output of method 1: Map of the intertidal habitats of Adonga. Classes are Sand-FBA, Sand, Muddy and Muddy-FBA.

IMPORTANCE OF THE DIFFERENT LAYERS IN SEPARATING HABITAT CLASSES

The habitat class *Sand-FBA* have a different spectral signature in the short-wave infra-red - B11 (1.538-1.681 μm) and B12 (2.072 – 2.312 μm) than the other habitats (Fig. 1.5, right side). In this region of the short-wave infrared (SWIR), reflectance values increase in *Sand-FBA* and decrease in the other classes of habitat type. In fact, in Table 1.4, one can verify that the SWIR region was the main responsible for distinguishing between these two classes, as B11 and B12 had the highest relative importance (score of 651 and 1264, respectively).

In step 2 (Fig. 1.6, left side), the main differences between *Muddy-FBA* and *not Muddy-FBA* concern the visible and near infra-red region. The green band B3 (0.573 – 0.582 μm) had the highest importance in separating these two classes, followed by PC2 (score of 2051 and 830, respectively, see Table 1.4).

The principal layers involved in discriminating *Muddy* and *Sand* classes were the red-edge bands B5 (0.694 – 0.714 μm), B6 (0.731-0.749 μm), B7 (0.783 – 0.796 μm) and PC3, with scores of 205, 224, 192 and 307, respectively (Table 1.4.).

The correlation of the principal components with the different spectral bands and the other layers are displayed on table 1 to 3 (Appendices), corresponding to step 1 to 3, respectively.

Table 1.4- Importance of different layers as measured by mean Gini index. Layers with higher values mean that those layers had higher importance in separating habitat classes

Layers	Step 1	Step 2	Step 3
Band 2	45	255	70
Band 3	53	**2051**	144
Band 4	101	57	182
Band 5	41	421	**205**
Band 6	32	53	**224**
Band 7	31	92	**192**
Band 8	24	65	158
Band 8A	28	41	152
Band 11	**652**	52	109
Band 12	**1265**	110	111
NDWI layer	59	22	186
Inund layer	62	191	173
PC1	203	22	113
PC2	59	**830**	106
PC3	68	215	**307**
PC4	146	64	125
PC5	39	154	155

ESTIMATION OF THE FINAL AREA OF THE DIFFERENT HABITAT CLASSES

The area occupied by the different habitat types (estimated by method 1) along the study site is given in Table 1.5. The total classified area covers approximately 1095 ha (109483 pixels). *Muddy-FBA* is the most widespread habitat type, followed by *Sand*. Habitats of *Sand-FBA* and *Muddy* have the

lowest total areas. The area of the habitat types estimated by method 2 is similar to method 1 (see Table 4, Appendices). The highest difference between methods was found for the habitat type *Sand* whose coverage decreased 2.2% from method 1 to method 2.

Table 1.5 -Number of classified pixels, total area and percentage of each habitat class of the intertidal area of Adonga, using method 1 (tile of 16/03/2019).

Land cover class	Number of pixels	Area (ha)	Percentage of each land cover area (%)
Sand-FBA	21506	215	19.6
Sand	31331	313	28.6
Muddy	18466	185	16.9
Muddy-FBA	38180	382	34.9
Total	109483	1095	100

CLASSIFICATION ACCURACY ASSESSMENT FOR BOTH METHODS

Method 1

The confusion matrix of the supervised classification using method 1 is presented on Table 1.6. The overall accuracy and the kappa coefficient had a value of 0.92 and 0.88, respectively. The class *Muddy-FBA* had the highest values for the balanced accuracy (0.99), producers' accuracy (0.99) and user's accuracy (0.97). The class *Muddy* had the lowest values for the balanced accuracy (0.89), producers' accuracy (0.80) and user's accuracy (0.86). The confusion matrix (Table 1.6) shows that the major limitation of the classification concerns the separation of the classes *Sand* and *Muddy*.

Table 1.6- Confusion matrix regarding method 1. Correct and incorrect classified pixels and derived performance statistics: Producers' accuracy and user's accuracy, omission and commission errors, overall accuracies, kappa coefficient and confidence interval.

Reference / Prediction	Sand- FBA	Sand	Muddy	Muddy-FBA	User's Accuracy	Commission error
Sand- FBA	204	9	1	0	0.95	0.05
Sand	21	519	51	3	0.87	0.13
Muddy	0	32	210	1	0.86	0.14
Muddy- FBA	0	19	2	637	0.97	0.03
Producer´s accuracy	0.91	0.90	0.80	0.99		
Omission error	0.09	0.10	0.20	0.01		
Balanced accuracy	0.95	0.92	0.89	0.99		
Overall accuracy: 0.92; Confidence interval: (0.90; 0.93); kappa:0.88						

Method 2

The confusion matrix of the supervised classification using method 2 is presented on Table 1.7. The overall accuracy and the kappa coefficient had a value of 0.90 and 0.86, respectively. The class *Muddy-FBA* had the highest values for the balanced accuracy (0.98), producers' accuracy (1) and user's accuracy (0.94). The class *Sand* had the lowest values for the balanced accuracy (0.88), producers' accuracy (0.88). The class *Sand-FBA* had the lowest users' accuracy (0.81). The major limitations are in the distinction between *Sand* and *Sand with FBA* and between *Sand* and *Muddy* (Table 1.7).

Table 1.7 - Confusion matrix regarding method 2. Correct and incorrect classified pixels and derived performance statistics: Producers' accuracy and user's accuracy, omission and commission errors, overall accuracies, kappa coefficient and confidence interval.

Reference / **Prediction**	**Sand-FBA**	**Sand**	**Muddy**	**Muddy- FBA**	**User's Accuracy**	**Comission error**
Sand-FBA	205	46	2	0	0.81	0.19
Sand	20	471	38	1	0.89	0.11
Muddy	0	25	220	0	0.90	0.10
Muddy-FBA	0	37	4	640	0.94	0.06
Producer´s accuracy	0.91	0.81	0.83	1		
Omission error	0.09	0.19	0.17	0		
Balanced accuracy	0.94	0.88	0.91	0.98		
Overall accuracy: 0.90; Confidence interval: (0.88; 0.91); kappa:0.86						

UNCERTAINTY ASSESSMENT FOR BOTH METHODS

The global uncertainty percentage was ca. 8% higher in method 2 than in method 1 (table 1.2). By observing the maps referent to method 1 (Fig. 1. Appendices), one notice that the major uncertainty appears in the borders of uniform areas, as they represent transition zones.

Table 1.8 - Number of uncertain pixels, number of classified pixels and ratio between these two parameters (percentage of uncertainty), for both methods

	Method 1	**Method 2**
Number of Classified pixels	109483	109483
Number of uncertain pixels ($0.4<p<0.6$)	20770	29797
Uncertainty (%)	19	27

COMPARISON OF THE CLASSIFICATION ACCURACIES BETWEEN METHODS

Both methods achieved high overall accuracies and kappa coefficients. Comparisons between the producer's and user's accuracy are graphically represented in figure 1.9 and 1.10, respectively. When applying method 1, the overall accuracy and the kappa coefficient were ca 2% and 3% higher, respectively. Producer's accuracy changed only slightly (Fig. 1.9). In the class *Sand*, method 1 showed better performance as it increased in approximately 9% when compared to method 2. For the

class *Muddy*, method 2 performed better as it increased the accuracy by 3%. The other two classes had a similar producer's accuracy (variations between methods were lower than 1%).

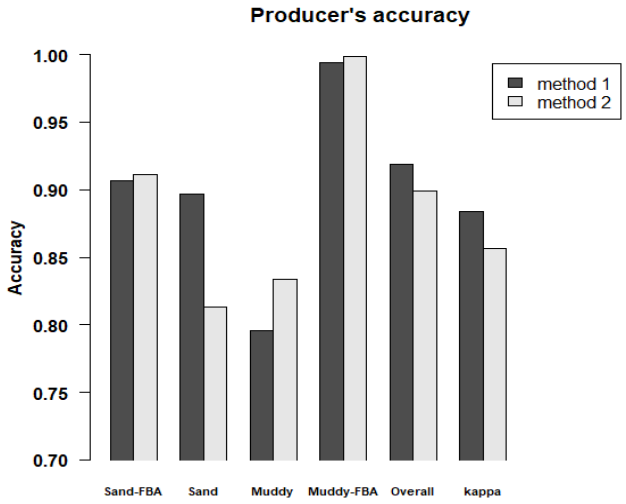

Figure 1.9 - Comparison between methods of the producer's accuracy of the four habitat classes, the overall accuracy and kapa coefficient.

User's accuracy of the class *Sand-FBA* had an increase of 14% in method 1 when compared to method 2. This also increased in the class *Muddy- FBA* by about 3 %. Method 2 had better accuracy in the classes *Sand* and *Muddy*, with an increment of 2 and 4%, respectively (Fig. 1.10).

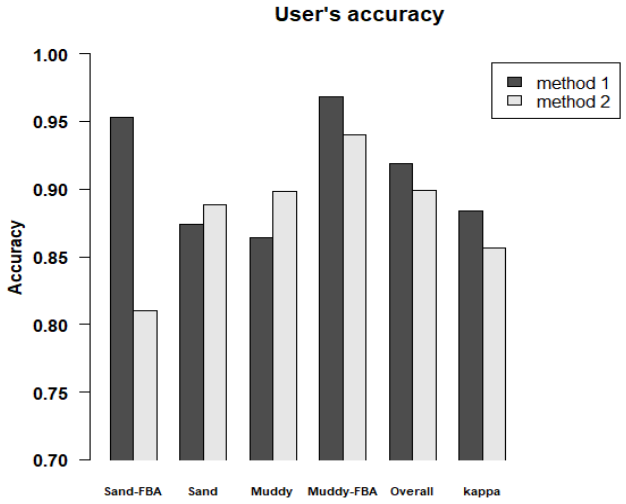

Figure 1.10- Comparison between methods of the user's accuracy of the four habitat classes, the overall accuracy and kapa coefficient.

We also assessed if the differences between methods were statistically significant, by applying the McNemar's test (see methods). Differences between the whole classification were not significant. Among classes, there were also no significant differences, except for *Sand-FBA*. The classification of this class was significantly better in method 1 (χ^2=13.1; p< 0.001).

REPEATABILITY OF THE METHODS

Both methods were highly accurate when applied to another image (15/04/2019). The accuracies were similar between the different dates (Table 5, Appendices). When applying method 1 to the second image, the overall accuracy was 91% and with method 2 was 90%. The areas of the different habitats, using the second tile (15/04/2019) estimated by method 1 and 2 are displayed on table 6 and 7 (Appendices), respectively. The proportion occupied by the different habitat types are similar. The highest difference recorded refers to the class *Sand* that had a decrease in 3.4% from method 1 to method 2. When comparing the results obtained by the application of method 1 in the two different tiles, the highest recorded variation was for the class *Muddy-FBA*, with a decrease of 2.8% from the tile of 16/03/2019 to the tile of 15/04/2019. In the case of method 2, the highest difference corresponded to the same habitat class (*Muddy-FBA*), with a decrease of 1.8% from the tile of 16/03/2019 to the tile of 15/04/2019.

DISCUSSION

Our results suggest that both classification methods used were highly capable of producing excellent results, with highly accurate classification for the different parameters, even in stringent validation condition (i.e., using pixels from polygons not used for training the models). This result is mainly due to a careful definition of the training and validation areas, which were selected to include only relatively homogeneous patches, and also to a collection of variables known to affect the spectral signature of intertidal sediments. This study adds to the growing evidence that Sentinel tiles deliver important improvement in classification efficiency over Landsat scenes, due to its higher spatial resolution of the and to the increased radiometric resolution.

Fiddler crab areas are widespread in our study area, occupying more than 50% of the total area and the area of mud (mud fraction > 10%) is similar to that of sand (mud fraction < 10 %). Both these observations are in agreement with the description of Zwarts (1988) for the whole archipelago.

COMPARISON BETWEEN AREAS OCCUPIED BY HABITAT TYPES USING DIFFERENT METHODS AND DIFFERENT TILES

When comparing the areas calculated using both methods, we could not find notable variations between the areas of the different habitats. Also, between different tiles, there were no major alterations. This can indicate that habitat areas did not change in one-month interval and that our method can be replicated with success, as it identified well our main habitat types in two different dates. However, to further monitor alterations, one should use the spectral signatures described above, instead of using the same sampling polygons, as intertidal areas change through the years and our sampling polygons were defined based on the date of our fieldwork.

COMPARISON OF CLASSIFICATION ACCURACIES BETWEEN BOTH METHODS

The differences between the two methods were in general low. Yet, method 1 allowed for a better identification of the differences in the spectral signature of different classes. Usually, classes with distinct spectral signature will be well identified by both methods, e.g. *Muddy-FBA*. Although, the class accuracy for *Sandy-FBA* was significantly higher in method 1. This is a consequence of higher confusion between *Sand-FBA* and *Sand* in method 2. Both methods presented higher confusion problems in distinguishing between *Muddy* and *Sand* areas, as these two habitat classes have very similar spectral signatures. Consequently, if we expand the variability between two classes only, e.g. using a Principal Component analysis, we can focus on the variables that allow better discrimination between classes.

The first method had a lower number of uncertain classified pixels. Classification uncertainty analysis can be a major help in evaluating the value of a map as well as its shortcomings (Wegmann et al., 2016). However, to do more accurately comparisons between uncertainties of both methods, one should focus on the uncertainties found in transition zones, i.e., the border zones of major habitat patches as these areas are often more difficult to accurately classify (Thomson et al., 2003).

We think that method 1 can have a better performance as it allowed to better discriminate between the habitat types *Sand-FBA* and *Sand*, and in general, had higher accuracies despite some of

them not being statistically significant. Also, this method allows a better understanding of the main variables that are distinguishing the different habitat types, as one can focus on the bands or layers that were critical for the classification of such habitat types.

IMPORTANCE OF THE DIFFERENT LAYERS AND VARIABLES IN SEPARATING HABITAT CLASSES

The analysis of the spectral signature of *sand-FBA* sites shows that the bands in the SWIR region have a different spectral signature from the other habitat classes. The reflectance of wavelengths in the SWIR region - B11 (1.538-1.681 μm) and B12 (2.072 – 2.312 μm) - is related to the water contents of the soil (Lobell & Asner, 2002) and this was the principal variable separating this class from the remaining ones. Although we did not estimate the water contents of the sediment due to lack of equipment, we estimated the surface water coverage. Kwon et al. (2016) showed that there is a linear relationship between the decline of the reflectance in the SWIR region and the increase of the water contents of the sediment. In fact, these authors established a relationship between the surface water and the interstitial water, where they argue that if the superficial water exceeds 35%, then the sediment is oversaturated. They also refer that the increase of the water contents of the sediment is positively related to the superficial water coverage. By consulting table 1.3, one can observe that *Sand-FBA* sites have the lowest mean superficial water cover (2.9 ± 6.0) and therefore, probably the lowest water contents.

The visible colour, superficial water coverage and the mean height were the main factors discriminating the class *Muddy-FBA* from the remaining ones. Areas of *Muddy-FBA* show lower reflectance values for the wavelengths in the visible, red-edge and near-infrared regions, which agrees with the fact that they are much darker than the other habitat types. This can be a result of the pseudo faeces produced by fiddler crab while feeding, as well as due to the small balls of mud resulting from burrow excavation. Hence, the green band B3 (0.537-0.582 μm) band played a major role in separating this class from the remaining ones, as darker objects reflect less radiation. PC 2 is correlated with NDWI values which are higher in pixels in the water areas (Catalão, 2018). PC 2 is also correlated with the visible bands and with the inundation layer (table 2, in annexes), and the mean height of muddy-FBA areas is lower than the other classes (table 1.3). *Muddy* and *sand* areas have higher superficial water coverage than *muddy-FBA* (see table 1.3).

Muddy and *Sand* classes were the classes with lower accuracy metrics in the final classification. The difficulties in this process are a result of the water coverage of both types of sediments (Ryu et al., 2004; Kwon et al., 2014) and often, of a thin layer of mud covering sandy areas (Yates et al., 1993). Despite this, the achieved result was overall positive, as these two classes had high overall accuracies values of 92% (*Sand)* and 89% (*Muddy*). The principal discriminant layers were PC3, the bands in the red-edge (B5 (0.694 – 0.714 μm), B6 (0.731-0.749 μm), B7 (0.783 – 0.796 μm)) and the NDWI layer. PC3 is negatively correlated with the inundation layer, B12 and B11. Muddy areas have lower mean heights than sandy ones (table 1.3). Also, muddy areas have higher superficial water coverage than sandy areas (table 1.3) and therefore higher water contents (Kwon et al., 2014). Hence, the correlation between PC3 and the SWIR bands shows that muddy areas contain more moisture than sandy ones. The NDWI layer was also important due to differences in the cover of superficial water. Muddy areas have more organic matter contents than sandy areas (table 1.3). It is known that the Chlorophyll-a reflects wavelengths between 700 and 750 nm (Seager et al., 2005) and the red-edge region of Sentinel-2 bands is located between that interval. Our muddy areas have a higher reflectance in that region, meaning they have more chlorophyll-a contents than sandy areas. Organic matter was a major factor discriminating those two classes, as well as the topography and the water contents of the substrate.

Despite not using the water coverage to form habitat classes, we think that our methodology, i.e., the incorporation of the NDWI values for each pixel, the usage of the short-wave infra-red bands and the principal component analysis, was successful in overcoming this major difficulty in separating habitat classes, as water coverage can cause similarities in the spectral signature of different sediments (Kwon et al., 2016).

LIMITATIONS

Despite the positive results, the number of classes was not very high, and, in some cases, the limits were too wide. Muddy areas comprise a wide range of fine particles contents (encompassing muddy-sand, sandy-mud and mud). However, the intermediate classes between mud and sand – muddy sand and sandy mud - are often difficult to classify consistently (Thomson, 2003). According to this author, this discrimination can be one major difficulty when mapping intertidal sediments as these areas comprise the transition between the two main classes. These types of areas may be also temporally inconstant as the thin coverage of fine sediment can rapidly change due to extreme tides or storm events (Thomson. 2003). In our study, we had a low number of samples from sandy-mud (50-90% of MF) and mud (90-100% of MF) areas, as the intertidal sediment of the Bijagós archipelago is mainly composed by muddy-sand (Zwarts, 1988). Therefore, we had to group all classes of sediment above 10%, in one single class. We also tried to differentiate more sediment classes based on the other collected features. However, they did not have a reasonable balance to form representative classes.

To avoid spatial autocorrelation between training and validation pixels, the later ones should not belong to the same polygons used for training the model and the locations of both sets of polygons should be spatially separated (Wegmann et al., 2016). Despite meeting the first criteria, our datasets were not completely independent as validation polygons were sampled in similar zones of training ones. This is the result of lack of sampling time and the fact that we defined training areas in major habitat patches. Hence, some of the validation areas were within these patches, meaning our datasets may have some spatial autocorrelation.

ECOLOGICAL IMPORTANCE OF THIS WORK

Intertidal areas of the Bijagós archipelago are extremely important to a large proportion of the East Atlantic Flyway wintering shorebirds (Zwarts et al., 1988; Dodman & Sá. 2005). Given that shorebirds are known to select different habitats within intertidal flats (Lunardi et al., 2012), mapping such habitats is critical to predict shorebird distribution.

The fiddler crab *Afruca tangeri* is widespread in the intertidal flats of the Bijagós archipelago (Zwarts, 1985). They are a key element of the ecosystem, as they model the occurrence patterns of several faunal groups within these flats, such as macroinvertebrates and foraging shorebirds (Paulino, 2019). Our work allowed us to clearly identify and map areas with high densities of fiddler crabs, using Sentinel-2 MSI imagery. This is an excellent result and to our knowledge, no studies have achieved this. These results can potentially be used to predict the spatial distribution of shorebirds and macroinvertebrates, which is of great importance, as populations of shorebirds are declining at a global scale (Thomas et al., 2006; Wilson et al., 2011; Moores et al., 2016; Studds et al., 2017). The repeatability of the method proved to be high when using two different images with a one-month interval. This suggests that our method is consistent and if we extract the spectral signatures of our habitat classes, our method may probably be used to monitor alterations in the intertidal habitats.

FINAL CONCLUSIONS

It is difficult to accurately classify intertidal areas in estuarine habitats, as there are several difficulties in discriminating different spectral signatures of the sediments existing there. The present study represents a relevant contribution to the classification of intertidal habitats in the Bijagós archipelago, as we achieved high accuracies for each sediment class. Another contribution of these work is referent to understanding which environmental variables allow better discrimination between classes. One of the possible applications of our work is the modelling of shorebirds occurrence inside and outside high-density fiddler crab areas, as the distribution of this crab is known to affect the distribution of foraging shorebirds. Also, it can be used to monitor changes in intertidal habitats over the years. This is of extreme importance as these areas are decreasing at a global level due to land-reclamation and sea level rise (Murray et al., 2019). However, to expand this exercise to the whole archipelago, further work is needed, mainly because the examination of the entire Sentinel tile indicated that the intertidal area of Adonga islet did not comprise the whole variability found in the tidal flats of the archipelago.

Chapter 2: MAPPING THE DISTRIBUTION OF FORAGING SHOREBIRDS REGARDING TO ENVIRONMENTAL VARIABLES, IN THE MUDFLATS OF THE BIJAGÓS ARCHIPELAGO

Abstract: Shorebird populations are threatened at a global scale, representing a matter of international concern. Foraging shorebird distributions at low tide may depend on macroinvertebrate abundances. However, this information is difficult to obtain at medium/large geographic scales. An alternative approach is to assess environmental factors affecting macroinvertebrate abundances and relate them to shorebird abundances. In this study, we investigate the biotic and abiotic variables driving foraging shorebird distributions in the Bijagós archipelago, an important East Atlantic Flyway non-breeding area. This allowed mapping important foraging areas for shorebird species on an important mudflat. To achieve this, we (1) counted shorebirds in 67 plots during low tide, (2) collected biotic and abiotic data within the counted plots, and (3) used species distribution models (GAMs) to test which variables can better explain the variations in shorebird occurrences (n=11 species) and abundances (n=7 species) throughout the sampling plots. The most significant predictors were the exposure period, mud fraction, fiddler crab burrow area, distance to mangrove patches (m) and distance to channels/creeks. GAMs offered accurate occurrence predictions and interpretable shorebird-habitat relationships. Overall explained deviances reached high values (e.g. abundance of whimbrels had 60% of its deviance explained). The best predictors for shorebird distributions were used to classify the intertidal area using remote sensing techniques (Sentinel-2A), and suggested predictions for shorebird distributions within the study area. This work can be expanded to the whole Bijagós archipelago, providing an important tool to identify priority areas and to inform conservation actions.

Key-words: Bijagós archipelago, generalized additive models, predictive maps, Sentinel-2A, shorebirds

INTRODUCTION

Shorebird populations are threatened at a global scale, representing a matter of international conservation concern (Russi et al. 2013; IUCN, 2019). Major population declines have been reported for several species worldwide (Thomas et al., 2006; Wilson et al., 2011; Moores et al., 2016; Studds et al., 2017). The main causes for population declines are related to direct impacts of human activities on estuarine areas, such as industrial development or sediment dredging (Goss-Custard & Yates, 1992; Cayford, 1993; Day Jr et al., 2013), and associated to the threat of sea-level rise as a result of global climate change (Watkinson et al., 2004; Galbraith et al., 2002). These threats ultimately result in habitat loss and degradation for shorebirds, as they depend on the invertebrate prey (e.g. polychaetes, bivalves and crustaceans) found on estuarine mudflats during the migratory and the non-breeding periods (Delany et al., 2009).

Patterns of macroinvertebrate distribution are known to drive the patterns of shorebirds occurrence in intertidal flats at low tide (Bryant, 1979; Yates et al., 1993; Stillman et al., 2005; Folmer & Piersma, 2012; Lourenço et al., 2005, 2017; Ponsero et al., 2016). This relationship can be found across all scales: from tens of square kilometres (Bryant et al., 1979; Yates et al., 1993) down to hundreds of square meters (Goss-Custard, 1970). However, predicting the distribution of feeding shorebirds based on prey distribution over medium/large areas is difficult to accomplish as it requires a huge sampling effort and complex logistics (Granadeiro et al., 2004). An alternative approach is to measure habitat features that explain the spatial distribution of macroinvertebrates which in turn, explain shorebird distribution patterns in feeding areas (Yates et al., 1993). Macroinvertebrates are distributed through intertidal gradients, according to their ability to cope with physical factors (e.g. desiccation, grain size) and biotic factors and biological processes (e.g. food availability, competition; Rafaelli & Hawkins, 1999; Gibson et al., 2001). This biological response is referred to habitat selection that leads to zonation. The sediment exposure period is a major constraint to macroinvertebrate distribution (Choi et al., 2014; Ponsero et al., 2016), as invertebrates tend to concentrate in areas where the stress to environmental conditions is relatively low and/or the submersion period is long enough to meet their energetic requirements (Peterson, 1991; Beninger & Paterson, 2018). Also, invertebrates are distributed according to the grain-size gradient, since different types of sediment provide suitable habitats for different species (Peterson, 1991; Yates et al., 1993; Ponsero et al., 2016). The distance to channels/creeks is also an important factor in explaining the biomass of invertebrate prey (Lourenço et al., 2005). These authors showed that despite the similarity of sediment features, macroinvertebrate biomass increases with the proximity to drainage channels.

Several studies tested different environmental variables in order to describe and predict shorebird spatial distribution. Sediment fine particle contents (Granadeiro et al., 2004; Granadeiro et al., 2007; Lunardi et al., 2012) and time of exposure (Burger et al., 1977; Colwell, 1993; Granadeiro et al., 2007; Calle et al., 2018) are among the most relevant predictors of shorebird distribution in foraging areas. The presence of shell banks and macrophyte algae was also referred to as a relevant factor for some species of shorebirds (Granadeiro et al., 2007). As previously referred, proximity to drainage channels is also relevant as invertebrate biomass tends to be higher (Lourenço et al., 2005) and these areas require less effort to probe and therefore increases the access to prey (Miller & de Rivera 2014). Predation risk is also a factor very influential when shorebirds have to decide the best areas to forage (Page & Whitacre, 1975; Folmer & Priesma, 2012). Yasué et al. (2006) concluded that shorebirds would prefer areas far from the forest canopy, as these areas can harbour higher numbers of predators.

Sound knowledge on the set of variables driving shorebird distribution is essential for conservation planning of wetlands, both at a local and a regional scale (Granadeiro et al., 2007). To assess shorebird distribution, the most common method used is visual counts (e.g. Zwarts et al., 1988; Yates et al., 1993; Ponsero et al., 2016). The link between bird counts and environmental variables can then be assessed by species distribution models (Wegmann et al., 2016). These models are not only widely used in scientific literature, but also in guiding conservation decisions, for example in identifying and protecting critical habitats (Guisan et al., 2013). Generalized additive models – GAM (Hastie and Tibshirani, 1990) have been used to model shorebirds occurrence (Granadeiro et al., 2004). They perform better than generalized linear models, as they allow to increase the response flexibility and to incorporate non-linear terms (Granadeiro et al., 2004).

The Bijagós archipelago is located off the coast of Guinea-Bissau (11º52' N, 15º 36' W) and it is one of the most important African sites along the East Atlantic Flyway (EAF; Fig. 2.1) for shorebirds (Dodman & Sá, 2005). The islands of the Bijagós support annually between 700000 and 900000 shorebirds during the non-breeding period (Zwarts et al., 1988; Dodman & Sá, 2005). The intertidal area of Bijagós archipelago extends over 140000 ha of mud and sand flats, 35000 ha of which are covered by mangroves (Campedron & Catry, 2016). Most of the tidal flats are composed of mixed sediments and surrounded by dense mangrove areas (Zwarts, 1988). These flats contain low macroinvertebrate biomass (Zwarts, 1985; Lourenço et al., 2017). However, the fiddler crab *Afruca tangeri* (Eidux, 1835) is widespread in the mudflats of this archipelago and acts as a key element in the diet of some shorebird species occurring there (Lourenço, et al., 2017).

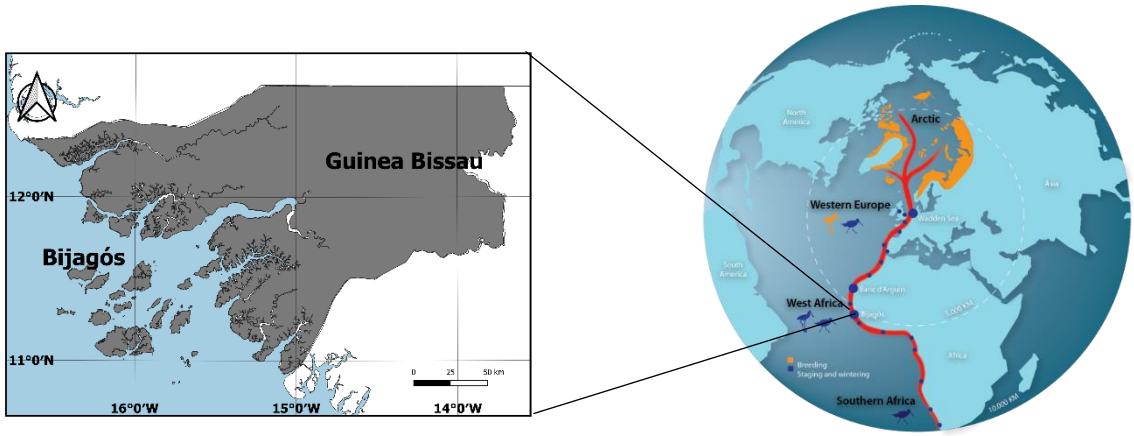

Figure 2.1 - Representation of the East Atlantic Flyway of Wadden Sea Flyway Initiative (WSFI, 2015) , on the right side, and the location of Guinea-Bissau and the Bijagós archipelago (left side) along the EAF

In this study, we aim to determine which are the biotic and abiotic variables explaining the distribution of shorebirds in their foraging areas in the Bijagos archipelago, to map their foraging distribution, regarding those variables.

METHODS

STUDY AREA

Fieldwork took place in an extensive intertidal flat in south part of Orango National Park, which comprises an area of roughly 1000 ha (Fig. 2.2.). Flats are surrounded by mangroves with a thin sandbank that acts as a barrier. The study area is characterized by a semi-diurnal tidal regime, where the tidal amplitude varies approximately 3m during neap tides and approximately 4.5m during spring tides (estimated from Instituto Hidrográfico da marinha portuguesa – IH, 2019).

SHOREBIRD COUNTS

We defined 67 counting plots (mostly within a 250*250 m grid) that were spread over the study area, in order to capture the maximum variability of conditions (Fig. 2.2.). In some areas, the limits of these plots had to be rearranged, to avoid the inclusion of land or water. The number of shorebirds of each species was counted during 19 field visits carried out between 7 February 2019 and 22 March 2019. Each plot was counted at least in two different days.

During each visit and in each plot, we performed 1-7 counts separated by 1 hour within +/- 3 h from low tide peak. The counts were performed by 3 observers, using 20-60x zoom telescopes and only under favourable weather conditions. At low tide, only some areas could be counted from the shoreline. To sample all other areas, we arrived (by boat) at the centre of the counting area between 4 and 3,5 hours before low tide peak, to avoid potential effects of disturbance in shorebirds occurrence and abundance. However, our presence in the area might have influenced the occurrence of some shorebird species, but whenever we noticed major alterations, we discarded that count. Also, we stopped our counts if all birds flew again from the plot, due to some sort of disturbance (e.g. presence of a raptor). Prior to the counts, we estimated the percentage of available foraging area for shorebird (i.e., the area of each plot that was not covered by water) and the percentage of this area covered by fiddler-crab burrows. In each count, we recorded the number of birds feeding and resting in areas with and without fiddler-crab burrows.

ABIOTIC AND BIOTIC VARIABLES IN COUNTING PLOTS

In each counting plot, we visually estimated the percentage cover of different types of habitats in terms of sediment granulometry: sand, muddy-sand, sandy-mud and mud. Also, within each habitat type, we estimated the percentage coverage of fiddler crab burrowing area (FBA), superficial water, macroalgae, shells and drainage channels. To assess the fraction of fine sediments (<0.063mm) and the organic matter of the sediment, we followed the procedures explained in Chapter 1 (see Methods, "Sediment sampling processing", page 10). We averaged all replicates of measurements made within each habitat type and then multiplied each collected variable value by the proportion of each habitat type, to obtain a final value per plot.

Using QGIS (v 3.6.1), we calculated the distances from the centroid of every plot to the limit of the nearest mangrove area, sandbank (as a proxy to the possible roost areas) and channel/creek, which were digitized from a satellite scene (see Chapter 1). To assess the exposure period of each plot, first we used heights previously estimated (see Chapter 1, Methods, "Intertidal area classification", Page 11). Using every pixel within a counting plot, we calculated the mean height of each plot. Afterwards, the exposure period (in hours) of each plot was estimated using the following equation (Hickey, 2019):

$$exp.P = 2 \times \pi - cos\left(2 \times \frac{(H - LW)}{(HW - LW)} - 1\right) \quad (2.1)$$

where exp.P is the exposure period of a plot in hours, LW(m) and HW(m) are the lowest and highest tide heights recorded on that tide cycle and H (m) is the mean height of each plot. Counts were carried out in different days and therefore each the exposition period associated with a given plot results from the mean of all counting days.

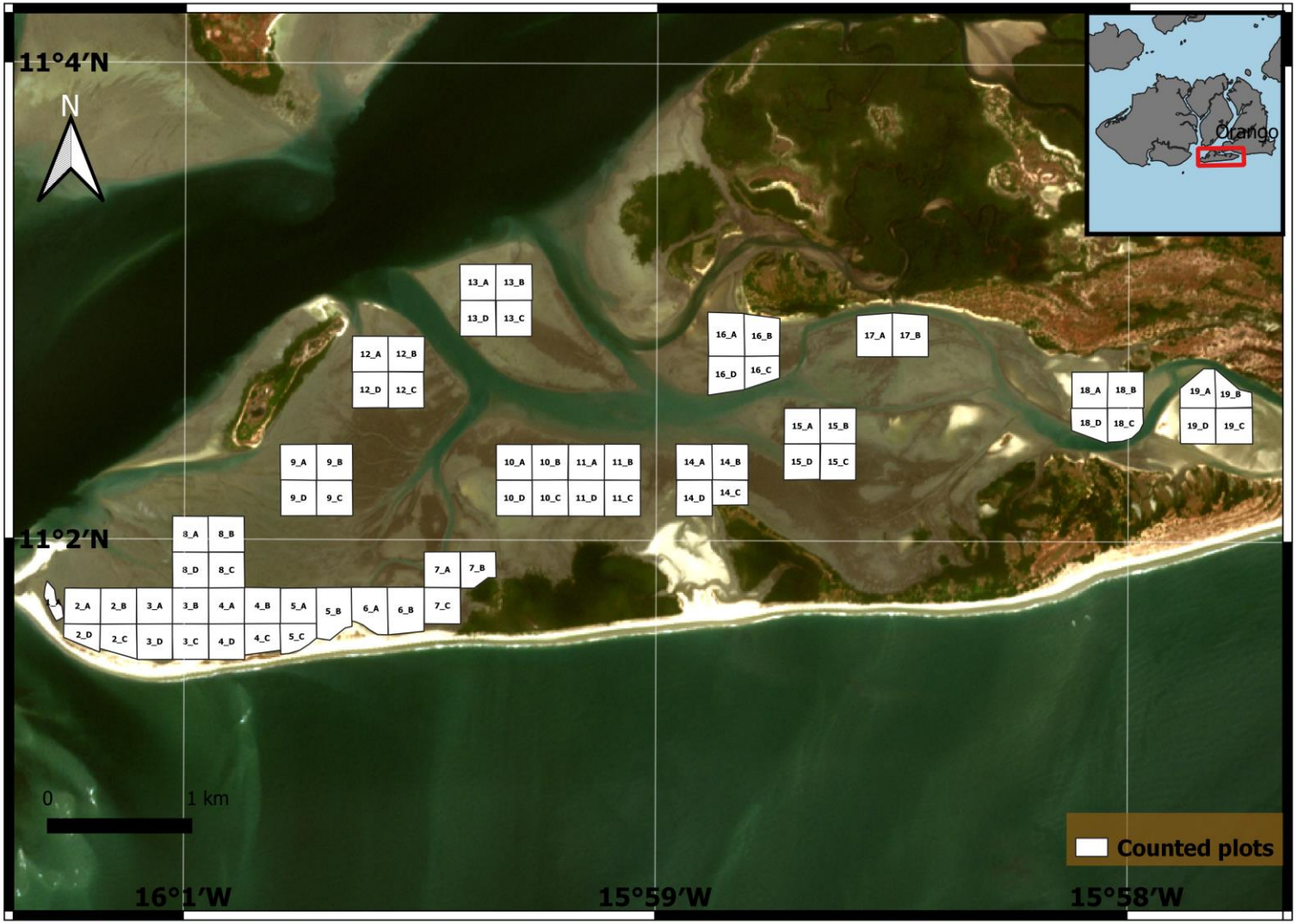

Figure 2.2- Study area: Adonga islet, part of the Orango National Park, and the counting plots (n=67)

DATA ANALYSIS

We only considered species with mean frequency of occurrence higher than 30% (n= 12 species). For each selected shorebird species, we modelled the relationship between presence/absence and the physical characteristics of the area where they occur. We did the same for species densities (only in species with mean densities above 0,5 individuals per hectare, 7 species). However, the mean frequency of occurrence of the Whimbrel *Numenius phaeopus* was higher than 90% (see table 2.1.), compromising the models of occurrence, and therefore we just used the abundances for this species. We selected only counts within +/- 2 h from the low tide peak, constrained to have an available area above 50%. Afterwards, we calculated the mean and the occurrence frequency between the counts of the two sampling days, resulting in between 8-10 counts per plot.

Previous studies focusing in describing habitat selection by shorebirds suggested that species show a non-linear nor monotonic response along the gradients found in intertidal areas (e.g. Yates et al., 1996; Austin, 1999; Granadeiro et al., 2004). Therefore, we used generalized additive models (GAMs), as it increases its flexibility (Granadeiro et al., 2004). Hence, a more flexible framework can produce more realistic and informative results.

The general form of a GAM is

$$E(y) = g^{-1} \times \left(\beta_0 + \sum_k s_k(x_k) \right) \tag{2.2}$$

where s(k) represents a one-dimensional smooth function of the predictors. A GAM is a general linear model with a linear predictor involving smooth functions of covariates (Marra & Wood, 2011). GAMs are considered to be semi-parametric models as they can model non-parametric terms, but the probability distribution of the response variable has to be specified (Guisan et al., 2002).

The selection of an appropriate level of "smoother" for a predictor is a critical step when applying a GAM (Guisan et al., 2002) and this selection should be based on a trade-off between fitting the data and avoiding unnecessary detail. This can be achieved by specifying the effective degrees of freedom (edf) of the splines and the choice of edf should maintain a reasonable balance between the total number of observations and the expected relationship between the response variable and the covariates (Granadeiro et al., 2004).

We modelled the presence/absence of selected species using GAMs with a binomial error structure, with logit as the link function, while for abundances, we used GAMs with a negative binomial error structure, as in all cases the data had overdispersion, and using a logarithmic link function. The predictors are listed in table 2.2. For every model, we used the area of each counted plot as an *offset*. The smoothers used in our models were penalised thin-plate splines with a modification of the smoothing penalty, so that the null space is also penalised, and the term can be shrunk to zero. This means that the level of smoothness can be downgraded to the point where the predictor is simply linear. Model fitting was carried out by using tools available in the package 'mgcv' running in R (developed by Wood, 2000, 2003). This package uses generalised cross-validation (GCV) to automatically select the smoothing parameters of each smoothing term. The GCV score provides a measure of the overall

balance between the gains in increasing the amount of smoothing and the costs of increasing or decreasing the number of degrees of freedom. We set knot values (k=edf+1) at a maximum of four to allow some flexibility of the response and to avoid over-fitting the data (Granadeiro et al., 2004) and the fitting procedure then downgrades them to minimise the GCV score of the whole model.

A high correlation between independent variables can be a concern when developing a model, as two correlated variables can explain less of the final model deviance than when used individually (Guisan et al., 2002). Therefore, we first build a correlation matrix and variables showing Pearson coefficients above 0.7 were excluded. The remaining variables were selected as candidate variables.

We used classification and regression trees in a complementary way to GAMs as they can be an accurate approach to identify the most influential predictors (following Guisan et al., 2002). We used the package 'party' (developed by Hothorn, et al., 2006) in R, which includes the function 'cforest' (Hothorn et al., 2006; Strobl et al., 2007; 2008). We used the candidate variables as an input to the classification tree. Classification trees are a nonparametric and highly nonlinear method. They are robust to outliers, invariant to monotonic transformations of numerical predictors and can also handle missing values (Strobl et al. 2008). We used the function '*varimp'* which provides the conditional variable importance, following the permutation principle of the 'mean decrease in Gini' importance in 'randomForest', explained in Chapter 1 (see Methods, "Importance of the different layers in separating habitat classes", Page 14). We then selected the five variables with higher values of relative importance for the final model construction.

After the most influential variables were selected, a GAM was fitted. We assessed the chi-squared value and the p-values of each variable to have a measure of deviance reduction and therefore model performance. Variables with p-values $p<0,05$ were maintained. We measured the concurvity which is extremely important when applying GAMs (Guisan et al., 2002). Concurvity is present when a smooth term in a model could be approximated by one or more of the other smooth terms in the model (Wood, 2006). Concurvity can be viewed as a generalization of collinearity and causes similar problems of interpretation. Concurvity indexes vary between zero and one, with one indicating high concurvity problems. They are based on the ratio of the squared Euclidean norms of the vectors evaluated at the observed covariates values. If two variables had concurvity values above 0.4, we discarded the one with the lowest chi-squared value. After this step, we obtained the most relevant predictors for species occurrence (Table 2.3) and for species abundances (Table 2.4). We also analysed the residual plots and values to exclude outliers.

PREDICTING SHOREBIRD OCCURRENCE IN THE ENTIRE INTERTIDAL AREA OF ADONGA

To generalise the prediction of the models to the entire Adonga area, required the construction of raster of the relevant predictor for the entire area. This was carried out using QGIS (v. 3.6.1) and R (v.3.5.1). We used the same tile of Sentinel-2A, described in Chapter 1 (see Methods, "Classification of the Intertidal Area of Adonga", page 11).

We calculated the Normalized Difference Vegetation Index (NDVI) values and converted the mangrove areas into a vector file.

$$NDVI = \frac{Band\ 8 - Band\ 4}{Band\ 8 + Band\ 4} \qquad (2.3.)$$

Where the bands correspond to the reflectance value found in Sentinel-2 Multi-Spectral Instrument bands 8 and 4(ESA, 2017c). Band 8 corresponds to the near infra-red region (wavelengths between 0.767 and 0.908 μm) and Band 4 corresponds to the visible, colour red, region (wavelengths between 0.646 and 0.685 μm). Vegetated areas will absorb most of the visible wavelengths and reflect a large proportion of the near infra/red light (ESA, 2017c). Therefore, mangrove areas will have higher NDVI values than sandbanks or intertidal areas, as the first areas have more vegetation than the later ones. Afterwards, we estimated the distance between each intertidal pixel and the nearest mangrove edge, in meters. We obtained a map where every pixel was associated with a distance value, in meters.

To build the predictor "distance to channels", we used the raster of inundation (see Chapter 1, Methods, "Classification of the Intertidal Area of Adonga", Page 11). We selected only the areas where the mean height was lower than 2.5 m as these areas are associated with channel/creeks. We then calculated the distance between every pixel and the nearest channel/creek, obtaining a map where every pixel was associated with a distance value, in meters.

The exposure period of each pixel in the intertidal area (in h) was calculated by applying equation 1 to the inundation raster (see Chapter 1, Methods, "Classification of the Intertidal Area of Adonga", Page 11).

All previous modelling procedures involved the use of mud fraction (%) and proportion of areas with fiddler crab burrows (%) observed in the plots. However, these variables could not be calculated efficiently for the entire intertidal area, so the generalization of the distribution models were based on the map of the intertidal habitats, composed by: Sand, Sand-FBA, Muddy and Muddy-FBA (see Chapter 1, Results, "Classification of the Intertidal Area of Adonga", Page 19). Therefore, we produced new GAM models replacing the mud fraction and fiddler crab burrow area by the classes of percentage these two predictors used in the classification of the satellite image (see Chap 1). The final results were predictive maps for the probability of occurrence of the 11 species and the respective frequencies of occurrence for each plot.

RESULTS

SHOREBIRD COUNTS

We carried out a total of 663 counts where we recorded the number of birds found in each. We recorded a total of 26 species of birds that use the intertidal flats for feeding. The most abundant species were the Curlew Sandpiper *Calidris ferruginea and* the Red Knot *Calidris canutus*, followed by the Whimbrel *Numenius phaeopus*, the Common Ringed Plover *Charadrius hiaticula* and the Bar-tailed Godwit *Limosa lapponica* (table 2.1.). The remaining species had densities lower than one individual per hectare.

Table 2.1- Frequency of occurrence (%) and mean densities (ind/ha) of the 12 most frequent specie, calculated from 663 counts in 67 counting plots (407 ha).

Species	Frequency of occurrence (% per counting plot)	Mean density (inds/ha)
Whimbrel *Numenius phaeopus*	97	1,7 ± 1,6
Grey Plover *Pluvialis squatarola*	84	0,6 ± 0,4
Redshank *Tringa totanus*	76	0,5 ± 0,3
Bar-tailed Godwit *Limosa lapponica*	72	1,0 ± 0,8
Common Ringed Plover *Charadrius hiaticla*	67	1,3 ± 1,5
Curlew Sandpiper *Calidris ferruginea*	63	2,3 ± 4,9
Sanderling *Calidris alba*	62	0,9 ± 1,1
Common Sandpiper *Actitis hypoleucos*	49	0,2 ± 0,2
Red Knot *Calidris canutus*	33	2,1 ± 5,1
White-fronted Plover *Charadrius marginatus*	33	0,1 ± 0,2
Turnstone *Arenaria interpres*	33	0,1 ± 0,1
African Sacred Ibis *Treskiornis aethiopicus*	33	0,2 ± 0,2

BIOTIC AND ABIOTIC VARIABLES IN COUNTING PLOTS

Results from the characterization of the study area (median, mean, minimum and maximum values of all counting plots) concerning environmental variables are presented in Table 2.2. One plot could encompass a wide variety of habitats. Organic contents of the sediment was highly correlated to their mud fraction (r^2=0.90, n=80). Hence, it was excluded as a candidate predictor for the models.

Table 2.2 - Median, mean, standard deviation, minimum and maximum values for the different environmental variables (used as predictors) of the 67 counting plots

Environmental variables (Predictors)	Median	Mean ± SD	Min	Max
Mud fraction (%)	18,6	24,8 ± 23,8	2,2	88,6
Water coverage (%)	14,9	17,9 ± 13,6	0	52,0
Macroalgae coverage (%)	0	0,4 ± 1,8	0	11,1
Shells coverage (%)	0,1	1,0 ± 2,2	0	13,6
Channels coverage (%)	2,0	4,6 ± 6,5	0	30,0
FBA coverage (%)	35,0	44,4 ± 34,7	0	100
Dist. to sand banks (m)	570	746 ± 605	7	2171
Dist. to mangrove (m)	560	650 ± 433	80	1642
Dist. to channels/creeks (m)	131	133 ± 91	0	337
Mean exposure period (h)	5,1	5,1 ± 0,2	4,72	5,9

MODELS OF SHOREBIRD OCCURRENCE

Table 2.3 presents the most influential selected predictors (from GAM modelling) explaining variations in the presence of each species within the foraging areas as well as the degree of each smooth term. We modelled the occurrence of 11 species and the most selected predictor was the mean exposure period of each counting plot (n=11). The estimated distance between the centroid of the plot and the edge of mangrove was selected for six species and the distance to the channels/creeks was selected for only one species.

Despite being selected as an important predictor to all species distributions models, the exposure period was only considered twice as the most influential predictor. Mud fraction of the sediment and the percentage of FBA coverage were selected five times each as an important predictor and as the most influential predictors for three species. The distance to mangrove edge were selected for six species and in three cases was considered the most relevant predictor. The distance to channels/creeks was selected for two species as an important predictor. The percentage of the deviance explained in the models ranged from 29,4 % (Common Sandpiper *Actitis hypoleucos*) to 58,7% (Common Ringed Plover).

The smooth terms obtained in the models are graphically presented in Figures 1.3 to 1.5, where the vertical axis represents the predictor contribution to the response. Species such as the Turnstone *Arenaria interpres*, Red Knot, Curlew Sandpiper, Common Ringed Plover and the Bar-tailed Godwit showed response with a similar shape, where the probability of occurrence remains relatively constant for plots with low to medium exposure periods and decrease in plots with higher exposure periods. The main difference between these species is that Bar-tailed Godwits and Common Ringed Plovers seem to have an earlier turning point (exposure period = ±5.0 hours) before the number of presences starts to decrease, while the turning point for the other three species is around 5.3 hours. The number of presences of Sanderling, Redshank *Tringa totanus*, Grey Plover *Pluvialis squatarola* and White-fronted Plover *Charadrius marginatus* increases between low and medium exposure periods till it reaches a peak and then declines from medium to longer exposure periods. The Common Sandpiper and the African Sacred

Ibis *Treskiornis aethiopicus* showed distinct responses, with a decrease in probability of occurrence from shorter exposure periods to longer ones.

The magnitude and direction of the responses to the mud fraction contents of the sediment varied among species. For instance, the number of presences of the Common Ringed Plover decreases linearly with the increase of mud fraction, while for Grey Plover we found the opposite trend. Sanderlings and White-fronted Plovers appear to prefer sandy areas as the occurrence of both species is significantly higher in areas with low mud fraction. The occurrence of White-fronted Plover declines abruptly until areas with ± 25% of mud fraction and then again after ±60%. Between these limits, the number of presences is approximately constant. The number of presences of Sanderlings declines abruptly from sandy to muddy areas. In the case of the African Sacred Ibis, the scenario is completely different: the number of occurrences increases from sandy to muddy-sand (± 30% of mud fraction) areas, where it reaches the maximum peak; then, the number of occurrences declines until stabilizing after ± 60% of mud fraction.

Species such as the Red Knot and the Curlew Sandpiper frequently occur in areas where the percentage cover of FBA ranges between 0 and 60%, but after that threshold, they experience a decline in the number of presences. Contrarily, the occurrence of the Common Sandpiper increases in areas with up to 40% of FBA cover and then remains relatively stable. Occurrence of Turnstones tends to increase in areas up to 60% of fiddler-crab burrow cover, but then also declines. The Redshank seems to be relatively indifferent to the percentage of FBA cover, as the occurrences of this species remain stable. However, there is a slightly increase until 60 % and then a slightly decrease on this species occurrences.

Overall, shorebird responses in relation to the distance between foraging areas and the edge of mangrove areas have a similar shape. We recorded a higher number of presences of the White-fronted Plover, Red Knot, Curlew Sandpiper and Redshank, with increasing distances to mangrove edge. These relationships are nearly linear. For the Common Ringed Plover, the number of presences also increases with the distance to the mangrove. Grey Plovers are more frequent in areas within intermedium distances (e.g. 900 m) to the mangrove and then become less frequent.

Finally, the occurrence of the Bar-tailed Godwit slightly increases until a distance of ±200 m and then decreases to higher distances. The Sanderling occurrence increases with the increasing distance to channels.

Table 2.3- Most relevant predictors selected after using GAMs for modelling species occurrences (n=11 species). Each predictor is associated with values of chi-square, significance values, degrees of freedom. Each final model is associated with UBRE score, R-square, Null deviance, explained deviance and number of samples used to build the model.

Species	Predictors	χ^2	p-value	DF	UBRE	R-sq. (adj)	Null deviance	Explained deviance (%)	No of samples
Common sandpiper	Cover FBA	59.71	<0.001	2.8	3.01	0.27	356.60	29.4	66
	Exposure period	28.57	<0.001	2.6					
Turnstone	Cover FBA	54.9	<0.001	2.9	2.68	0.08	334.08	32.3	65
	Exposure period	16.24	<0.001	2.8					
	Dist. to channels/creeks	18.21	<0.001	2.0					
Sanderling	Exposure period	58.30	<0.001	2.8	3.28	0.41	554.71	52.1	66
	Mud fraction	141.69	<0.001	2.4					
	Cover FBA	26.14	<0.001	2.9					
Red knot	Dist. to mangrove	47.86	<0.001	1.3	2.37	0.35	351.51	41.3	66
	Exposure period	11.49	<0.01	2.9					
	Cover FBA	84.19	<0.001	2.7					
Curlew sandpiper	Dist. to mangrove	35.4	<0.001	1.1	2.88	0.48	530.74	55.3	65
	Exposure period	24.72	<0.001	2.9					
	Dist. to mangrove	68.94	<0.001	2.1					
Ringed plover	Exposure period	45.66	<0.001	2.3	2.42	0.52	508.18	58.7	65
	Mud fraction	63.26	<0.001	1.0					
	Dist. to mangrove	29.55	<0.001	1.1					
White-fronted plot	Exposure period	21.08	<0.001	2.5	2.33	0.30	384.86	46.8	66
	Mud fraction	89.52	<0.001	2.9					
Bar-tailed godwit	Dist. to channels/creeks	10.38	<0.01	2.5	1.57	0.42	232.59	32.1	66
	Exposure period	43.23	<0.001	2.4					
	Dist. to mangrove	50.54	<0.001	2.4					
Grey plover	Exposure period	41.37	<0.001	2.7	2.14	0.29	357.67	46.9	65
	Mud fraction	7.364	<0.01	0.9					
African sacred ibis	Exposure period	21.87	<0.001	1.6	2.16	0.40	356.77	45.6	65
	Mud fraction	81.53	<0.001	3					
	Cover FBA	6.26	<0.05	2					
Redshank	Dist. to mangrove	12.45	<0.001	0.9	2.87	0.23	394.10	37.2	67
	Exposure period	58.13	<0.001	2					

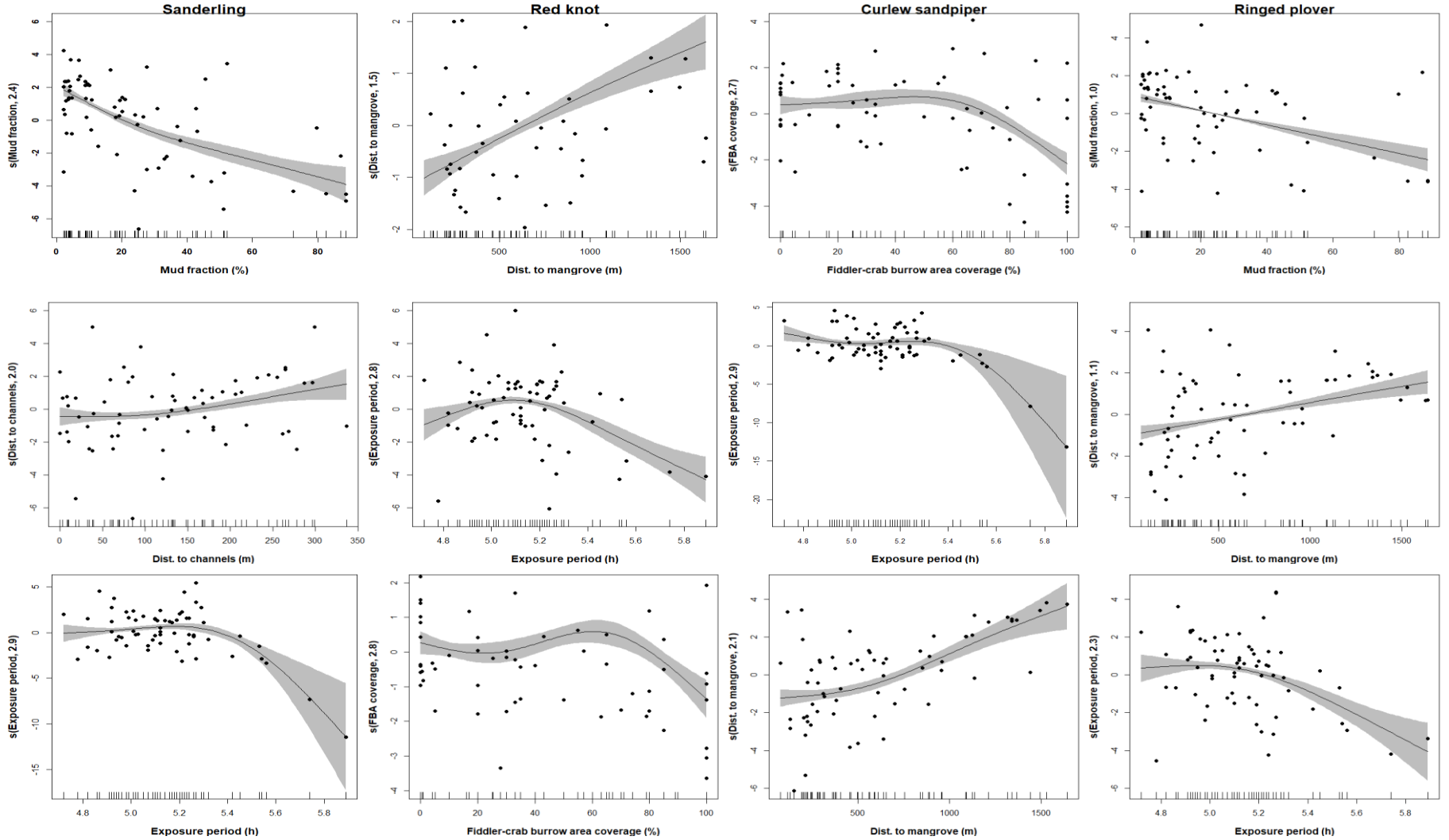

Figure 2.3- Fitted smooth terms indicated as s(name of the predictor, degrees of freedom) for the occurrences of four shorebird species (Sanderling, Red Knot, Curlew Sandpiper and Common Ringed Plover) in solid lines. The limit of the shades corresponds to ± 95% confidence intervals. The thick marks in the x-axis represent the location of the observations along the predictors. The plots for each species are ordered from the most significative predictor (top) to less significative predictor (bottom).

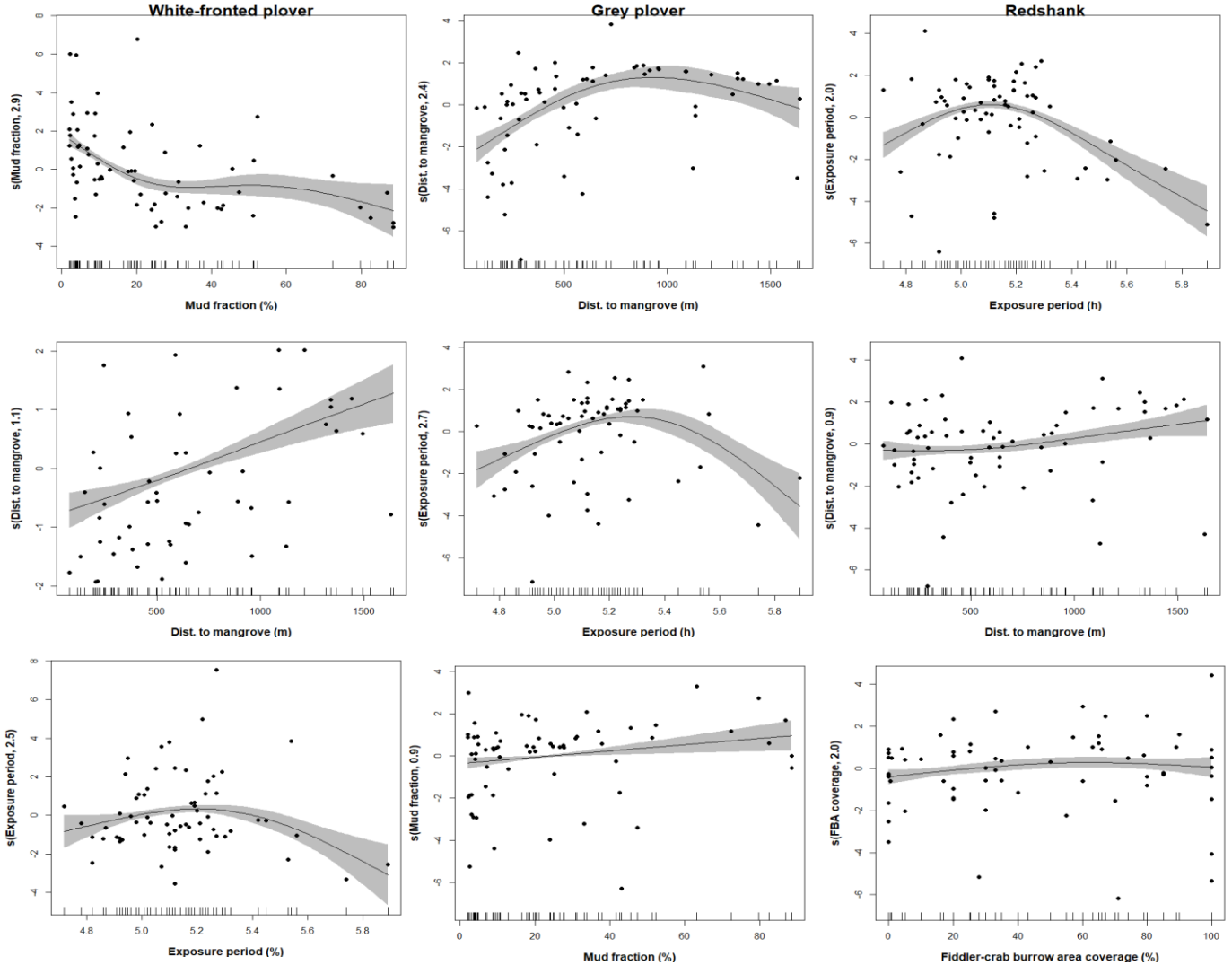

Figure 2.4- Fitted smooth terms indicated as s(name of the predictor, degrees of freedom) for the occurrences of three shorebird species (Whit- fronted Plover , Grey Plover and the Redshank) in solid lines. The limit of the shades corresponds to ± 95% confidence intervals. The thick marks in the x-axis represent the location of the observations along the predictors. The plots for each species are ordered from the most significative predictor (top) to less significative predictor (bottom).

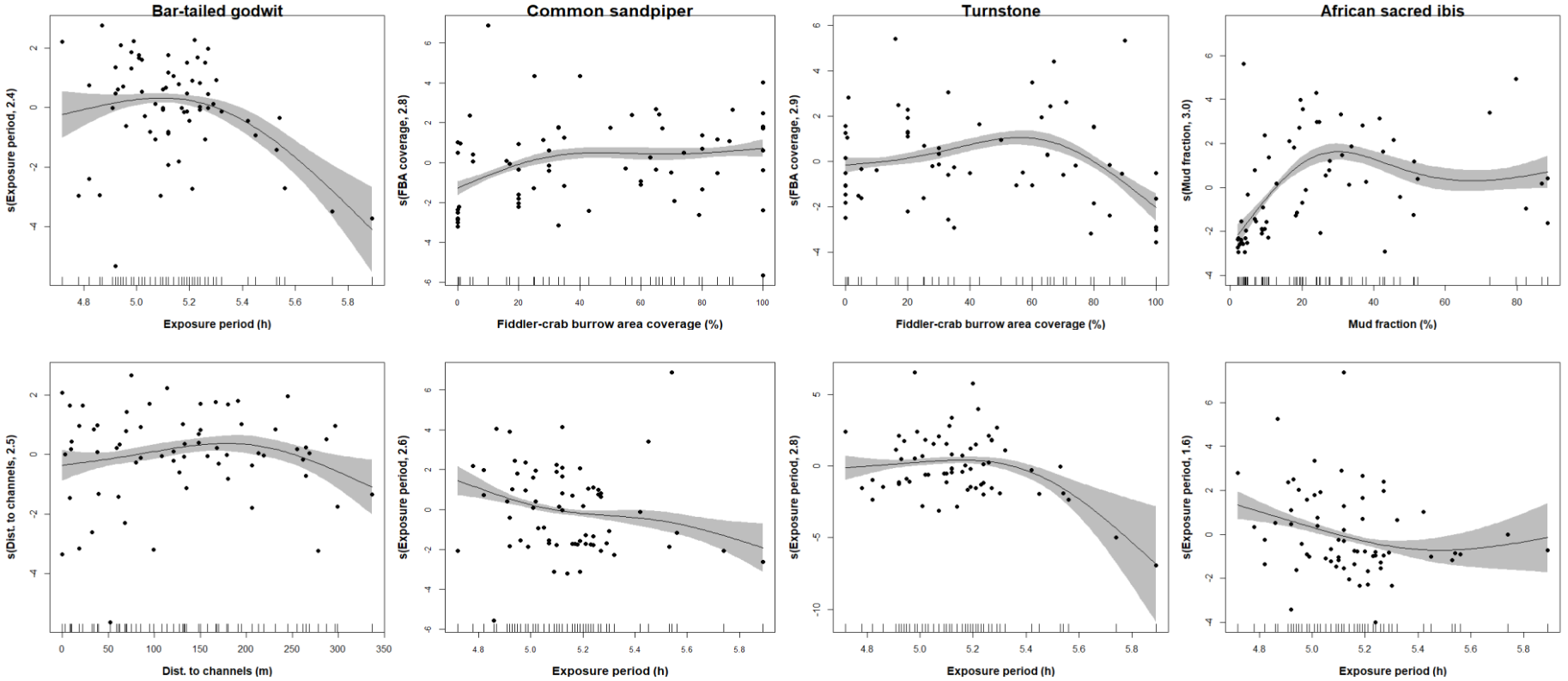

Figure 2.5- Fitted smooth terms indicated as s(name of the predictor, degrees of freedom) for the occurrences of four shorebird species (Bar-tailed Godwit, Common Sandpiper, Turnstone and African sacred Ibis) in solid lines. The limit of the shades corresponds to ± 95% confidence intervals. The thick marks in the x-axis represent the location of the observations along the predictors. The plots for each species are ordered from the most significative predictor (top) to less significative predictor (bottom).

MODELS OF SHOREBIRD ABUNDANCE

Regarding the identification of variables driving shorebird abundance, the main results are presented on table 2.4. The distance to the edge of mangrove areas was selected as one of the most relevant predictors for six out of seven species. The exposure period was selected for four species, while the mud fraction of the sediment and the percentage cover of FBA were selected for two species. The explained deviance ranged from 26,4 % (Grey Plover) to 60,4 % (Whimbrel).

Figures 2.6 and 2.7 show the smooth terms of the responses of shorebird abundances to the selected linear predictors. Overall, the distance to mangrove areas seems to be the main factor influencing variation in shorebird abundances in foraging areas. The abundance of Bar-tailed Godwit, Ringed Plover and Grey Plover increased almost linearly with distance to the mangrove. The abundance of Curlew Sandpiper and Whimbrel slightly declined in areas distanced to the mangrove up to approximately 500 and 900m, respectively, and then increase at higher distances. The abundance of Red Knot increased until 1000 m and then appear to be stabilizing. Concerning the mean exposure period of each counted plot, shorebirds seem to be concentrated in areas with lower exposure periods. Bar-tailed Godwit, Red Knot and Ringed Plover showed higher abundances in plots with lower exposure periods, while Sanderling abundances had a similar variation to the ones recorded in the occurrence models. As the cover of FBA increases, the abundances of Curlew Sandpiper decline linearly, while the opposite trend is found for Whimbrel. Abundance of the Common Ringed Plover and Sanderling decrease almost linearly with the increase in the mud fraction of the sediment.

COMPARISON BETWEEN THE SELECTED PREDICTORS FOR OCCURRENCE AND ABUNDANCE MODELS

In general, most of the selected predictors explaining the occurrence of shorebirds were also selected as significant predictors in explaining the abundance for the same species. However, not every predictor was selected for both models. In the case of the Red Knot, one occurrence's predictor was not selected for the abundance model of this species (coverage of fiddler crab burrow area). The model using the abundance of the Curlew Sandpiper did not selected exposure period as a relevant predictor. For the Grey Plover abundances, the predictors selection did not include the exposure period nor the mud fraction. The important predictors for the Common Ringed Plover were equally selected for both models. In the case of the Bar-Tailed Godwit and the Sanderling, the distance to mangrove was an important predictor explaining the abundance of these species instead of the distance to channels that was important in explaining the occurrence of these species.

Table 2.4 - Most relevant predictors selected after using GAMs for modelling species abundances (n=11 species). Each predictor is associated with values of chi-square, significance values, degrees of freedom. Each final model is associated with UBRE score, R-square, Null deviance, explained deviance and number of samples used to build the model.

Species	Predictors	χ^2	p-value	DF	(-) REML	R-sq. (adj)	Null deviance	Explained deviance (%)	No of samples
Sanderling	Exposure period	12.16	p<0.01	2	176.07	0.20	145.76	46.6	66
	Mud fraction	49.76	p<0.001	1.3					
Red knot	Dist. To mangrove	39.3	p<0.001	1.9	181.86	0.29	135.79	51.0	65
	Exposure period	33.76	p<0.001	1.7					
Curlew sandpiper	Cover FBA	6.911	p<0.01	1	209.14	0.67	167.28	57.3	65
	Dist. to mangrove	57.928	p<0.001	2.3					
Common Ringed plover	Dist. To mangrove	46.74	p<0.001	1.3	195.52	0.08	155.43	50.0	66
	Exposure period	11.86	p<0.001	1					
	Mud fraction	25.09	p<0.001	1.2					
Bar-tailed godwit	Dist. To mangrove	10.65	p<0.001	1	184.65	-0.54	113.11	36.2	67
	Exposure period	27.15	p<0.001	1.1					
Whrimbel	Dist. To mangrove	54.2	p<0.001	2.7	236.27	-8.31	171.15	60.4	67
	Cover FBA	17.13	p<0.001	1.1					
Grey plover	Dist. To mangrove	22.86	p<0.001	1.1	153.44	-1.35	92.24	26.4	66

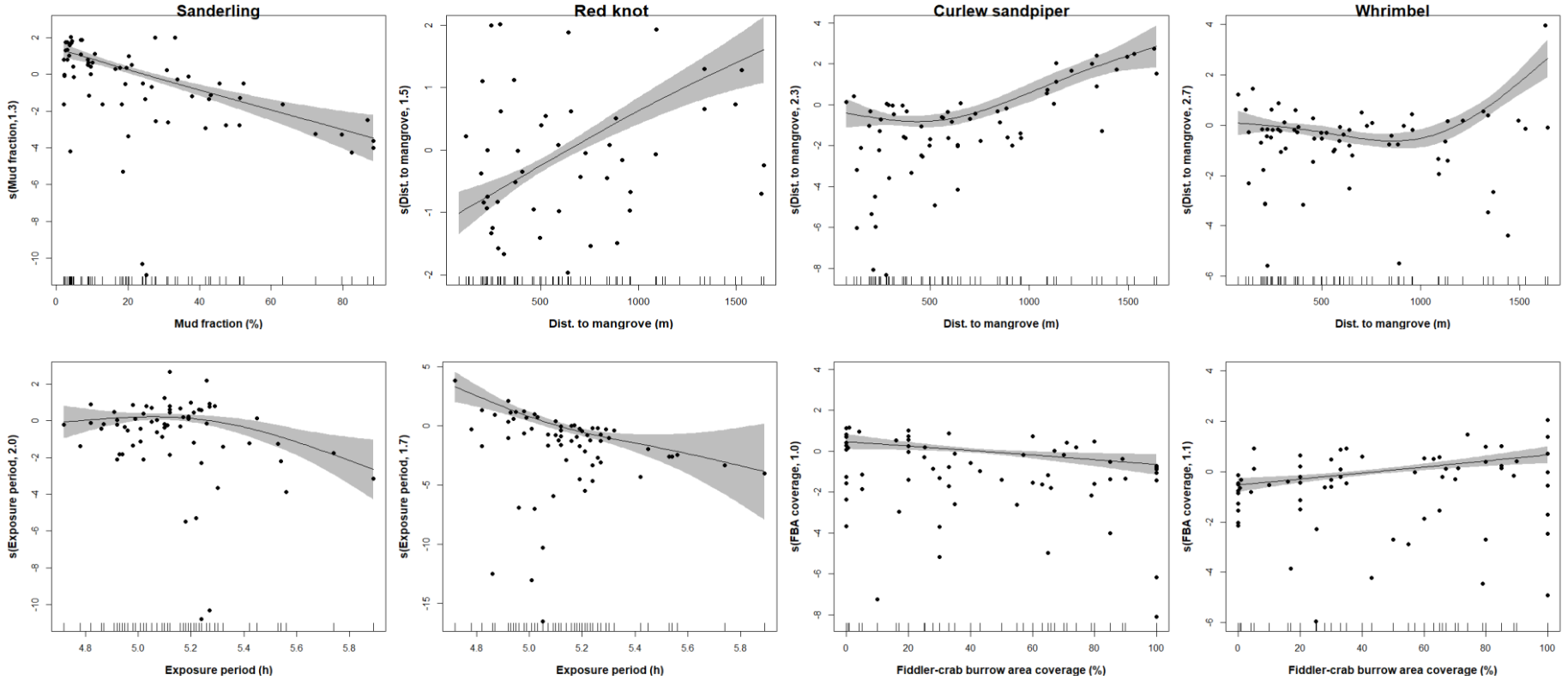

Figure 2.6 - Fitted smooth terms indicated as s(name of the predictor, degrees of freedom) for the abundances of four shorebird species (Sanderling, Red Knot, Curlew Sandpiper and Whimbrel) in solid lines. The limit of the shades corresponds to ± 95% confidence intervals. The thick marks in the x-axis represent the location of the observations along the predictors. The plots for each species are ordered from the most significative predictor (top) to less significative predictor (bottom).

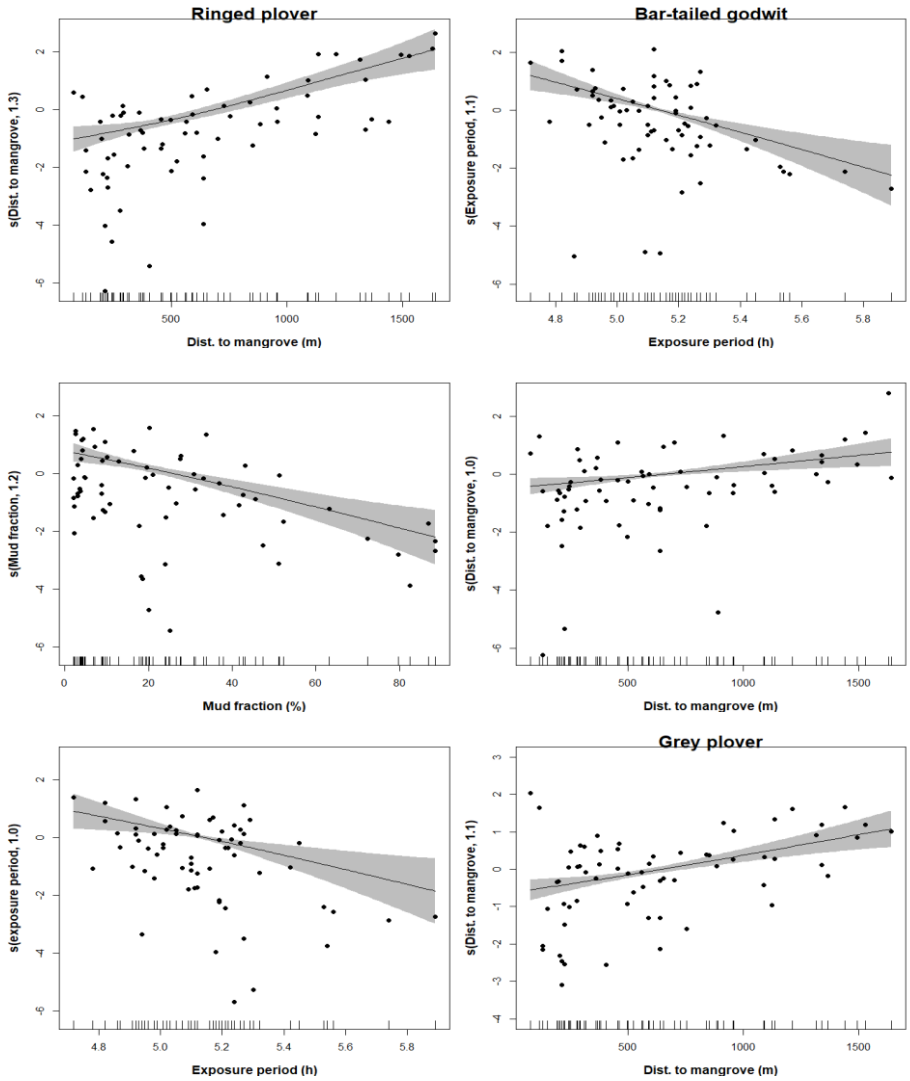

Figure 2.7- Fitted smooth terms indicated as s(name of the predictor, degrees of freedom) for the abundances of three shorebird species (Common Ringed Plover, Bar-tailed Godwit and Grey Plover) in solid lines. The limit of the shades corresponds to ± 95% confidence intervals. The thick marks in the x-axis represent the location of the observations along the predictors. The plots for each species are ordered from the most significative predictor (top) to less significative predictor (bottom).

PREDICTING SHOREBIRD OCCURRENCE IN THE ENTIRE INTERTIDAL AREA OF ADONGA

The maps produced for each relevant predictor are displayed on Figures 2.8 to 2.10. The predictive maps for the different species are displayed in Figure 2.11 to 2.21. In the same maps, we have the observed frequencies of occurrence for each species represented by circles (the size of each circle is proportional to the value of the observed frequency of occurrence). In general, when the observed frequency of occurrence increases, the predicted probability of occurrence also increases. As one can note, preferences between species are distinct. The Whimbrel occurs regularly through all area; therefore, the predictive map is not represented.

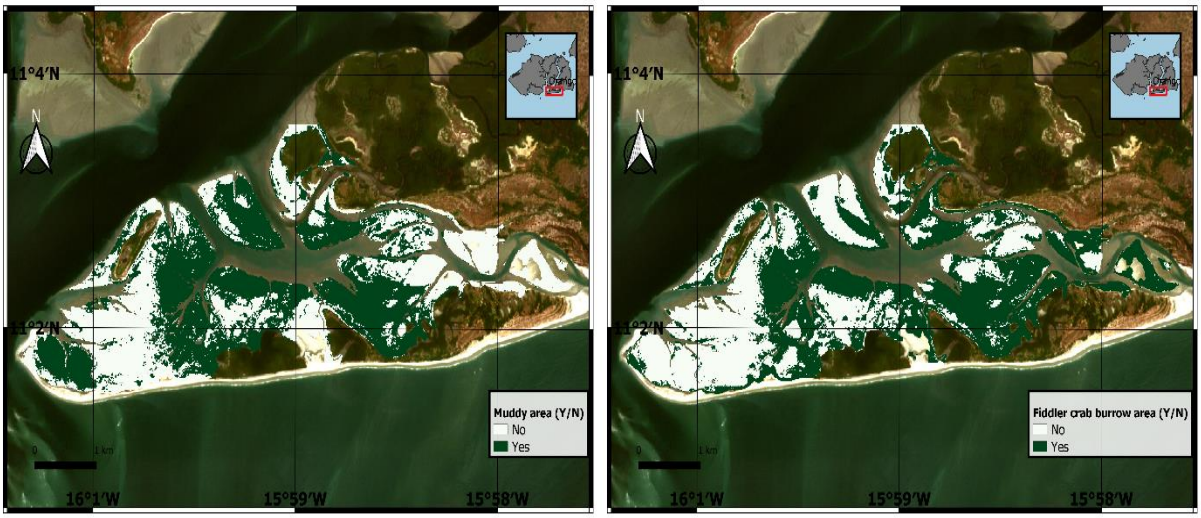

Figure 2.8 - Map of muddy and sand areas (Yes/No, respectively), on the left side, and map of areas with (Yes) and without (No) fiddler crab burrow coverage, on the right side.

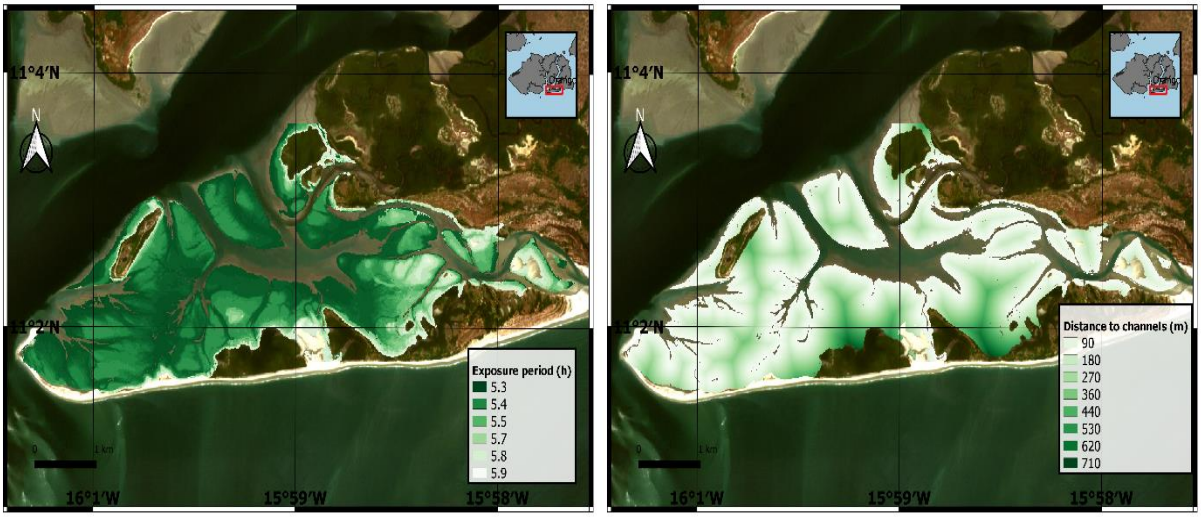

Figure 2.9 - Map of the exposure periods on the left side (each pixel is associated with time of exposure, in hours) and map of distance to channels/creeks on the right side (each pixel is associated with a distance value, in meters).

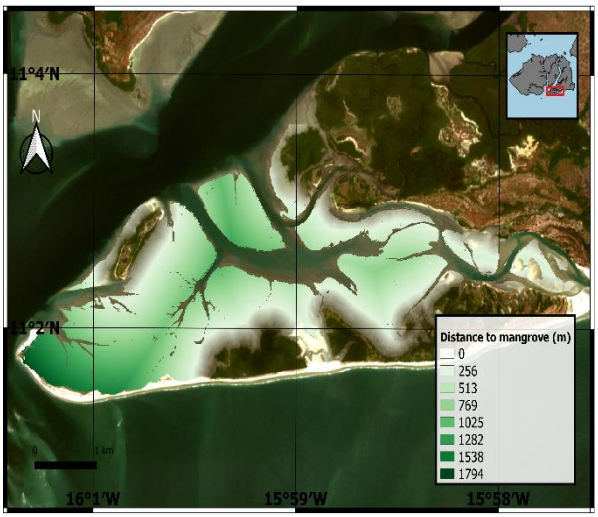

Figure 2.10- Map of distance to mangrove patches (each pixel is associated with a distance value, in meters).

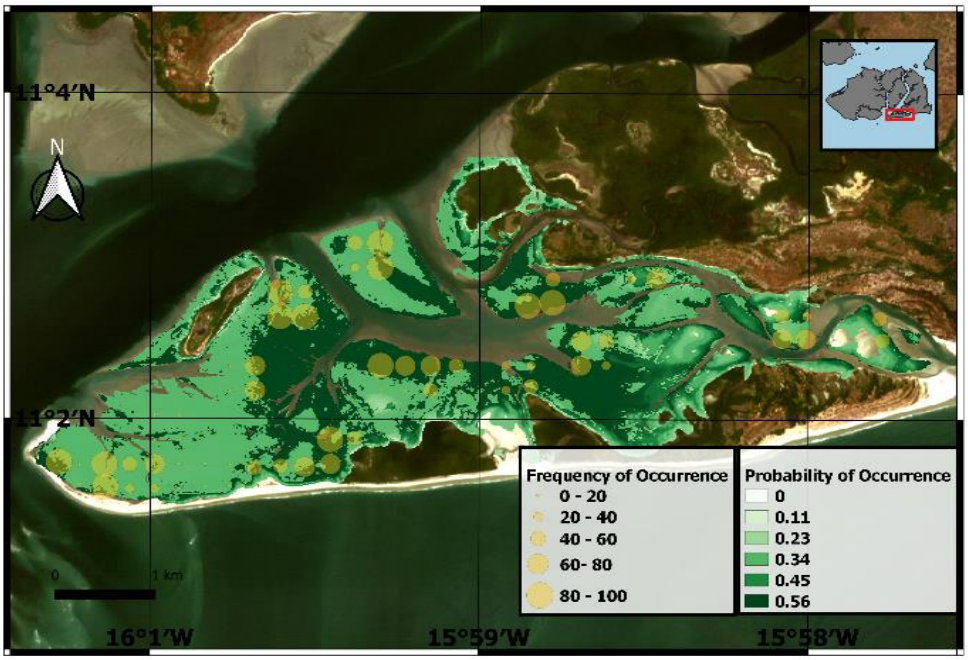

Figure 2.11- Predictive map for the Common Sandpiper occurrences. White areas correspond to low values for the probability of occurrence and dark green areas correspond to higher values of probability of occurrence. Smaller orange circles correspond to lower frequencies of occurrence and bigger orange circles correspond to higher frequencies of occurrence.

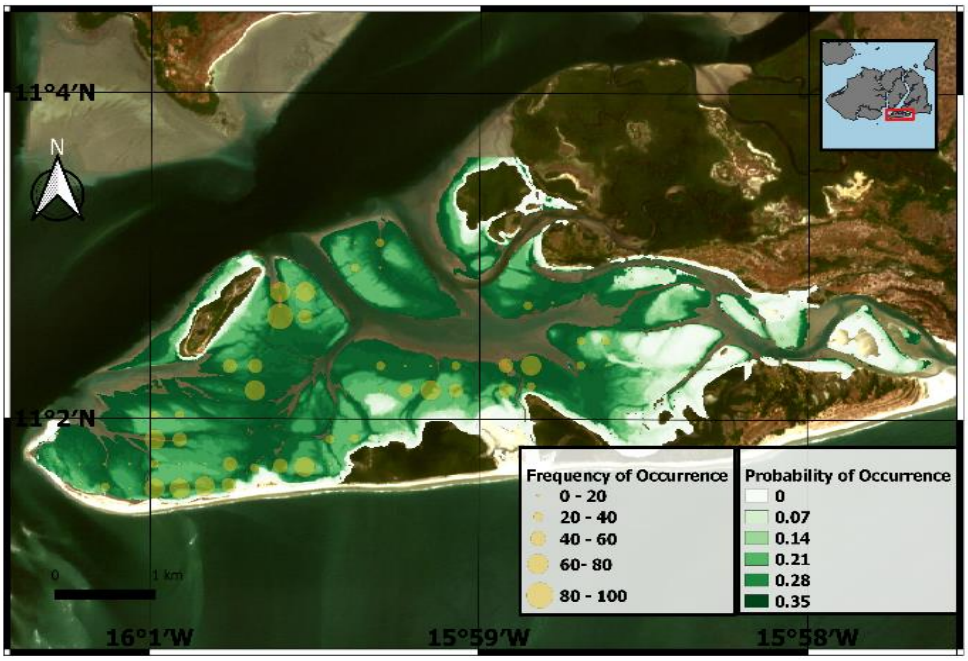

Figure 2.12 - Predictive map for the Turnstone occurrences. White areas correspond to low values for the probability of occurrence and dark green areas correspond to higher values of probability of occurrence. Smaller orange circles correspond to lower frequencies of occurrence and bigger orange circles correspond to higher frequencies of occurrence.

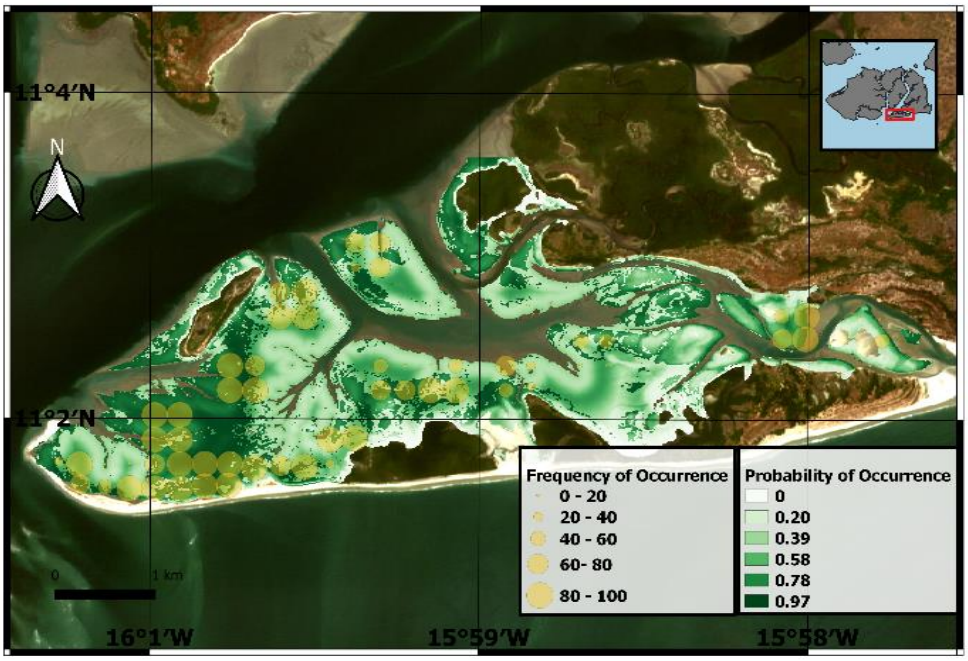

Figure 2.13 - Predictive map for the Sanderling occurrences. White areas correspond to low values for the probability of occurrence and dark green areas correspond to higher values of probability of occurrence. Smaller orange circles correspond to lower frequencies of occurrence and bigger orange circles correspond to higher frequencies of occurrence.

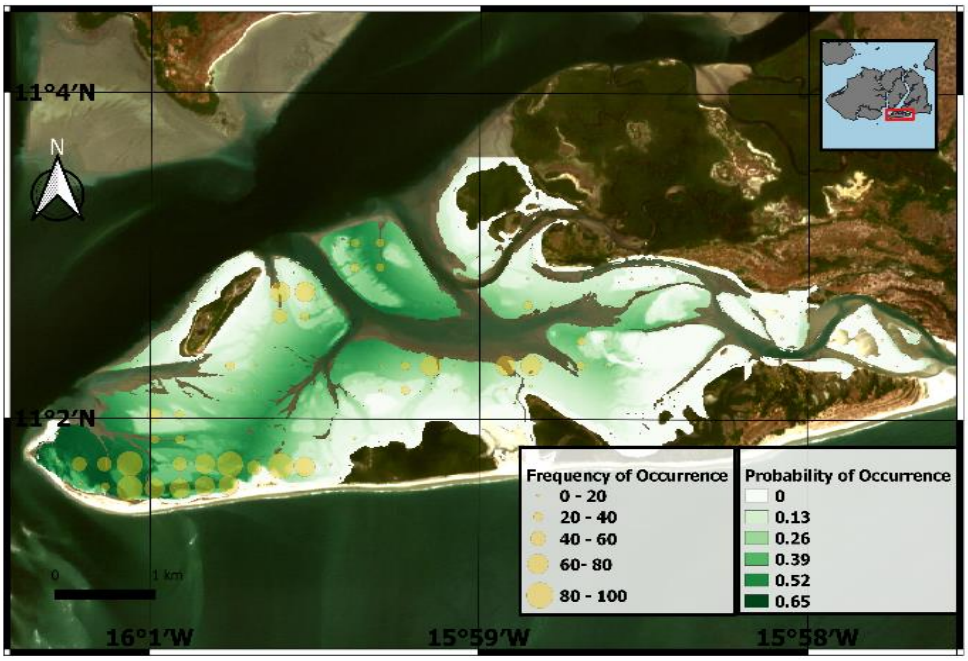

Figure 2.14 - Predictive map for the Red Knot occurrences. White areas correspond to low values for the probability of occurrence and dark green areas correspond to higher values of probability of occurrence. Smaller orange circles correspond to lower frequencies of occurrence and bigger orange circles correspond to higher frequencies of occurrence.

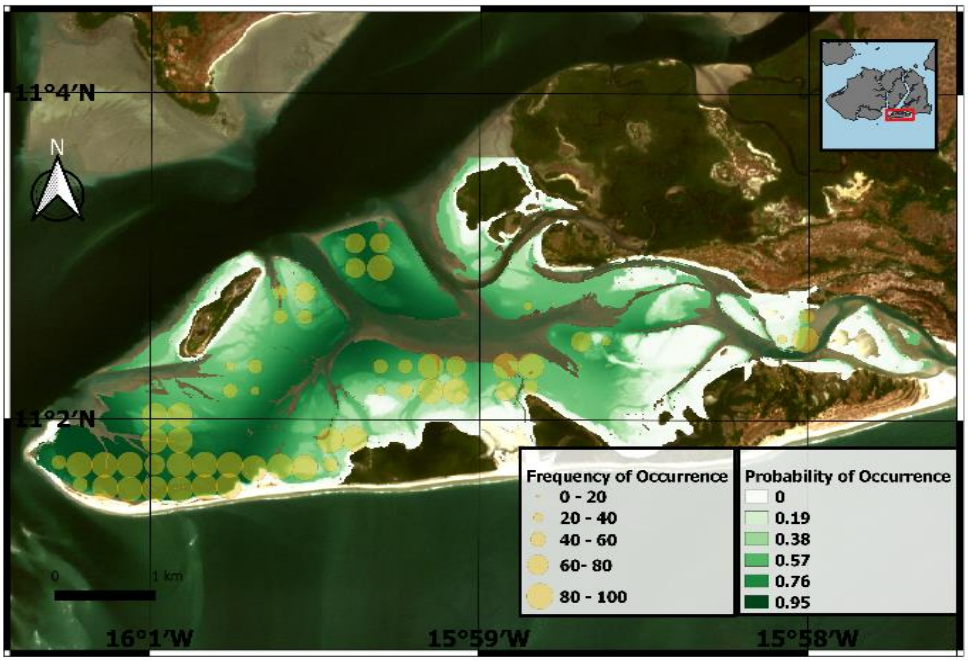

Figure 2.15- Predictive map for the Curlew Sandpiper occurrences. White areas correspond to low values for the probability of occurrence and dark green areas correspond to higher values of probability of occurrence. Smaller orange circles correspond to lower frequencies of occurrence and bigger orange circles correspond to higher frequencies of occurrence.

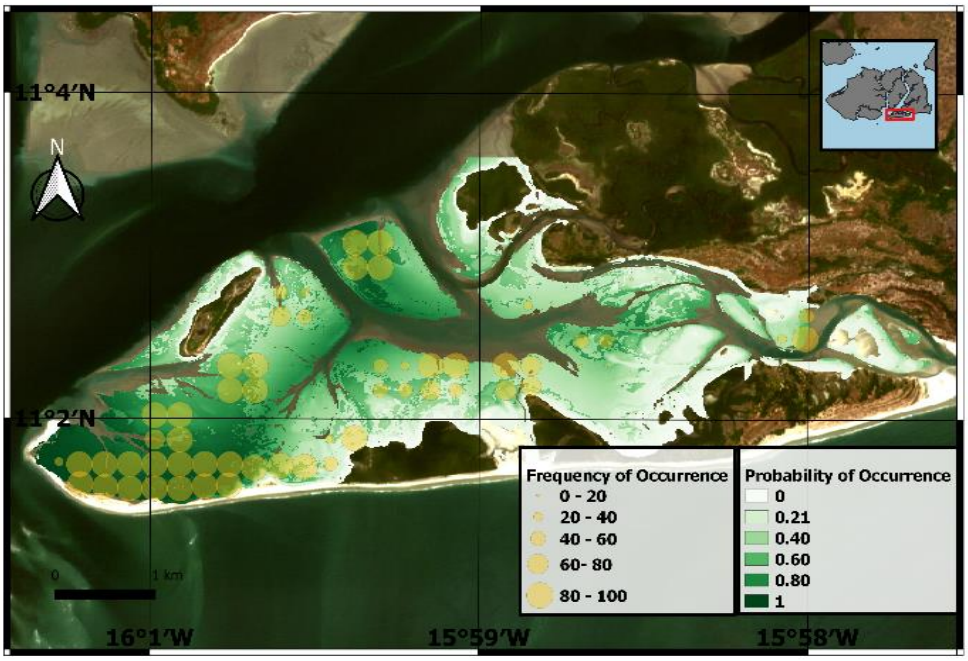

Figure 2.16 - Predictive map for the Common Ringed Plover occurrences. White areas correspond to low values for the probability of occurrence and dark green areas correspond to higher values of probability of occurrence. Smaller orange circles correspond to lower frequencies of occurrence and bigger orange circles correspond to higher frequencies of occurrence.

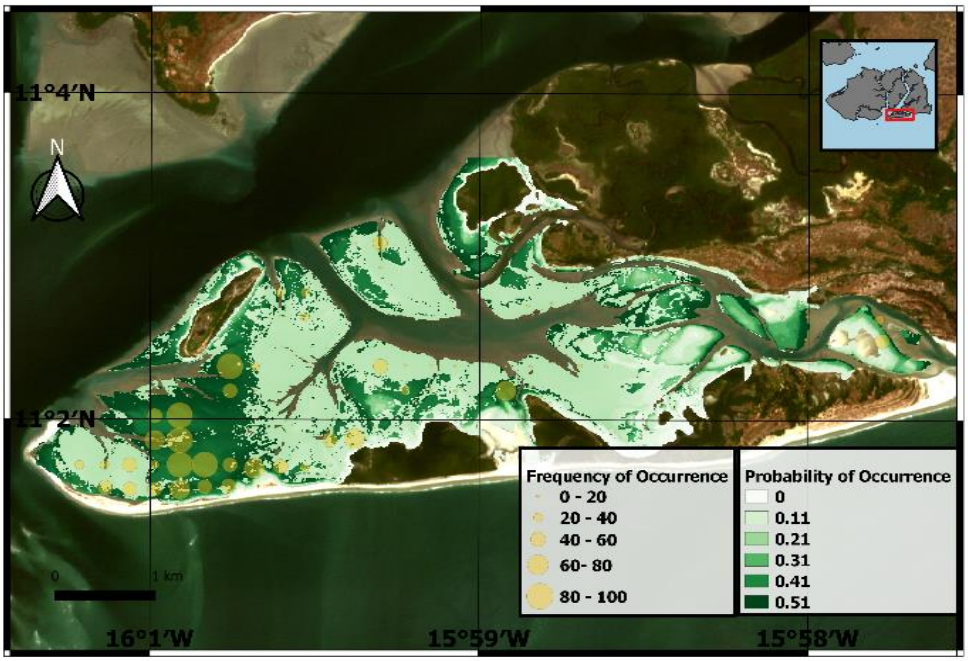

Figure 2.17- Predictive map for the White-Fronted Plover occurrences. White areas correspond to low values for the probability of occurrence and dark green areas correspond to higher values of probability of occurrence. Smaller orange circles correspond to lower frequencies of occurrence and bigger orange circles correspond to higher frequencies of occurrence.

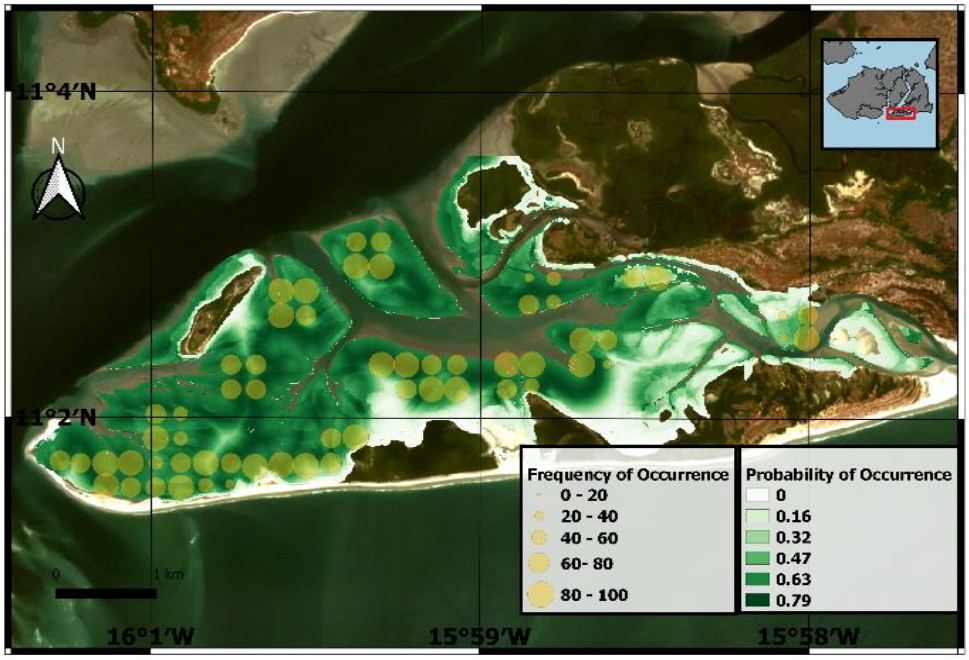

Figure 2.18 - Predictive map for the Bar-tailed Godwit occurrences. White areas correspond to low values for the probability of occurrence and dark green areas correspond to higher values of probability of occurrence. Smaller orange circles correspond to lower frequencies of occurrence and bigger orange circles correspond to higher frequencies of occurrence.

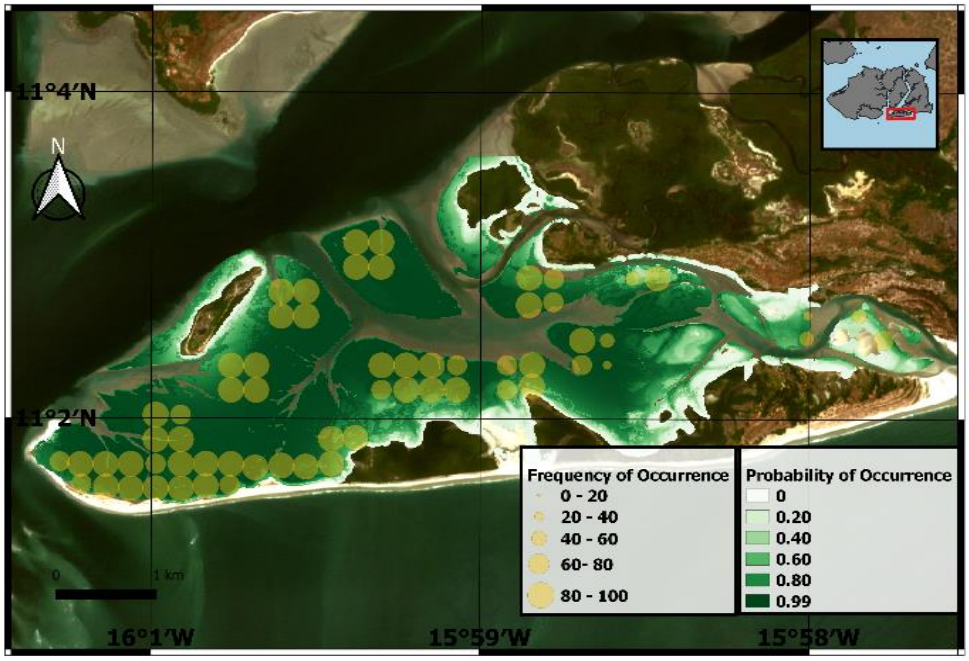

Figure 2.19 - Predictive map for the Grey Plover occurrences. White areas correspond to low values for the probability of occurrence and dark green areas correspond to higher values of probability of occurrence. Smaller orange circles correspond to lower frequencies of occurrence and bigger orange circles correspond to higher frequencies of occurrence.

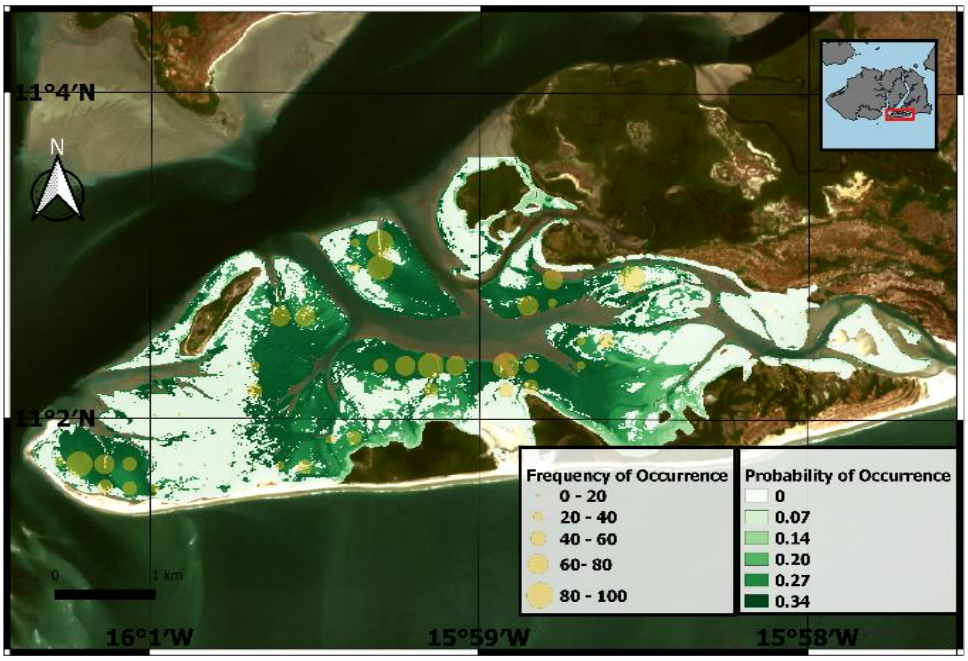

Figure 2.20 - Predictive map for the African Sacred Ibis occurrences. White areas correspond to low values for the probability of occurrence and dark green areas correspond to higher values of probability of occurrence. Smaller orange circles correspond to lower frequencies of occurrence and bigger orange circles correspond to higher frequencies of occurrence.

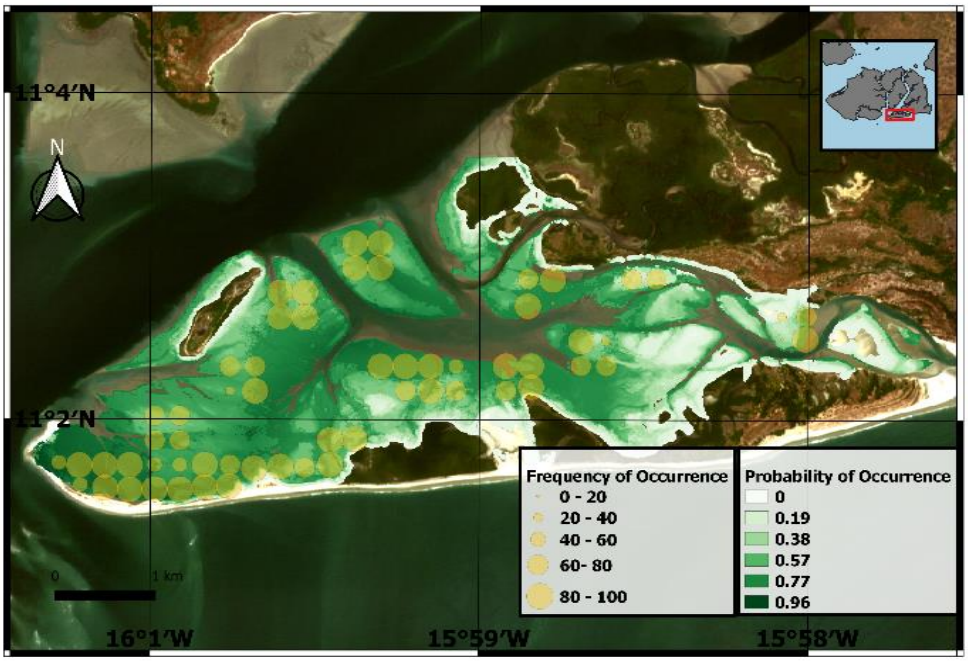

Figure 2.21 - Predictive map for the Redshank occurrences. White areas correspond to low values for the probability of occurrence and dark green areas correspond to higher values of probability of occurrence. Smaller orange circles correspond to lower frequencies of occurrence and bigger orange circles correspond to higher frequencies of occurrence.

DISCUSSION

This study presents data on the spatial distribution of shorebirds feeding on intertidal flats in Adonga islet, in the Bijagós archipelago and investigate the factors that are determinant for such distribution. Although our counting plots covered only 37% of the potential foraging area, they were distributed across the whole study area, capturing virtually all types of habitats occurring there. The relative abundance of each species within the shorebird community recorded in this study is in agreement with data from previous studies conducted at the archipelago scale (e.g. Zwarts, 1988; Salvig et al., 1994). The main difference concerns the much lower abundance of little stint *Calidris minuta* in our study area in comparison to previous studies (Zwarts, 1988; Salvig et al., 1994). This may be explained by a likely dramatic decline of the species in the whole archipelago (T. Catry & J.P. Granadeiro, pers.comm.) rather than by the lack of suitable habitat for the species within the mudflats of Adonga.

MAIN SELECTED PREDICTORS EXPLAINING SHOREBIRD'S OCCURRENCES AND ABUNDANCES

Exposure period

The variation of the exposure period between counting plots ranged from 4.72 to 5.87 hours, which is a low range when compared with other studies (e.g. Granadeiro et al., 2004; 2007). Also, the sediment in plots with higher emersion periods was mainly constituted by coarser sand and higher proportion of fiddler crab burrow area (n=6 counting plots), which can also explain differences in the occurrence and abundance of all species as macroinvertebrate densities in these areas are probably lower (Beninger & Paterson, 2018; Paulino, 2019). Nevertheless, our results suggest that shorebird's occurrence is high and relatively constant in plots with low and medium exposure periods. Still, birds tend to be more abundant in plots with lower exposure periods. The general tendencies described in the literature seem to agree with our results (Granadeiro et al., 2004, Ponsero et al., 2016). Macroinvertebrate abundance and composition are dramatically constrained by the exposure period of the intertidal flats (Yates et al., 1993; Choi et al., 2014; Ponsero et al., 2016). Macroinvertebrates tend to concentrate in areas where the stress to environmental conditions is relatively low, as they cannot tolerate high levels of dissection, and the exposure period is long enough to allow meeting their energetic requirements, as they feed during the emerged period (Beninger & Paterson, 2018). The exposure period had also been recognized as an important factor in shaping the foraging shorebird community through previous studies (Granadeiro et al., 2007; Ponsero et al., 2016).

Mud fraction

Higher values of mud fraction were rare and normally associated with fiddler crab high-density areas. Sanderlings were more frequent but also more abundant in sandy areas, which is in agreement with previous studies (Zwarts, 1988; Summers et al., 2002; Granadeiro et al., 2004). White-fronted Plovers were also more frequent in sandy areas (we could not model abundance for this species) also in accordance to what has been recorded before (Winterbottom, 1967). The Common Ringed Plover showed higher frequency and abundance in sandy areas, which have been previously observed (Summers et al., 2002). However, several studies indicated that the Common Ringed Plover is associated to muddier areas (Moreira, 1998). Our results are expected as this bird species forages preferably in areas without fiddler crab burrow areas (Paulino, 2019), as this crab is not an essential prey item in the diet of this by species (Lourenço et al., 2017). In the case of Grey Plover, this species was more likely to be found in muddy areas (in agreement with e.g. Zwarts (1988) and Rosa et al. (2003)), although mud contents of the sediment failed to explain their abundance patterns. In fact, the mud fraction of the sediment had been described by several studies, as one of the main drivers of the macroinvertebrate community (e.g. Goss-Custard and Yates, 1992; Yates et al., 1993; Choi et al., 2014; Ponsero et al.,

2016) and it had been selected and used as one of the principal factors possibly associated with shorebird distribution (Scheiffarth et al., 1996; Grandadeiro et al., 2004; Granadeiro et al. 2007; Lunardi et al., 2011).

Fiddler crab burrow area coverage

The percentage of fiddler crab burrowing area coverage was selected as an important predictor explaining foraging distribution of several species. Some species such as the Common Sandpiper and the Turnstone were more frequent in areas with high FBA coverage (Zwarts, 1988). Redshanks also tend to be more frequent in areas with a high density of fiddler crabs, which is likely explained by the high proportion of this crustacean in the diet composition of Redshanks in the Bijagós archipelago (Lourenço et al., 2017). Whimbrels were more abundant in areas with high cover of FBA. Previous studies confirm this observation as they suggest Whimbrels are fiddler-crab predator specialists (Zwarts, 1988; Lourenço et al., 2017). This has also been observed in South America with another fiddler-crab species (Iribarne & Marinez, 1999). For some species, such as the Red Knot and the Curlew Sandpiper, the number of presences remains constant in areas with low FBA cover to areas with up to approximately 60% of FBA cover, only decreasing after the 60% threshold. Given that both species consume low numbers of fiddler crabs (Lourenço et al., 2017), these results can be explained by the fact that plots covered by 60% of FBA still comprise more suitable habitats in the remaining areas. Moreover, the abundance of Curlew Sandpiper declines linearly with the increase in the percentage of FBA, which is also in agreement with the results found by Zwarts (1988). While being an important prey for different shorebird species (e.g. Zwarts, 1988; Lourenço et al., 2017) fiddler crabs are also known to impact the patterns of macroinvertebrate abundance and biomass (Zwarts, 1988; Paulino, 2019). Hence, shorebird species composition is different inside and outside fiddler-crab burrowing areas (Zwarts, 1988; Paulino, 2019).

Distance to mangrove patches

Our results suggest that majority of the shorebirds species tend to be more frequent and abundant in areas away from mangrove patches. Mangrove areas are widespread by the whole archipelago and are also present in our study area. Despite being used by several shorebird species as roosts (Zwarts, 1988), these areas can harbour raptors, which use mangrove trees as privileged (high) perches to hunt. In the Bijagós archipelago, the Peregrine falcon *Falco peregrinus* (Zwarts, 1988) is one of the most known raptors hunting shorebirds (Page & Whitacre, 1975). Although not previously described as a shorebird predator, we recorded the presence of Palm-nut vultures *Gypohierax angolensis* in counting plots at least 20 times, in 15 of which vultures were eating a shorebird (e.g. Curlew Sandpiper, Ringed Plover, Turnstone). This suggests that this species may be seen as a significant threat by shorebirds, and therefore contribute to a "landscape of fear". In addition, we recorded significant movements of shorebird flocks when Peregrine falcon or the African fish eagle *Pandion haliealetus* flew over counting areas. Shorebirds select feeding areas based on a compromise between invertebrate prey availability and surveillance from predators (Beninger & Paterson, 2018). Near to mangrove areas, the risk of being predated is higher, hence shorebirds tend to avoid these areas. In temperate zones, this has been observed in several studies (Page & Whitacre, 1975; Bryant, 1979; Van Dunsen et al., 2012). Overall, we found that the abundance of shorebirds was lower in areas close from mangrove patches which is in accordance with a strategy to minimize predation risk described for temperate zones (Page & Whitacre, 1975; Folmer & Piersma, 2012). Quantifying the predation (or the fear) pressure could be interesting for future work in order to support this hypothesis. Another probable reason why most of the birds were found foraging in areas far from mangrove areas is that the soluble tannins associated with mangrove leaf litter deposits can reduce macroinvertebrate abundance (Lee, 1999). Thus, it is expected that shorebirds tend to occur and to be more abundant in areas away from mangrove trees, as the macroinvertebrate abundance is higher in such areas. However, only areas in the vicinity of mangrove patches are affected and this do not explain every part of the shorebird's response concerning this variable.

Distance to channel/creeks

The responses of the Sanderling and Bar-tailed Godwit to the distance to channels seem to be different from those found in previous studies (e.g. Granadeiro et al., 2004; 2007). The Sanderling seem to more frequent in areas away from channels. One probable reason is that fiddler crab areas tend to be more concentrated near channels and fiddler crabs are not a common item in the diet of this species (Lourenço et al., 2017). Also, Sanderling densities are lower in fiddler crab high density areas (Paulino, 2019). Despite feeding on fiddler crab (Lourenço et al., 2017), the Bar-tailed Godwit seems to be more frequent in areas located at intermediate distances from channels. This might be related to the fact that this shorebird species has a diversified diet (Lourenço et al., 2019) and areas with fiddler crabs have lower macroinvertebrate diversity and densities (Paulino, 2019).

LIMITATIONS

The abundances values were calculated as the mean between two-days counting. In order to have more robust values, more counting days are needed. In general, confidence intervals were broad for higher values. For instance, we had few points of high mud fraction of the sediment and therefore the confidence interval is boarder than in areas with less mud contents. This is mainly caused by the characteristics of the intertidal flats of Adonga, that in general have low mud contents. The same happened with the mean exposure period. This can be improved by having a higher sampling size.

FINAL CONCLUSIONS

Intertidal systems are rapidly losing area at a global scale (Murray et al., 2019) mainly due to global climate changes, sea-level rise and human activities (Galbairth et al., 2002; Murray et al., 2019). Many populations of shorebirds are threatened at a global scale, mainly due to the loss/degradation of these intertidal foraging habitats (Russi et al., 2013; IUCN, 2019). Most of these birds are highly migratory and depend on a network of wintering and stopover sites to complete their annual cycles (Morrison, 1984). In this study, we provided a detailed description on the most important factors explaining the selection of foraging area by the 12 most abundant species in one important non-breeding area.

Generalized additive models offered accurate occurrence predictions and interpretable shorebird-habitat relationships. All species showed a non-linear response to at least one predictor and the representation of some smooth terms required more than two degrees of freedom. In general, the explained deviances were high. Remote sensing techniques allowed the identification of important variables influencing shorebirds distribution, including exposure period, (classes of) grain-size and presence of fiddler crabs. Our results show that when the observed frequency of occurrence is higher, the predicted probability of occurrence is also higher, suggesting that our predictive maps are accurate. Our results also suggest that different habitats within the intertidal area are exploited in distinct forms by different species, highlighting the need to preserve this diversity in order to meet each species requirements. With further work, predictive maps can be expanded to the whole archipelago and provide an important and powerful tool in identifying priority areas, for the definition of conservation actions at this critical wintering site.

FINAL CONSIDERATIONS

This study proposed an effective approach to identify foraging habitats for shorebirds. It is often difficult to map distribution at a medium/large scale in intertidal areas, some of which are dangerous to access. As mentioned before, the distribution patterns of shorebirds often respond to the patterns of occurrence and abundance of macroinvertebrate prey, in intertidal mudflats. It is known that these patterns of macroinvertebrate distribution are difficult to quantify at medium/large scales. To address this issue, we collected environmental variables that have been previously described as relevant factors affecting both macroinvertebrate and shorebird distribution.

Remote sensing proved to be a valuable tool. In Chapter 1, profiting the high spatial and radiometric resolution of Sentinel 2 images, we built a highly accurate map regarding two variables: mud fraction and fiddler crab burrow area. This result had major importance as intertidal areas are difficult to classify due the reasons explained along Chapter 1. Also, mapping areas with fiddler crab areas are crucial to predict shorebird distribution, as the composition of shorebird assemblage inside and outside such areas is quite different. To our knowledge, there are no studies that accomplished this. Intertidal areas are decreasing their area at an accelerated rhythm and our results can be used to monitor changes in intertidal habitats.

In Chapter 2, we successfully modelled the patterns of occurrence and abundance of several shorebird species. We also provided a detailed description of the most influential predictors affecting foraging shorebird distribution. Our GAM models achieved a high power in explaining deviances values, and they offered interpretable bird-habitat relationships. As expected, we could observe that different species have different habitat preferences. Therefore, maintaining the diversity in intertidal areas is crucial to meet each species requirements.

The link between the two chapters are the predictive maps. We could predict areas with higher probability of occurrence for 11 shorebird species, using information that could hardly be obtained without the use of remote sensing tools. The exercise used in this thesis can be expanded to larger scales if the sampling effort is higher. We consider our work to be relevant in terms of conservation, as intertidal areas and shorebirds face several threats. Although being poorly studied, the Bijagós archipelago is one of the key non-breeding areas for shorebirds along the East Atlantic Flyway. Therefore, identifying priority areas for shorebirds in this critical site can be of major importance for the definition of conservation actions.

REFERENCES

According to Hydrobiologia

Amanollahi J, Abdullah AM, & G. A. D. Tilaki, 2011. Relationship between plants evening and soil properties in the rangeland, Lar National Park, Iran. African Journal of Agricultural Research 6: 5551-5557.

Attarchi, S., & R. Gloaguen, 2014. Improving the estimation of above ground biomass using dual polarimetric PALSAR and ETM+ data in the Hyrcanian mountain forest (Iran). Remote Sensing 6: 3693-3715.

Austin, M. P., 1999. A silent clash of paradigms: some inconsistencies in community ecology. Oikos 86: 170-178.

Beninger, P. G., & D. M. Paterson, 2018. Introduction: Mudflat Basics. In Mudflat Ecology. Springer, Cham.

Botto, F., & O. Iribarne, 2000. Contrasting effects of two burrowing crabs (Chasmagnathus *Granulata* and *Uca uruguayensis*) on sediment composition and transport in estuarine environments. Estuarine, Coastal and Shelf Science 51: 141-151.

Breiman, L., 2001. Random forests. Machine Learning 45: 5-32.

Brito, A., Benyoucef, I., Jesus, B., Brotas, V., Gernez, P., Mendes, C., Luneau, P., Dias, M. & L. Barillé, 2013. Seasonality of microphytobentos revealed by remote-sensing in a South European estuary. Continental Shelf Research 66: 83-91.

Brockman, C., & K. Stelzer, 2008. Optical remote sensing of intertidal flats. In Barale V. & M. Gade (eds), Remote Sensing of the European Seas. Springer, Dordrecht.

Brown, M., 2018. Shorebirds in action: an introduction to waders and their behaviour, Richard Chandler. African Journal of Wildlife Research 48: 1-3.

Bryant, D.M., 1979. Effects of prey density and site character on estuary usage by overwintering 384 waders (Charadrii). Estuarine and Coastal Marine Science 9: 369-384.

Bryant, R., Tyler, A., Gilvear, D., McDonald, P., Teasdale, I., Brown, J., & G. Ferrier, 1996. A preliminary investigation into the spectral characteristics of inter-tidal estuarine sediments. International Journal of Remote Sensing 17: 405-412.

Burger, J., Howe, M.A., Hahn, D.C. & J. Chase, 1977. Effects of tide cycles on habitat selection and habitat partitioning by migrating shorebirds. The Auk 94: 743-758.

Calle, L., Green, L., Strong, A., & D. E. Gawlik, 2018. Time- integrated habitat availability is a resource attribute that informs patterns of use in intertidal areas. Ecological Monographs 88: 600-620.

Campbell, J.B. & R. H. Wynne, 2011. Introduction to Remote Sensing (5th. Ed.). The Guilford Press, New York.

Campredon, P., & P. Catry, 2016. Bijagos Archipelago (Guinea-Bissau). In Finlayson C., Milton G., Prentice R. & N. Davidson, (eds), The Wetland Book. Springer, Dordrecht.

Cardoso, P., 2017. Os mangais da Guiné-Bissau: análise a 40 anos de evolução da sua extensão. Masters dissertation, Universidade de Lisboa.

Catalão, J., 2018. Uma nova técnica para determinar a batimetria intertidal com imagens multiespectrais do satélite Sentinel-2. 5as Jornadas de Engenharia Hidrográfica.

Cayford, J., 1993. Wader disturbance: a theoretical overview. Wader Study Group Bulletin 68: 3-5.

Chen, C., Liaw, A., & L. Breiman, 2004. Using random forest to learn imbalanced data. University of California, Berkeley 110: 1-12.

Choi, C. Y., Battley, P. F., Potter, M. A., Ma, Z., & W. Liu, 2014. Factors affecting the distribution patterns of benthic invertebrates at a major shorebird staging site in the Yellow Sea, China. Wetlands 34: 1085-1096.

Cingolani, A.M., Renison, D., Zak, M.R. & M. R. Cabido, 2004. Mapping vegetation in a heterogeneous mountain rangeland using Landsat data: an alternative method to define and classify land-cover units. Remote Sensing of Environment 92: 84-97.

Colwell, M. A., 1993. Shorebird community patterns in a seasonally dynamic estuary. The Condor 95: 104-114.

Congalton, R.G., 1991. A review of assessing the accuracy of classifications of remotely sensed data. Remote Sensing of Environment 37: 35-46.

Dahl, T. E., 2006. Status and Trends in the Conterminous United States 1998 to 2004. Washington D.C.: U.S. Department of the Interior, Fish and Wildlife Service Publication.

Day Jr, J. W., Yanez-Arancibia, A., Kemp, W. M. & B. C. Crump, 2013. Introduction to estuarine ecology. Estuarine Ecology (second ed).

Delany, S., Scott, D., Dodman, T., & D. Stroud, 2009. An atlas of wader populations in Africa and Western Eurasia. Brit Birds, 102: 639-642.

Deronde, B., Kempeneers, P., & R. M. Forster, 2006. Imaging spectroscopy as a tool to study sediment characteristics on a tidal sandbank in the Westerschelde. Estuarine, Coastal and Shelf Science 69: 580-590.

Dietterich, T. G., 1998. Approximate statistical tests for comparing supervised classification learning algorithms. Neural computation 10: 1895-1923.

Doerffer, R., & D. Murphy, 1989. Factor analysis and classification of remotely sensed data for monitoring tidal flats. Helgoländer Meeresuntersuchungen 43: 275-293.

Dodman, T., & J. Sá, 2005. Monitorização de aves aquáticas no Arquipélago dos Bijagós, Guiné-Bissau. Wetlands International, Bissau.

Drusch, M., Del Bello, U., Carlier, S., Colin, O., Fernandez, V., Gascon, F., Hoersch, B., Isola, C., Labertenti, P., Martimort, P., Meygret, A. Spoto, F., Sy, O., Marchese, F. & P. Bargellini, 2012. Sentinel-2: ESA's optical high-resolution mission for GMES operational services. Remote Sensing of Environment 120: 25-36.

Dyer, K. R., Christie, M. C., & E. W. Wright, 2000. The classification of intertidal mudflats. Continental Shelf Research 20: 1039-1060.

ESA, 2017a. Sentinel Online. Missions. Sentinel/2. Data products. Available in: https://sentinel.esa.int/web/sentinel/missions/sentinel-2/data-products. Accessed November 5, 2019.

ESA, 2017b. Sentinel Online; Radiometric Resolutions. Available in: https://earth.esa.int/web/sentinel/user-guides/sentinel-2-msi/resolutions/radiometric. Accessed November, 5, 2018

ESA, 2017c. Sentinel Online. Technical Guides. Level -2A Algorithm Overview. Available in: https://earth.esa.int/web/sentinel/technical-guides/sentinel-2-msi/level-2a/algorithm. Accessed September 25, 2019.

Foody, G. M., 2004. Thematic map comparison. Photogrammetric Engineering & Remote Sensing 70: 627-633.

Folmer, E. O., & T. Piersma, 2012. The contributions of resource availability and social forces to foraging distributions: a spatial lag modelling approach. Animal Behaviour 84: 1371-1380.

Forkuor, G., Dimobe, K., Serme, I., & J. E. Tondoh, 2018. Landsat-8 vs. Sentinel-2: examining the added value of sentinel-2's red-edge bands to land-use and land-cover mapping in Burkina Faso. GIScience & Remote Sensing 55: 331-354.

Galbraith, H., Jones, R., Park, R., Clough, J., Herrod-Julius, S., Harrington, B., & G. Page, 2002. Global climate change and sea level rise: potential losses of intertidal habitat for shorebirds. Waterbirds 25: 173-183.

Gibson, R. N., Barnes, M., & R. J. A. Atkinson, 2001. Selective tidal-stream transport of marine animals. Oceanography and Marine Biology 39: 305-353.

Genoni, G.P., 1991. Increased burrowing by fiddler crabs *Uca rapax* (Smith) (Decapoda: Ocypodidae) in response to low food supply. Journal of Experimental Marine Biology and Ecology 147: 267-285.

Goss-Custard, J. D., 1970. The responses of redshank (*Tringa totanus* (L.)) to spatial variations in the density of their prey. The Journal of Animal Ecology 39: 91-113.

Goss-Custard, J. D., & M. G. Yates, 1992. Towards predicting the effect of salt-marsh reclamation on feeding bird numbers on the Wash. Journal of Applied Ecology 29: 330-340.

Granadeiro, J. P., Andrade, J., & J. M. Palmeirim, 2004. Modelling the distribution of shorebirds in estuarine areas using generalised additive models. Journal of Sea Research 52: 227-240.

Granadeiro, J. P., Santos, C. D., Dias, M. P., & J. M. Palmeirim, 2007. Environmental factors drive habitat partitioning in birds feeding in intertidal flats: implications for conservation. Hydrobiologia 587: 291-302.

Granadeiro, J. P., Dias, M. P., Martins, R. C., & J. M. Palmeirim, 2006. Variation in numbers and behaviour of waders during the tidal cycle: implications for the use of estuarine sediment flats. Acta Oecologia 29: 293-300.

Guisan, A., Edwards Jr, T. C., & T. Hastie, 2002. Generalized linear and generalized additive models in studies of species distributions: setting the scene. Ecological Modelling 157: 89-100.

Guisan, A., Tingley, R., Baumgartner, J. B., Naujokaitis- Lewis, I., Sutcliffe, P. R., Tulloch, A. I., Regan, T. J., Brotons, L., McDonald-Maddem, E., Mantyca-Pringle, C., Martin, T. G., Rhodes, J. R., Maggini, R., Setterfield, S. A., Elith, J., Schwartz, M. W., Wintle, B. A., Broenniman, O., Austin, M., Ferrier, S., Kearney, M. R., Posssingham, H. P., & Y. M. Buckley, 2013. Predicting species distributions for conservation decisions. Ecology Letters 16: 1424-1435.

Gutiérrez, J. L., Jones, C. G., Groffman, P. M., Findlay, S. E. G., Iribarne, O. O., Ribeiro, P. D., & C. M. Bruschetti, C.M., 2006. The contribution of crab burrow excavation to carbon availability in surficial saltmarsh sediments. Ecosystems 9: 647–658.

Han, J., Zhu, L., Kulldorff, M., Hostovich, S., Stinchcomb, D. G., Tatalovich, Z., Lewis, D. R. & E. J. Feuer, 2016. Using Gini coefficient to determining optimal cluster reporting sizes for spatial scan statistics. International Journal of Health Geographics 15.

Hastie, T., & R. Tibshirani, 1990. Exploring the nature of covariate effects in the proportional hazards model. Biometrics 46: 1005-1016.

Hedley, J., Roelfsema, C., Koetz, B., & S. Phinn, 2012. Capability of the Sentinel 2 mission for tropical coral reef mapping and coral bleaching detection. Remote Sensing of Environment 120: 145-155.

Hothorn, T., Hornik, K., & A. Zeileis, 2006. Unbiased recursive partitioning: A conditional inference framework. Journal of Computational and Graphical statistics 15: 651-674.

Hickey, R., 2019. Tidal inundation modeling within GIS. Journal of Coastal Conservation 23: 1-8.

IH, 2019. Instituto Hidrográfico da Marinha Portuguesa. Available in: http://www.hidrografico.pt. Accessed September 25, 2019.

Iribarne, O. O., & M. M. Martinez, 1999. Predation on the southwestern Atlantic fiddler crab (*Uca uruguayensis*) by migratory shorebirds (*Pluvialis dominica*, *P. squatarola*, *Arenaria interpres*, and *Numenius phaeopus*). Estuaries 22: 47-54.

IUCN, 2019. The IUCN Red List of Threatened Species. Version 2019-2. Available from http://www.iucnredlist.org/. Accessed September 25, 2019.

Khatami, R., Mountrakis, G., & S. V Stehman, 2016. A meta-analysis of remote sensing research on supervised pixel-based land-cover image classification processes: General guidelines for practitioners and future research. Remote Sensing of Environment 177: 89-100.

Klemas, V., 2011. Remote sensing of wetlands: case studies comparing practical techniques. Journal of Coastal Research 27: 418-427.

Korhonen, L., Packalen, P., & M. Rautiainen, 2017. Comparison of Sentinel-2 and Landsat 8 in the estimation of boreal forest canopy cover and leaf area index. Remote Sensing of Environment 195: 259-274.

Kristensen E., 2008. Mangrove crabs as ecosystem engineers; with emphasis on sediment processes. Journal of Sea Research 59: 30-43.

Kwang, C., Jnr, E. M. O., & A. S. Amoah, 2017. Comparing of Landsat 8 and Sentinel 2A using Water Extraction Indexes over Volta River. Journal of Geography and Geology 10.

Kwon, D. J., Park, W., & J. S. Won, 2016. Classification of intertidal sediment using a two-step principal component analysis (PCA) of optical reflectance: A case study in Ganghwa tidal flats. Journal of Marine Science and Technology 24: 1136-1145.

Lee, S. Y., 1999. The effect of mangrove leaf litter enrichment on macrobenthic colonization of defaunated sandy substrates. Estuarine, Coastal and Shelf Science 49: 703-712.

Leutner, B., Horning, N., & J. Schwalb-Willmann, 2018. RStoolbox: tools for remote sensing data analysis. R package version 0.2. 4. Available in: https://CRAN.R-project.org/package=RStoolbox. Accessed August 16, 2019.

Lhermitte S, Verbesselt J, Verstraaten WW, & P. Coppin, 2011. A comparison of time series similarity measures for classification and change detection of ecosystems dynamics. Remote Sensing of the Environment 115: 3129-3152.

Li, J., & D. P. Roy, 2017. A global analysis of Sentinel-2A, Sentinel-2B and Landsat-8 data revisit intervals and implications for terrestrial monitoring. Remote Sensing 9: 902-913.

Li, W., & P. Gong, 2016. Continuous monitoring of coastline dynamics in western Florida with a 30-year time series of Landsat imagery. Remote Sensing of Environment 179: 196-209.

Liu, H., & K. C. Jezek, 2004. Automated extraction of coastline from satellite imagery by integrating Canny edge detection and locally adaptive thresholding methods. International Journal of Remote Sensing 25: 937-958.

Liu, R., Men, C., Liu, Y., Yu, W., Xu, F., & Z. Shen, 2016. Spatial distribution and pollution evaluation of heavy metals in Yangtze estuary sediment. Marine Pollution Bulletin 110: 564-571.

Lobell, D. B., & G. P. Asner, 2002. Moisture effects on soil reflectance. Soil Science Society of America Journal 66: 722-727.

Lotze, H., Lenihan, H., Bourque, B., Bradbury, R., Cooke, R., Kay, M., Kidwell, S., Kirby, M., Peterson, C., & J. Jackson, 2006. Depletion, degradation, and recovery potential of estuaries and coastal seas. Science 312: 1806-1809.

Lourenco, P. M., Granadeiro, J. P., & J. M. Palmeirim, 2005. Importance of drainage channels for waders foraging on tidal flats: relevance for the management of estuarine wetlands. Journal of Applied Ecology 42: 477-486.

Lourenço, P. M., Catry, T., & J. P. Granadeiro, 2017. Diet and feeding ecology of the wintering shorebird assemblage in the Bijagós archipelago, Guinea-Bissau. Journal of Sea Research 128: 52-60.

Lunardi, V. O., Macedo, R. H., Granadeiro, J. P., & J. M. Palmeirim, 2012. Migratory flows and foraging habitat selection by shorebirds along the northeastern coast of Brazil: the case of Baía de Todos os Santos. Estuarine, Coastal and Shelf Science 96: 179-187.

Manzo, C., Bresciani, M., Giardino, C., Braga, F., & C. Bassani, 2015. Sensitivity analysis of a bio-optical model for Italian lakes focused on Landsat-8, Sentinel-2 and Sentinel-3. European Journal of Remote Sensing 48: 17-32.

Marra, G., & S. N. Wood, 2011. Practical variable selection for generalized additive models. Computational Statistics & Data Analysis 55: 2372-2387.

Mertes, L. A., Smith, M. O., & J. B. Adams,1993. Estimating suspended sediment concentrations in surface waters of the Amazon River wetlands from Landsat images. Remote Sensing of Environment 43: 281-301.

Miller, A. K., & C. E. de Rivera, 2014. Small tidal channels improve foraging opportunities for *Calidris* shorebirds. The Condor: Ornithological Applications 116: 113-121.

Moores, N., Rogers, D. I., Rogers, K., & P. M. Hansbro, 2016. Reclamation of tidal flats and shorebird declines in Saemangeum and elsewhere in the Republic of Korea. Emu-Austral Ornithology 116: 136-146.

Morrison, R. I. G., 1984. Migration systems of some New World shorebirds. Behavior of Marine Animals: Current Perspectives in Research 6: 125-202.

Moreira, J., 1998. On the use by birds of intertidal areas of the Tagus estuary: implications for management. Aquatic Ecology 33: 301-390.

Mouton, E.C. & D.L. Felder, 1996. Burrow distributions and population estimates for the fiddler crabs *Uca spinicarpa* and *Uca longisignalis* in a Gulf of Mexico salt marsh. Estuaries 19: 51–61.

Muñoz-Robles C, Frazier P, Tighe M, Reid N, Briggs SV, & B. Wilson, 2012. Assessing Ground Cover at Patch and Hillslope Scale in Semi-arid Woody Vegetation and Pasture Using Fused Quickbird Data. International Journal of Applied Earth Observation and Geoinformation 14: 94-102.

Murray, N. J., Phinn, S. R., DeWitt, M., Ferrari., R., Johnstone, R., Lyons, M. B., Clinton, N., Thau, D. & R. A. Fuller, 2019. The global distribution and trajectory of tidal flats. Nature 565: 222-225.

Na, X., Zhang, S., Li, X., Yu, H., & C. Liu, 2010. Improved land cover mapping using random forests combined with Landsat thematic mapper imagery and ancillary geographic data. Photogrammetric Engineering & Remote Sensing 76*:* 833-840.

NASA, 2015. USGS EROS Archive - Sentinel-2 - Comparison of Sentinel-2 and Landsat. Available in: https://landsat.gsfc.nasa.gov/wp-content/uploads/2015/06/Landsat.v.Sentinel-2.png. Accessed November 5, 2018.

NASA, 2017. Spectral Response of the Operational Land Imager In-Band, Band-Average Relative Spectral Response. Available in: https://landsat.gsfc.nasa.gov/preliminary-spectral-response-of-the-operational-land-imager-in-band-band-average-relative-spectral-response/. Accessed November 5, 2018.

Page, G., & D. F. Whitacre, 1975. Raptor predation on wintering shorebirds. The Condor 77: 73-83.

Pesaresi, M., Corbane, C., Julea, A., Florczyk, A. J., Syrris, V., & P. Soille, 2016. Assessment of the added-value of Sentinel-2 for detecting built-up areas. Remote Sensing 84: 299.

Peterson, C. H., 1991. Intertidal zonation of marine invertebrates in sand and mud. American Scientist 7: 236-249.

Quintino, V., Rodrigues, A. M. & F. Gentil, 1989. Assessment of macrozoobenthic communities in the Lagoon of Obidos, western coast of Portugal. Scientia Marina 53: 645–654.

Paulino, J., 2019. Fiddler crabs impact the structure of the benthic macroinvertebrate community and the spatial distribution of foraging shorebirds in tropical intertidal mudflats. Master dissertation, Universidade de Lisboa.

Ponsero, A., Sturbois, A., Desroy, N., Le Mao, P., Jones, A., & J. Fournier, 2016. How do macrobenthic resources concentrate foraging waders in large megatidal sandflats? Estuarine, Coastal and Shelf Science 178: 120-128.

Raffaelli, D., & S. J. Hawkins, 1999. Intertidal ecology. Klewer Academic Publishers, Dordrecht.

Rainey, M. P., Tyler, A. N., Bryant, R. G., Gilvear, D. J., & P. McDonald, 2000. The influence of surface and interstitial moisture on the spectral characteristics of intertidal sediments: implications for airborne image acquisition and processing. International Journal of Remote Sensing 21: 3025-3038.

Rainey, M. P., Tyler, A. N., Gilvear, D. J., Bryant, R. G., & P. McDonald, 2003. Mapping intertidal estuarine sediment grain size distributions through airborne remote sensing. Remote Sensing of Environment 86: 480-490.

Rebelo, R., & P. Catry, 2011. O arquipélago dos Bijagós (Guiné-Bissau) - valores de biodiversidade e potencialidades para a investigação científica. Ecologia 2: 8-15.

Rodriguez-Galiano, V. F., Ghimire, B., Rogan, J., Chica-Olmo, M., & J. P. Rigol-Sanchez, 2012. An assessment of the effectiveness of a random forest classifier for land-cover classification. ISPRS Journal of Photogrammetry and Remote Sensing 67: 93-104.

Rosa, S., Palmeirim, J. M., & F. Moreira, 2003. Factors affecting waterbird abundance and species richness in an increasingly urbanized area of the Tagus estuary in Portugal. Waterbirds 26: 226-232.

Rozenstein, O., & A. Karnieli, 2011. Comparison of methods for land-use classification incorporating remote sensing and GIS inputs. Applied Geography 31: 533-544.

Russi, D., ten Brink, P., Farmer, A., Badura, T., Coates, D., Förster, J., Kumar, R., & N. Davidson, 2013. The economics of ecosystems and biodiversity for water and wetlands. IEEP, London and Brussels, 78.

Ryu, J. H., Na, Y. H., Won, J. S., & R. Doerffer, 2004. A critical grain size for Landsat ETM+ investigations into intertidal sediments: a case study of the Gomso tidal flats, Korea. Estuarine, Coastal and Shelf Science 60: 491-502.

Sagar, S., Roberts, D., Bala, B., & L. Lymburner, 2017. Extracting the intertidal extent and topography of the Australian coastline from a 28 year time series of Landsat observations. Remote Sensing of Environment 195: 153-169.

Salvig, J. C., Asbirk, S., Kjeldsen, J.P. & P. A. Rasmussen,1994. Wintering waders in the Bijagos Archipelago, Guinea-Bissau 1992-1993. Ardea 82: 137-142.

Scheiffarth, G., Nehls, G., & I. Austen, 1996. Modelling distribution of shorebirds on tidal flats in the Wadden Sea and visualisation of results with the GIS IDRISI. IDRISI GIS 96 25.

Schelske C.L, & E. P. Odum, 1962. Mechanisms maintaining high productivity in Georgia estuaries. Proceedings of the Gulf and Caribbean Fisheries Institute 14: 75–80

Seager, S., Turner, E. L., Schafer, J., & E. B. Ford, 2005. Vegetation's red edge: a possible spectroscopic biosignature of extraterrestrial plants. Astrobiology 5: 372-390.

Stelzer, K., Brockmann, C., Murphy, D., & U. Krämer, 2004. Applicability of remote sensing in monitoring coastal zones. Coastline Reports 1: 249-253.

Stillman, R. A., West, A. D., Goss-Custard, J. D., McGrorty, S., Frost, N. J., Morrisey, D. J., Kenny, A. J. & A. L. Drewitt, 2005. Predicting site quality for shorebird communities: a case study on the Humber estuary, UK. Marine. Ecology Progress Series 305: 203-217.

Strobl, C., Boulesteix, A. L., Zeileis, A., & T. Hothorn, 2007. Bias in random forest variable importance measures: Illustrations, sources and a solution. BMC bioinformatics 8.

Strobl, C., Boulesteix, A. L., Kneib, T., Augustin, T., & A. Zeileis, 2008. Conditional variable importance for random forests. BMC Bioinformatics 9.

Studds, C. E., Kendall, B. E., Murray, N. J., Wilson, H. B., Rogers, D. I., Clemens, R. S., Gosbell, K., Hassel, C., Jessop, R., Melville, D., Milton, D., Minton, C., Possingham, H., Riegen, A., Straw, P., Woehler, E. & Fuller, R., 2017. Rapid population decline in migratory shorebirds relying on Yellow Sea tidal mudflats as stopover sites. Nature Communications 8.

Summers, R. W., Underhill, L. G., & A. Simpson, 2002. Habitat preferences of waders (Charadrii) on the coast of the Orkney Islands. Bird Study, 49: 60-66.

Thomas, G. H., Lanctot, R. B., & T. Szekely, 2006. Can intrinsic factors explain population declines in North American breeding shorebirds? A comparative analysis. Animal Conservation, 9: 252-258.

Thomson, A. G., Fuller, R. M., Sparks, T. H., Yates, M. G., & J. A. Eastwood, 1998. Ground and airborne radiometry over intertidal surfaces: waveband selection for cover classification. International Journal of Remote Sensing 19: 1189-1205.

Thomson, A. G., Fuller, R. M., Yates, M. G., Brown, S. L., Cox, R., & R. A. Wadsworth, 2003. The use of airborne remote sensing for extensive mapping of intertidal sediments and saltmarshes in eastern England. International Journal of Remote Sensing 24: 2717-2737.

Topaloglu, R. H., Sertel, E., & N. Musaoglu, 2016. Assessment of classification accuracies of Sentinel-2 and Landsat-8 data for land cover/use mapping. International Archives of the Photogrammetry, Remote Sensing & Spatial Information Sciences 41: 1055-1059.

Tiner, R. W., 1996. Wetlands. Manual of Phorographic Interpretation, 2nd edition. Falls Church, Virginia: American Society for Photogrammetry and Remote Sensing.

UNESCO, 2011. Biosphere Reserves, UNESCO. Accessed December 10, 2018.

VanDusen, B. M., Fegley, S. R., & C. H. Peterson, 2012. Prey distribution, physical habitat features, and guild traits interact to produce contrasting shorebird assemblages among foraging patches. PlosOne 7.

Van Roomen, M., Nagy, S., Citegeste, G. & H. Shekkerman, 2018. Introduction. In: Van Roomen, M., Nagy, S., Citegeste, G. & H. Shekkerman, 2018 (eds). East Atlantic Flyway Assessment 2017: the status of coastal waterbird populations and their sites.

WSI, 2015. Wadden Sea Flyway Initiative. Available in: https://www.unep-aewa.org/en/news/joining-efforts-protect-migratory-birds-along-east-atlantic-flyway/. Accessed September 20, 2019.

Watkinson, A. R., Gill, J. A., & M. Hulme, 2004. Flying in the face of climate change: a review of climate change, past, present and future. Ibis 146: 4-10.

Wallace, J. H., Kok, H. M., Beckley, L. E., Bennett, B., Blaber, S. J. M. & A. K. Whitfield, 1984. South African estuaries and their importance to fishes. South African Journal of Science 80: 203–207.

Wegmann, M., Leutner, B. & S. Dech, 2016 Remote Sensing and GIS for Ecologists: Using Open Source Software. Pelagic Publishing, UK.

Wilson, H. B., Kendall, B. E., Fuller, R. A., Milton, D. A., & H. P. Possingham, 2011. Analyzing variability and the rate of decline of migratory shorebirds in Moreton Bay, Australia. Conservation Biology 25: 758-766.

Winterbottom, J. M. (1967). The Birds of Three Salt-Water Habitats in the South West Cape. Ostrich, 38: 148-154.

Wood, S. N., 2000. Modelling and smoothing parameter estimation with multiple quadratic penalties. Journal of the Royal Statistical Society: Series B (Statistical Methodology) 62: 413-428.

Wood, S. N., 2003. Thin plate regression splines. Journal of the Royal Statistical Society: Series B (Statistical Methodology) 65: 95-114.

Wood, S. N., 2017. Generalized additive models: an introduction with R. Chapman and Hall/CRC.

Yates, M. G., Goss-Custard, J. D., McGrorty, S., Lakhani, K. H., dit Durell, S. L. V. D., Clarke, R. T., Rispin, W. E., Moy, I., Yates, T., Plant, R. A. & A. J. Frost, 1993. Sediment characteristics, invertebrate densities and shorebird densities on the inner banks of the Wash. Journal of Applied Ecology 30: 599-614.

Yates, M. G., Goss-Custard, J. D., & W. E. Rispin, 1996. Towards predicting the effect of loss of intertidal feeding areas on overwintering shorebirds (Charadrii) and shelduck (*Tadorna tadorna*): refinements and tests of a model developed for the Wash, east England. Journal of Applied Ecology 33: 944-954.

Yasué, M., 2006. Environmental factors and spatial scale influence shorebirds' responses to human disturbance. Biological Conservation, 128: 47-54.

Yu, Y., & S. T. Acton, 2004. Automated delineation of coastline from polarimetric SAR imagery. International Journal of Remote Sensing 25: 3423-3438.

Zwarts, L., 1985. The winter exploitation of fiddler crabs *Uca tangeri* by waders in Guinea -Bissau. Ardea 73: 3–12.

Zwarts, L., 1988. Numbers and distribution of coastal waders in Guinea-Bissau. Ardea, 76: 42-55.

APPENDICES

Table 1- Pearson correlations between the principal components used for supervised classification of Sand-FBA and the other classes

Layers	PC1	PC2	PC3	PC4	PC5
B2	0.295	0.317	---------	0.135	0.441
B3	0.310	0.251	---------	0.146	0.138
B4	0.314	0.203	---------	---------	0.452
B5	0.324	---------	---------	---------	0.107
B6	0.319	-0.130	0.163	0.180	-0.155
B7	0.316	-0.166	0.161	0.179	-0.265
B8	0.314	-0.178	0.173	0.153	-0.149
B8A	0.314	-0.199	0.138	0.148	-0.337
B11	0.300	---------	-0.165	-0.538	-0.188
B12	0.308	---------	-0.148	-0.659	---------
Inundation layer	0.170	-0.353	-0.867	0.281	-0.105
NDWI layer	----------	0.737	-0.299	0.198	-0.538

Table 2 - Pearson correlations between the principal components used for supervised classification of Muddy-FBA and the other classes

Layers	PC1	PC2	PC3	PC4	PC5
B2	0.271	0.405	---------	---------	0.140
B3	0.297	0.353	---------	---------	---------
B4	0.304	0.316	---------	---------	0.561
B5	0.346	0.157	0.108	---------	0.235
B6	0.347	-0.127	0.198	---------	-0.107
B7	0.340	-0.169	0.208	---------	-0.217
B8	0.335	-0.191	0.198	-0.118	-0.178
B8A	0.333	-0.210	0.189	---------	-0.278
B11	0.291	-0.135	-0.558	---------	---------
B12	0.251	---------	-0.711	---------	---------
Inundation layer	0.129	-0.306	0.935	0.935	---------
NDWI layer	---------	0.584	0.265	0.265	-0.643

Table 2 - Pearson correlations between the principal components used for supervised classification of Sand and Muddy

Layers	PC1	PC2	PC3	PC4	PC5
B2	0.282	0.363	---------	0.138	0.433
B3	0.312	0.295	---------	0.164	0.155
B4	0.314	0.272	0.102	0.122	-0.661
B5	0.343	0.103	0.201	0.105	-0.408
B6	0.336	-0.196	0.176	---------	0.177
B7	0.328	-0.243	0.158	---------	0.188
B8	0.327	-0.246	0.146	---------	---------
B8A	0.322	-0.275	---------	---------	0.150
B11	0.298	---------	-0.470	-0.371	-0.125
B12	0.273	0.118	-0.505	-0.453	---------
Inundation layer	0.106	-0.265	-0.606	0.738	---------
NDWI layer	---------	0.614	---------	0.198	0.251

Table 4 - Number of classified pixels, total area and percentage of each habitat class of the intertidal area of Adonga, using method 2 (tile of 16/03/2019).

Land cover class	Area (ha)	Percentage of each land cover area (%)
Sand-FBA	230	21.0
Sand	289	26.4
Muddy	182	16.5
Muddy-FBA	395	36.1
Total	1096	100

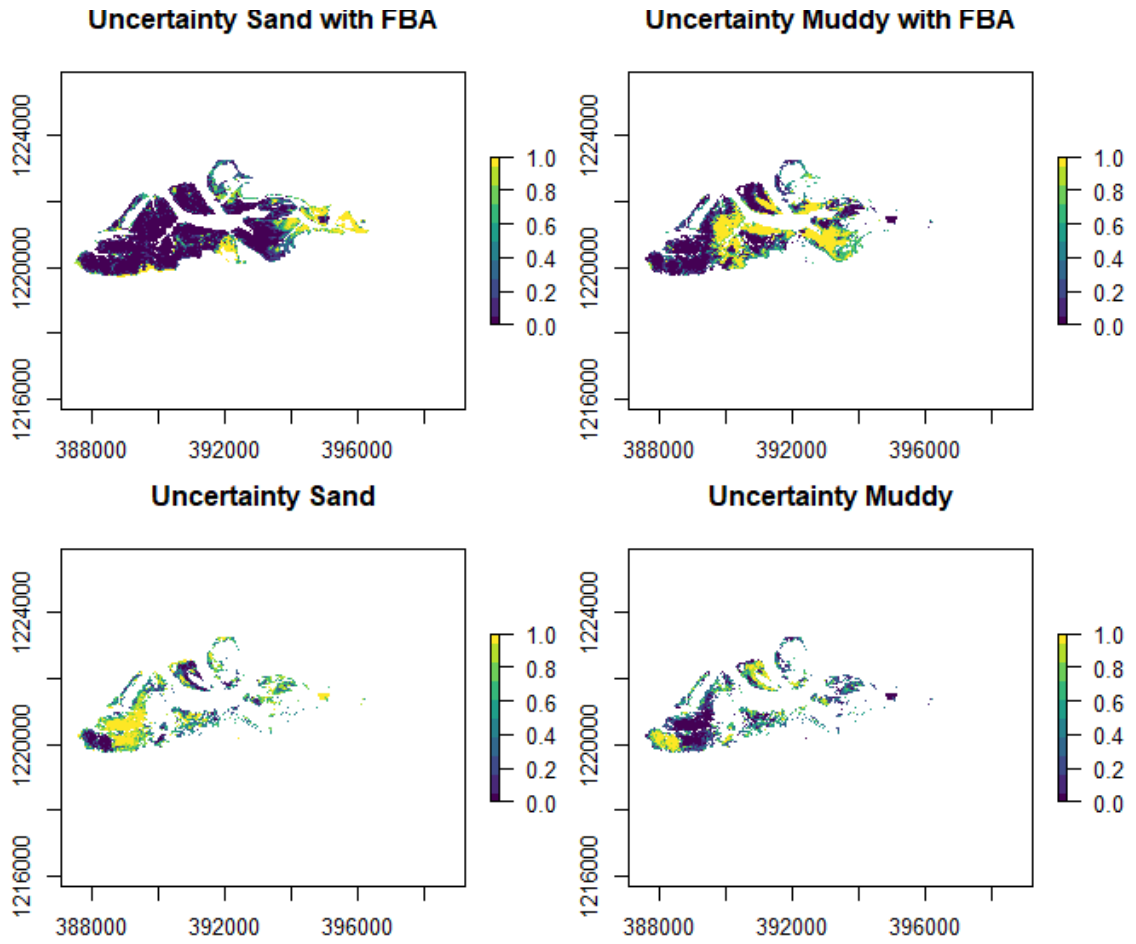

Figure 1 - Spatial distribution of uncertainty pixels (0.4<probability<0.6). Step 1: Sand-FBA (top left); Step 2: Muddy-FBA (top right); Step 3: Sand (bottom left) and Step 3: Muddy (bottom right).

Table 5 - Comparison of balanced accuracies for the different classes of the sediment(Sand-FBA, Sand, Muddy and Muddy FBA), overall accuracies and kappa coefficients for both methods, applied to the image of 15/04/2019

15/04/2019	Accuracies					
	Sand-FBA	Sand	Muddy	Muddy-FBA	Overall	kappa
Method 1	0.96	0.90	0.85	0.98	0.91	0.87
Method 2	0.96	0.90	0.84	0.97	0.90	0.85

Table 6 - Number of classified pixels, total area and percentage of each habitat class of the intertidal area of Adonga, using method 1 (tile of 15/04/2019).

Land cover class	Area (ha)	Percentage of each land cover area (%)
Sand-FBA	224	20.5
Sand	317	28.9
Muddy	202	18.5
Muddy-FBA	351	32.1
Total	1095	100

Table 7 - Number of classified pixels, total area and percentage of each habitat class of the intertidal area of Adonga, using method 2 (tile of 15/04/2019).

Land cover class	Area (ha)	Percentage of each land cover area (%)
Sand-FBA	243	22.2
Sand	280	25.5
Muddy	197	18.0
Muddy-FBA	376	34.3
Total	1096	100